# S T A B I L I T Y  A N D  N O I S E

# O F  E L E C T R O N  B E A M S

Thesis Submitted by

John E. Ryley

for the Degree of

Doctor of Philosophy

Faculty of Engineering

Department of Electronics

University of Southampton

April 1964

Summary

The noise figure of a travelling-wave tube or backward-wave amplifier is limited by electron-beam noise, the most important cause of which is random electron emission at the cathode. Beam-noise theory shows that the minimum noise figure of a t.w.t. or b.w.a. depends on $(S - \Pi)$, where S and $\Pi$ are two parameters which remain constant on a single-velocity beam. The noise figure thus depends on the processes in the multi-velocity region near the cathode in which S and $\Pi$ are determined. Practical work, by Currie in particular, has shown that $(S - \Pi)$ can be considerably reduced by extending the multi-velocity region using a special electrode near the cathode. Analysis of the noise-reducing processes in this region is difficult. A review of the several different theories put forward is presented here.

The work reported in this thesis is a study of the Currie gun which has been found to exhibit unusual changes in the beam structure and d.c. characteristics. The construction of equipment for tube processing and operation is described, including an all-semiconductor high-power d.c. supply for a focusing solenoid. Two tubes for studying beam structure using fluorescent screens were used. Details of a third tube with a movable gun and noise-pick-up cavity with associated microwave measuring apparatus are also given. Results of investigations into the effects of virtual cathode formation on the d.c. characteristics and beam structure are discussed. Unusual hysteresis effects observed in the beam current are

explained by the presence of positive ions. The method of measuring the noise parameter S using the moving-gun tube is described. A new method of measuring both S and $\pi$ by simply adding a second fixed cavity to the tube is put forward.

Index

# 1. INTRODUCTION

## 1.1 Low-Noise Microwave Amplifiers

Three main types of low-noise microwave amplifier exist - electron tubes, masers and parametric amplifiers.

The electron tubes may be sub-divided into three types - the travelling-wave tube (t.w.t.) or forward-wave amplifier, the backward-wave amplifier (b.w.a.) and the cyclotron-wave amplifier. All three of these employ an electron beam, but the cyclotron-wave amplifier differs considerably from the other two types and will not be considered here.

The b.w.a. and t.w.t. are very similar in construction and operation. Both use a similar type of slow-wave structure, usually a helix. In the t.w.t. the electron beam interacts with the fundamental of the wave on the helix and this type of amplifier has a very wide bandwidth. In the b.w.a. the beam is made to interact with a backward space harmonic of the wave on the helix resulting in an amplifier with a relatively narrow bandwidth. The b.w.a. can, however, be easily tuned over a wide range simply by changing the helix voltage.

Three fundamental factors limit the terminal noise figure of a t.w.t. or b.w.a. These are:

a) Electron-beam noise.

b) Loss on the slow-wave structure.

c) Loss at the input coupling to the slow-wave structure.

Beam noise is by far the most important of these three sources of noise as the other two can, in principle, be reduced to negligible levels by careful tube design.

1.2. Causes of Beam Noise

a) Electron-emission noise.

Noise is excited in the beam due to the random velocity, and rate of emission, of electrons from the cathode. Reduction of this noise can be achieved as the beam passes through the electron gun by suitable gun design.

b) Cathode defects.

Defects in the cathode surface cause non-uniformity of emission velocity across the cathode area resulting in increased beam noise. It is found generally that the more smooth and homogeneous the cathode surface the less noisy the beam is. A sharply defined cathode edge is also important for low noise. The improvement of the cathode emission properties is mainly a technological problem of evolving better cathode materials and application techniques.

c) Beam-transmission defects.

Beam noisiness is increased if the beam is allowed to intercept any structures, e.g. electrodes, or to collide with residual gas molecules. Interception can be eliminated by careful design, by working to close tolerances and by using a

strong magnetic focusing field. To avoid appreciable residual gas it is essential that the tube should have a high vacuum.

d) Secondary-emission noise

Noise may be caused by secondary electrons emitted when the primary electrons intercept some part of the structure, usually the collector. This noise can be minimized by suitable design of the collector, such as by applying a transverse electric field to trap the secondary electrons.

e) Ion-oscillation noise

Noise caused by plasma oscillations of ions in the electron beam is of a relatively low frequency but could cause unwanted modulation of the gain of the tube. To avoid this type of noise the formation of an ion trap in the beam must be avoided.

The last four sources of noise listed above can be reduced to negligible levels by suitable tube design and careful construction, by using a strong uniform magnetic focusing field and by providing a high vacuum. The most important cause of beam noisiness, and the factor which limits the attainable noise figure, is therefore random electron emission at the cathode. The design of a low-noise tube is mainly a problem of minimizing electron-emission noise by the design of a suitable low-noise electron gun. It is the

investigation of the characteristics and performance of such a gun that is the subject of the research project reported here.

## 2. BASIC THEORY

### 2.1 Development of Noise Theory

The analysis of noise propagation along single-velocity electron beams was developed by a number of authors[1-7] in the period 1954-5. This work led to an expression for the minimum noise figure of the t.w.t. and b.w.a. This theory is summarized below, the notation being that of Haus.[8]

### 2.2 Assumptions

Provided that certain assumptions are made, the propagation of noise along electron beams is well understood. The assumptions are that:

a) Electron flow is in the axial direction only and only one co-ordinate is used in the analysis (one-dimensional assumption).

b) Time-varying quantities are small compared with corresponding time-average quantities (small-signal assumption).

c) All the electrons passing any beam cross-section have the same velocity (single-velocity assumption).

These assumptions are believed to be applicable all along the beam except in the cathode-potential minimum region where the spread in electron velocities is not small compared with the average velocity. Where they are not applicable the analysis is extremely complex.

### 2.3 Signal Propagation along Electron Beams

In order to analyse the propagation of noise along an

electron beam it is best to consider first the propagation of a signal of discrete frequency.

The basic equations used in the analysis are as follows:

(a) Maxwell's equations:

$$\text{curl } \vec{E}(\vec{r},t) = -\mu_o \frac{\partial}{\partial t}\vec{H}(\vec{r},t) \qquad (2.1)$$

where $\vec{E}$ = electric field

$\mu_o$ = permeability of free space

$\vec{H}$ = magnetic field

$\vec{r}$ = radius vector

$t$ = time

($\vec{\ }$ denotes a vector quantity)

$$\text{and curl } \vec{H}(\vec{r},t) = J(\vec{r},t) + \epsilon_o \frac{\partial}{\partial t}\vec{E}(\vec{r},t) \qquad (2.2)$$

where $J$ = current density

$\epsilon_o$ = permittivity of free space

(b) Assuming a totally z-directed (axial) electron velocity, the force equation gives:

$$\frac{\partial v(\vec{r},t)}{\partial t} + v(\vec{r},t)\frac{\partial v(\vec{r},t)}{\partial z} = \frac{e}{m}E_z(\vec{r},t) \qquad (2.3)$$

where $v$ = electron velocity

$\frac{e}{m}$ = electron charge/mass ratio

(c) Under the same assumption the continuity equation gives:

$$\frac{\partial}{\partial z}J(\vec{r},t) = -\frac{\partial}{\partial t}\rho(\vec{r},t) \qquad (2.4)$$

where $\rho$ = charge density

(d) Under the single-velocity assumption:

$$J(\vec{r},t) = v(\vec{r},t)\rho(\vec{r},t) \qquad (2.5)$$

(e) From Gauss's law:

$$\text{div } \vec{E}(\vec{r},t) = \frac{\rho(\vec{r},t)}{\epsilon_o} \qquad (2.6)$$

The small-signal assumption allows the electric and magnetic fields, the charge and current densities and the electron velocity to be split into time-average and very much smaller time-varying parts, i.e.:

$$\vec{E}(\vec{r},t) = E_o(\vec{r}) + E(\vec{r})\cos\omega t \qquad (2.7)$$

$$\vec{H}(\vec{r},t) = H_o(\vec{r}) + H(\vec{r})\cos\omega t \qquad (2.8)$$

$$\rho(\vec{r},t) = \rho_o(\vec{r}) + \rho(\vec{r})\cos\omega t \qquad (2.9)$$

$$J(\vec{r},t) = J_o(\vec{r}) + J(\vec{r})\cos\omega t \qquad (2.10)$$

$$v(\vec{r},t) = u(\vec{r}) + v(\vec{r})\cos\omega t \qquad (2.11)$$

where $\omega = 2\pi$ x signal frequency

For simplicity these equations are solved first for an infinite-parallel-plane beam, where the time-average current density, velocity and charge density are constant in the x and y directions. As the beam is confined to the z-direction (e.g. by an infinite magnetic field) the $E_x$ and $E_y$ fields do not affect the beam. Making these assumptions the space-charge equations are obtained:

$$j\omega v + \frac{d}{dz}(uv) = -\frac{e}{m}\frac{1}{j\omega\epsilon_o}J \qquad (2.12)$$

$$j\omega J + u\frac{d}{dz}J = j\omega\rho_o v \qquad (2.13)$$

To simplify these equations the following parameters are introduced:

Kinetic voltage modulation $V = \frac{m}{e}uv$ (2.14)

D.C. voltage $V_o = \frac{1}{2}\frac{m}{e}u^2$ (2.15)

Electronic propagation 'constant' $\beta_e = \frac{\omega}{u}$ (2.16)

Plasma propagation 'constant' $\beta_p = \frac{1}{u}\left[\frac{e\rho_o}{m\epsilon_o}\right]^{\frac{1}{2}}$ (2.17)

Equations 2.12 and 2.13 become:

$$\left[j\beta_e + \frac{d}{dz}\right]V = j\beta_p{}^2\frac{2V_o}{\beta_e J_o}J \qquad (2.18)$$

$$\left[j\beta_e + \frac{d}{dz}\right]J = j\frac{\beta_e J_o}{2V_o}V \qquad (2.19)$$

Considering a thin beam (radius $< \frac{1}{\beta_e}$), an infinite number of space-charge modes exist but only the lowest order mode couples strongly to the slow-wave structure. For this reason a similar analysis to that worked out for the infinite-parallel-plane beam can be applied to a thin beam. The only difference is that a modified plasma propagation constant $\beta_q$ is used related to $\beta_p$ by:

$$\beta_q = p\beta_p \qquad (2.20)$$

where p is the plasma-frequency reduction factor, the value of which depends on various beam operating conditions. Details for calculating p are given by Branch and Mihran[9].

The modified versions of equations 2.18 and 2.19 are thus:

$$\left[j\beta_e + \frac{d}{dz}\right]V = j\beta_q{}^2\frac{2V_o}{\beta_e I_o}i \qquad (2.21)$$

$$\left[j\beta_e + \frac{d}{dz}\right]i = j\frac{\beta_e I_o}{2V_o}V \qquad (2.22)$$

where i = a.c. current modulation

$I_o$ = d.c. current

In order to solve equations 2.21 and 2.22 the following parameters are introduced:

Beam characteristic impedance $W = \frac{2V_o}{I_o}\frac{\beta_q}{\beta_e}$ (2.23)

Plasma transit angle $\phi = \int_0^z \beta_q dz$ (2.24)

and $\theta = \int_0^z \beta_e dz$ (2.25)

Equations 2.21 and 2.22 now transform to:

$$\frac{d}{d\phi}\left[Ve^{j\theta}\right] = jW\left[ie^{j\theta}\right] \qquad (2.26)$$

$$\frac{d}{d\phi}\left[ie^{j\theta}\right] = \frac{j}{W}\left[Ve^{j\theta}\right] \qquad (2.27)$$

Separating the variables we get the following equations relating a.c. voltage and current

$$\frac{d^2}{d\phi^2}\left[Ve^{j\theta}\right] - \frac{1}{W}\frac{dW}{d\phi}\frac{d}{d\phi}\left[Ve^{j\theta}\right] + \left[Ve^{j\theta}\right] = 0 \qquad (2.28)$$

$$\frac{d^2}{d\phi^2}\left[ie^{j\theta}\right] + \frac{1}{W}\frac{dW}{d\phi}\frac{d}{d\phi}\left[ie^{j\theta}\right] + \left[ie^{j\theta}\right] = 0 \qquad (2.29)$$

## 2.4 Lossless Beam Transducers

Equations 2.26 and 2.27 are analagous to lossless tapered transmission line equations. The r.f. power on such a line, and the r.f. beam power, is given by:

$$P = \tfrac{1}{2}\mathrm{Re}(Vi^{*}) \qquad (2.30)$$

($^{*}$ denotes the complex conjugate of a complex quantity)

From equations 2.26 and 2.27 it can be proved that $\frac{dP}{d\phi} = 0$ and $\frac{dP}{dW} = 0$ showing that the r.f. power in the beam remains constant with change of plasma transit angle (i.e. with distance along the beam) and with change of beam impedance brought about by changing the d.c. voltage or cross-sectional area of the beam. Because of this conservation of r.f. power any region in which the beam impedance is made to change with variation of plasma transit angle is known as a lossless transducer.

Assuming that the electron flow is maintained parallel to the beam axis by means of a large axial magnetic field, the beam impedance W is altered in a lossless transducer by changing the beam voltage $V_o$

using a series of electrodes at various potentials (W is proportional to $V_o^{\frac{3}{4}}$). The way in which the impedance transformation is brought about is characterized by the relationship between W and $\phi$. This is controlled in practice by the choice of electrode spacing and potentials.

Three fundamental types of lossless transducer which give fairly simple solutions to equations 2.28 and 2.29 are:

(a) A drift region where W is constant.

(b) An exponential transformer where $W = W_1 e^{k\phi}$

($W_1$ and k are constant).

(c) A Bessel transformer where $W = W_2 \phi^n$

($W_2$ and n are constant).

The exponential and Bessel transformers offer no practical advantage over other ways of transforming impedance. They do have the advantage, however, of giving exact solutions to equations 2.28 and 2.29. For this reason they are used as a basis for the design of impedance transforming sections of low-noise electron guns.

The drift region is the simplest type of transducer. No change of impedance takes place along the beam which is allowed to drift at constant potential. The solutions of equations 2.28 and 2.29 with $\frac{dW}{d\phi} = 0$ are particularly simple:

$$V = \left[V_1 e^{j\beta_q z} + V_2 e^{-j\beta_q z}\right] e^{-j\beta_e z} \qquad (2.31)$$

$$i = \frac{1}{W}\left[V_1 e^{j\beta_q z} - V_2 e^{-j\beta_q z}\right] e^{-j\beta_e z} \qquad (2.32)$$

These equations indicate the existence of two waves in the beam, a 'fast wave' with a propagation constant of $(\beta_e - \beta_q)$ and a 'slow wave' with a propagation constant of $(\beta_e + \beta_q)$. The phase velocities differ from the electron velocity by factors of $\frac{\beta_e}{\beta_e - \beta_q}$ and $\frac{\beta_e}{\beta_e + \beta_q}$ respectively. As $\beta_q$ is independent of W, the group velocity of both waves is equal to the electron velocity.

## 2.5 Analysis of Noise

The theory so far is for signals of discrete frequency. In order to apply it to noise quantities it is necessary to express the noise in terms of frequency-dependent voltage and current modulation.

The magnitude of the noise at any point along the electron beam is given by the time-dependent voltage and current modulation V(t) and i(t) which are non-periodic, noise being a random process. A Fourier integral cannot be formed for a function over an infinite time interval, hence the funtion $V_T(t)$ shown in fig.2.1 is considered.

By letting $T \to \infty$, the Fourier integral:

$$V_T(t) = \int_{-\infty}^{\infty} V_T(\omega) e^{j\omega t} dt \qquad (2.33)$$

is obtained,

and the corresponding Fourier transform is:

$$V_T(\omega) = \frac{1}{2\pi}\int_{-\infty}^{\infty} V_T(t)e^{-j\omega t}dt \qquad (2.34)$$

similarly:

$$i_T(\omega) = \frac{1}{2\pi}\int_{-\infty}^{\infty} i_T(t)e^{-j\omega t}dt \qquad (2.35)$$

$V_T(t) = 0$ if $T < t$ or $t < -T$

$V_T(t) = V(t)$ if $-T < t < T$

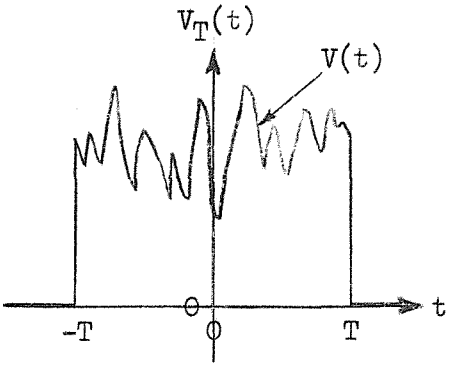


FIG. 2.1

As T is allowed to go to infinity $V_T(t)$ and $i_T(t)$ represent the random functions V(t) and i(t). The Fourier transforms thus give the frequency-dependent voltage and current modulations $V_T(\omega)$ and $i_T(\omega)$ in terms of the time-dependent modulation V(t) and i(t).

The theory of signal propagation can now be applied to noise using the quantities $V_T(\omega)$ and $i_T(\omega)$. Just as a signal on a beam in a drift region consists of a fast and

slow wave, so fast and slow noise waves can exist, one of each for each of the infinite number of frequencies in the bandwidth under consideration. There are thus an infinite number of waves, all with differing propagation constants. However, if noise at a single frequency only could be observed, just one fast and one slow wave would be found.

In common with other linear, passive networks the relationship between current and voltage modulation at any point along a beam undergoing a lossless transformation is linear. Considering any two cross-sections of the beam at a and b on the beam axis, the frequency-dependent noise modulations are related by the following matrix equation:

$$\underline{w_{bT}}(\omega) = \underline{K}\ \underline{w_{aT}}(\omega) \tag{2.36}$$

where $$\underline{w_{aT}}(\omega) = \begin{bmatrix} V_{aT}(\omega) \\ i_{aT}(\omega) \end{bmatrix} \tag{2.37}$$

and $$\underline{w_{bT}}(\omega) = \begin{bmatrix} V_{bT}(\omega) \\ i_{bT}(\omega) \end{bmatrix} \tag{2.38}$$

(_ denotes a matrix quantity)

In order to satisfy the condition of conservation of power, the 2 x 2 matrix $\underline{K}$ must satisfy the equation:

$$\underline{K}^{+} = \underline{R}\ \underline{K}^{-1}\ \underline{R} \tag{2.39}$$

where $$R = \begin{bmatrix} 0 & 1 \\ 1 & 0 \end{bmatrix} \tag{2.40}$$

($^{+}$ denotes the Hermitian conjugate and $^{-1}$ the inverse)

By definition let:

$$\Phi(\omega) = \lim_{T\to\infty} \frac{\pi}{T} \overline{\left|V_T(\omega)\right|^2} \qquad (2.41)$$

= self power density spectrum of the noise voltage modulation.

$$\Psi(\omega) = \lim_{T\to\infty} \frac{\pi}{T} \overline{\left|i_T(\omega)\right|^2} \qquad (2.42)$$

= self power density spectrum of the noise current modulation.

$$\Theta(\omega) = \lim_{T\to\infty} \frac{\pi}{T} \overline{V_T(\omega) i_T(\omega)^*} \qquad (2.43)$$

= cross power density spectrum between noise voltage and current modulations.

($\bar{}$ signifies an ensemble average)

Then $$\lim_{T\to\infty} \frac{\pi}{T} \overline{\underline{w}_T(\omega)\underline{w}_T(\omega)^+} = \begin{bmatrix} \Phi & \Theta \\ \Theta^* & \Psi \end{bmatrix} = \underline{W} \qquad (2.44)$$

and from equations 2.36 and 2.39 the relationship between the $\underline{W}$ matrix at a and b when the beam passes through a lossless transducer is:

$$\underline{W}_b \, \underline{R} = \underline{K} \, \underline{W}_a \, \underline{R} \, \underline{K}^{-1} \qquad (2.45)$$

Equation 2.45 shows that the trace and determinant of the matrix $\underline{W}\,\underline{R} = \begin{bmatrix} \Theta & \Phi \\ \Psi & \Theta^* \end{bmatrix}$ remain constant when the beam

undergoes a lossless transformation.

Let $\quad \mathrm{Re}\,\Theta = \Pi \qquad (2.46)$

$\quad \mathrm{Im}\,\Theta = \Lambda \qquad (2.47)$

and $(\Phi\Psi - \Lambda^2)^{\frac{1}{2}} = S \qquad (2.48)$

Then the trace of $\underline{W}\,\underline{R}$ is $2\Pi$ and the determinant is $\Pi^2 - S^2$.

S and $\Pi$ are thus two quantities which remain constant throughout any lossless transformation.

## 2.6 Minimum Noise Figure of a Microwave Amplifier

To carry out calculations for an amplifier as a whole it is more convenient to work with wave amplitudes instead of current and voltage modulation. The amplitudes of the fast and slow noise voltage waves in a drift region (see equations 2.31 and 2.32), normalized by multiplying by $\frac{1}{2W}$ are used.

At a point a on the beam the relationship between the normalized noise wave amplitudes and the voltage and current modulation is given by equations 2.31 and 2.32 as:

$$\underline{a_T}(\omega) = \underline{T_a}\ \underline{w_{aT}}(\omega) \qquad (2.49)$$

where $$\underline{a_T}(\omega) = \begin{bmatrix} a_{1T}(\omega) \\ a_{2T}(\omega) \end{bmatrix} \qquad (2.50)$$

and $$\underline{T_a} = \frac{1}{2\sqrt{2W_a}} \begin{bmatrix} 1 & W_a \\ -1 & W_a \end{bmatrix} \qquad (2.51)$$

A similar relationship exists at point b.

Defining the 2 x 2 matrix:

$$\underline{A} = \lim_{T\to\infty} \frac{2\pi}{T} \underline{a_T(\omega)}\, \underline{a_T(\omega)^+} \qquad (2.52)$$

From equations 2.44 and 2.49:

$$\underline{A} = 2\, \underline{T_a}\, \underline{W_a}\, \underline{T^+} \qquad (2.53)$$

giving the following relationships between the elements of the $\underline{A}$ and $\underline{W_a}$ matrices:

$$A_{11} = \tfrac{1}{4}\left[\frac{\Phi}{W} + W\Psi + 2\Pi\right] \qquad (2.54)$$

$$A_{12} = A_{21}^{*} = \tfrac{1}{4}\left[-\frac{\Phi}{W} + W\Psi + 2jA\right] \qquad (2.55)$$

$$A_{22} = \tfrac{1}{4}\left[\frac{\Phi}{W} + W\Psi - 2\Pi\right] \qquad (2.56)$$

From which the invariants S and $\Pi$ are given by:

$$S = \left[(A_{11} + A_{22})^2 - 4|A_{12}|^2\right]^{\frac{1}{2}} \qquad (2.57)$$

$$\Pi = A_{11} - A_{22} \qquad (2.58)$$

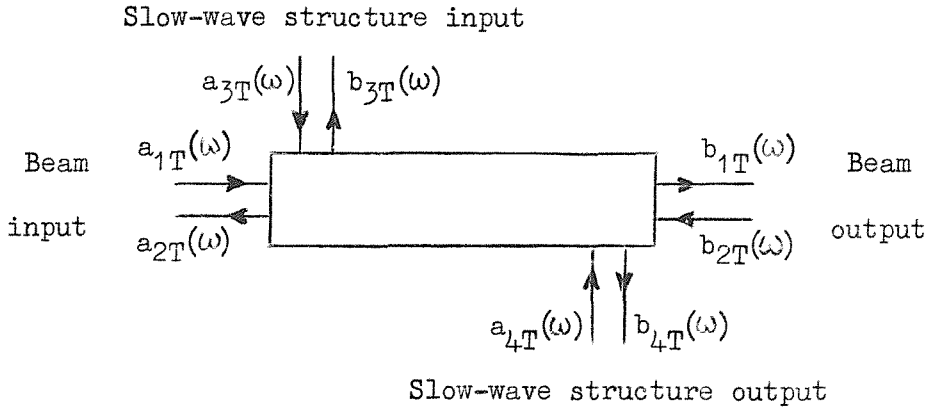


FIG. 2.2

Consider a beam-type microwave amplifier as shown in fig.2.2. The normalized amplitudes of the fast and slow noise waves on the beam are $a_{1T}(\omega)$ and $a_{2T}(\omega)$ at the input to the slow-wave structure, and $b_{1T}(\omega)$ and $b_{2T}(\omega)$ at the output. Similarly the incident and reflected noise waves at the amplifier input and output are $a_{3T}(\omega)$ and $b_{3T}(\omega)$, $a_{4T}(\omega)$ and $b_{4T}(\omega)$.

Under the small-signal assumption the relationships between the a's and b's is linear and can be represented in matrix form by:

$$\underline{b_T}(\omega) = \underline{G}\ \underline{a_T}(\omega) \tag{2.59}$$

where $$\underline{a_T}(\omega) = \begin{bmatrix} a_{1T}(\omega) \\ a_{2T}(\omega) \\ a_{3T}(\omega) \\ a_{4T}(\omega) \end{bmatrix} \tag{2.60}$$

and $$\underline{b_T}(\omega) = \begin{bmatrix} b_{1T}(\omega) \\ b_{2T}(\omega) \\ b_{3T}(\omega) \\ b_{4T}(\omega) \end{bmatrix} \tag{2.61}$$

It can be shown that if the amplifier is lossless, $\underline{G}$ must satisfy the condition:

$$\underline{G}\ \underline{P}\ \underline{G}^{+} = \underline{P} \tag{2.62}$$

where $P = \begin{bmatrix} 1 & 0 & 0 & 0 \\ 0 & -1 & 0 & 0 \\ 0 & 0 & 1 & 0 \\ 0 & 0 & 0 & 1 \end{bmatrix}$ (2.63)

Assuming that the amplifier input and output are matched to the source and the load respectively, $b_{3T}(\omega) = 0$ and $a_{4T}(\omega) = 0$.

Then the noise at the amplifier output produced by the beam noise within the narrow frequency band $\Delta f$ is:

$$N_i = \lim_{T\to\infty} \frac{2\pi}{T} \overline{\left[G_{41}a_{1T}(\omega) + G_{42}a_{2T}(\omega)\right]\left[G_{41}a_{1T}(\omega) + G_{42}a_{2T}(\omega)\right]^*} \times 4\pi\Delta f$$

$$= 4\pi\Delta f \left[|G_{41}|^2 A_{11} + |G_{42}|^2 A_{22} + G_{41}G_{42}^* A_{12} + G_{41}^* G_{42} A_{21}\right]$$

from equation 2.52.

$$= 4\pi\Delta f \Big[ \left(|G_{41}|^2 + |G_{42}|^2\right)\left(W_a\Psi_a + \frac{\Phi_a}{W_a}\right) + \left(G_{41}G_{42}^* + G_{41}^*G_{42}\right)\left(W_a\Psi_a - \frac{\Phi_a}{W_a}\right) + 2\left(|G_{41}|^2 - |G_{42}|^2\right)\Pi + 2\left(G_{41}G_{42}^* - G_{41}^*G_{42}\right)\left(\Phi\Psi - S^2\right)^{\frac{1}{2}} \Big]$$ (2.64)

from equations 2.46 - 2.48 and 2.54 - 2.56.

The noise at the amplifier output produced by the input circuit is:

$$N_o = \lim_{T\to\infty} \frac{2\pi}{T} \overline{\left[G_{43}a_{3T}(\omega)\right]\left[G_{43}a_{3T}(\omega)\right]^*} 4\pi\Delta f$$ (2.65)

According to Nyquist[10] the power at the amplifier input within the frequency band $\Delta f$ is:

$$\lim_{T\to\infty}\frac{2\pi}{T}\overline{a_{3T}(\omega)a_{3T}(\omega)^{*}}4\pi\Delta f = kT\Delta f \qquad (2.66)$$

where k = Boltzmann's constant

T = input circuit temperature

$$\text{Hence } N_o = |G_{43}|^2 kT\Delta f \qquad (2.67)$$

The noise figure of the amplifier is given by:

$$F = 1 + \frac{N_i}{N_o} \qquad (2.68)$$

Assuming a fixed input circuit temperature, $N_o$ is constant. The noise figure is minimized by adjusting the beam parameters $W_a\Psi_a$ and $\frac{\Phi_a}{W_a}$ at the slow-wave structure input to give as low a value as possible for $N_i$. This is achieved in practice by adjusting the gun electrode voltages and also possibly the length of the drift space between the final anode of the gun and the slow-wave structure. For conservation of power, S and $\Pi$ remain constant.

For minimum $N_i$ it is found that:

$$W_a\Psi_a = \left|\frac{|G_{41} - G_{42}|^2}{|G_{41}|^2 - |G_{42}|^2}\right| S \qquad (2.69)$$

$$\frac{\Phi_a}{W_a} = \left|\frac{|G_{41} + G_{42}|^2}{|G_{41}|^2 - |G_{42}|^2}\right| S \qquad (2.70)$$

From equations 2.64 and 2.67 - 2.70 the minimum noise figure:

$$F_{min} = 1 + \frac{2\pi}{kT}\frac{1}{|G_{43}|^2}\left[\left|\,|G_{41}|^2 - |G_{42}|^2\right|S + (|G_{41}|^2 - |G_{42}|^2)\Pi\right] \qquad (2.72)$$

where $|G_{43}|^2$ is the power gain of the amplifier and $G_{44}$ is the output reflection coefficient.

The maximum available power gain G is obtained when the output reflection coefficient is zero, i.e. from equation 2.72:

$$|G_{41}|^2 - |G_{42}|^2 = 1 - G \qquad (2.73)$$

Substituting equation 2.73 into 2.71:

$$F_{min} = 1 + \frac{2\pi}{kT}(1 - \frac{1}{G})(S - \Pi) \qquad (2.74)$$

Equation 2.74 gives the lowest possible noise figure for a t.w.t. or b.w.a.. It is achieved by:

a) Matching the amplifier input and output to the source and load respectively

b) Optimizing the beam operating conditions at the slow-wave structure input by the correct adjustment of the voltages on the transducer section of the electron gun.

The only beam parameters appearing in the expression for $F_{min}$ are S and $\Pi$. These remain constant when the beam is subjected to any lossless transformation, provided that the conditions stated in section 2.2 apply. These conditions

can be assumed to apply along the beam from a point just beyond the potential minimum where the beam has been accelerated to a potential of a few volts. From the cathode to this point the velocity spread is comparable with the mean velocity. Here the single-velocity assumption can no longer be made and S and $\Pi$ do not necessarily remain constant. The best noise figure is thus a function only of the processes in the multi-velocity region which determine S and $\Pi$ at the input to the single-velocity region. The nature of these processes is obviously of prime importance and has been the subject of much of the published work on low-noise t.w.t's and b.w.a's. Mathematical analysis of multi-velocity flow is difficult, often involving computer calculations, and no complete theory has yet been put forward. Encouraging practical results have been obtained recently, however, using an extended low-velocity region immediately in front of the cathode. This appears to bring about a considerable reduction in the value $(S - \Pi)$.

## 3. REVIEW OF PUBLISHED WORK

### 3.1 Early Work

The earliest measured t.w.t. noise figure was 11dB reported by Kompfner[11] in 1947. By 1952 8.2dB had been achieved by Peter[12].

Soon afterwards the theory presented in chapter 2 was developed. However, considerable doubt still remained as to the processes which determined S and $\Pi$ in the multi-velocity region.

A number of authors[1-5,7,8] obtained a value for $F_{min}$ by taking the potential minimum which occurs in space-charge limited flow as the reference plane after which single-velocity flow could be assumed. To evaluate S and $\Pi$ at that plane the following assumptions were made:

a) The noise current corresponded to full shot noise[13],

i.e. $\overline{i^2} = \Psi 4\pi\Delta f = 2ei\Delta f$

hence $\Psi = \frac{eI}{2\pi}$ (3.1)

b) The velocity modulation was that given by Rack[14],

i.e. $\overline{v^2} = \frac{\Phi 4\pi\Delta f e^2}{(mu)^2} = \frac{e\Delta f kT_c}{mI}(4 - \pi)$

where $u = \left[\frac{2kT_c}{m}\right]^{\frac{1}{2}}$ = average electron velocity at the reference plane.

and $T_c$ = cathode temperature.

hence $\Phi = \frac{k^2 T_c^2}{2\pi eI}(4 - \pi)$ (3.2)

c) The current and velocity fluctuations were uncorrelated,

i.e. $\Lambda = \Pi = 0$ (3.3)

From equations 2.48 and 3.1-3.3:

$$S = (\Phi\Psi)^{\frac{1}{2}} = (4 - \pi)^{\frac{1}{2}}\frac{kT_c}{2\pi} \qquad (3.4)$$

Substituting equation 3.4 into 2.74:

$$F_{min} = 1 + (1 - \frac{1}{G})(4 - \pi)^{\frac{1}{2}}\frac{T_c}{T} \qquad (3.5)$$

Substituting typical values into equation 3.5:

gain $G \gg 1$

cathode temperature $T_c = 1200^{o}K$

input temperature $T = 300^{o}K$

$F_{min} = 4.4$ or $6.4dB$

The most dubious assumption made in this calculation was the use of full shot noise at the input to the single-velocity region. It is well known that at low frequencies the potential minimum has a smoothing effect on the noise current. It seemed likely that a similar effect could occur at high frequencies although no simple analysis was available.

The disadvantage of having to make rather severe assumptions in order to obtain an analytical solution was overcome by Tien and Moshman[15,16] by a 'Monte Carlo' calculation. They carried out a computer analysis using random numbers to simulate the rate, time and velocity of electron emission. Numerical integration was used to trace

the individual electrons through the multi-velocity region of a typical space-charge-limited diode. They found that the potential minimum affected only the noise current modulation. This varied considerably with frequency, the corresponding minimum noise figure varying between about 1.5dB at 2.5kMc/s to 7.5dB at 4kMc/s. At very high frequencies the noise current approached the full-shot-noise value.

An approximate analysis of a high-frequency diode under space-charge-limited conditions was carried out by Siegman and Watkins[17]. They calculated the response of the potential minimum to a fluctuation in time of the cathode emission. Assuming full shot noise at the cathode, the noise at the potential minimum was found to be reduced at high frequencies. At lower frequencies (about 0.7 times the plasma frequency), and at high degrees of space-charge limitation, a maximum greater than shot noise was predicted similar to that found by Tien and Moshamn.

Siegman, Watkins and Hsieh[18] used a 'density function' method[19] of analysing propagation through a multi-velocity region. This method also employed numerical integration. They assumed full uncorrelated shot noise at the potential minimum. The multi-velocity flow beyond that point resulted in a lowering of S by a factor of 0.7, and an increase of $\Pi$ to above 0.3 times the initial value of S.

The minimum noise figure was thus about $3\frac{1}{2}$dB, compared with $6\frac{1}{2}$dB if S and $\Pi$ had remained constant.

3.2 The Currie Gun

In 1958 it was proved that noise figures considerably lower than $6\frac{1}{2}$dB could, in fact, be attained when Currie and Forster[20,21] reported a figure of 3.7dB for a b.w.a. Since then further improvements have been made,[22-27] the best figure being 1dB reported by Hammer and Thomas[27] for a liquid-nitrogen cooled tube.

Fig.3.1 shows the electrode arrangement of the original Currie gun. An annular cathode was used, producing an annular beam. Similar results have been obtained using a conventional button cathode and a solid cylindrical beam[23-26]. The electrode arrangement was somewhat similar to that of Peter's electron gun[12], a control electrode being used near the cathode. However, whereas Peter used a negative control electrode, Currie operated his gun with the control electrode positive with respect to the cathode. The resulting potential profile allowed the electrons to drift at a low velocity before reaching the potential minimum. The electrons were prevented from moving sideways by immersing the gun in a strong axial magnetic field (up to 0.16Wb/$m^2$).

Keeping the average beam current constant by adjusting anode 1 voltage and the control electrode voltage, Currie and Forster[22] observed a fairly sharp minimum in the noise figure.

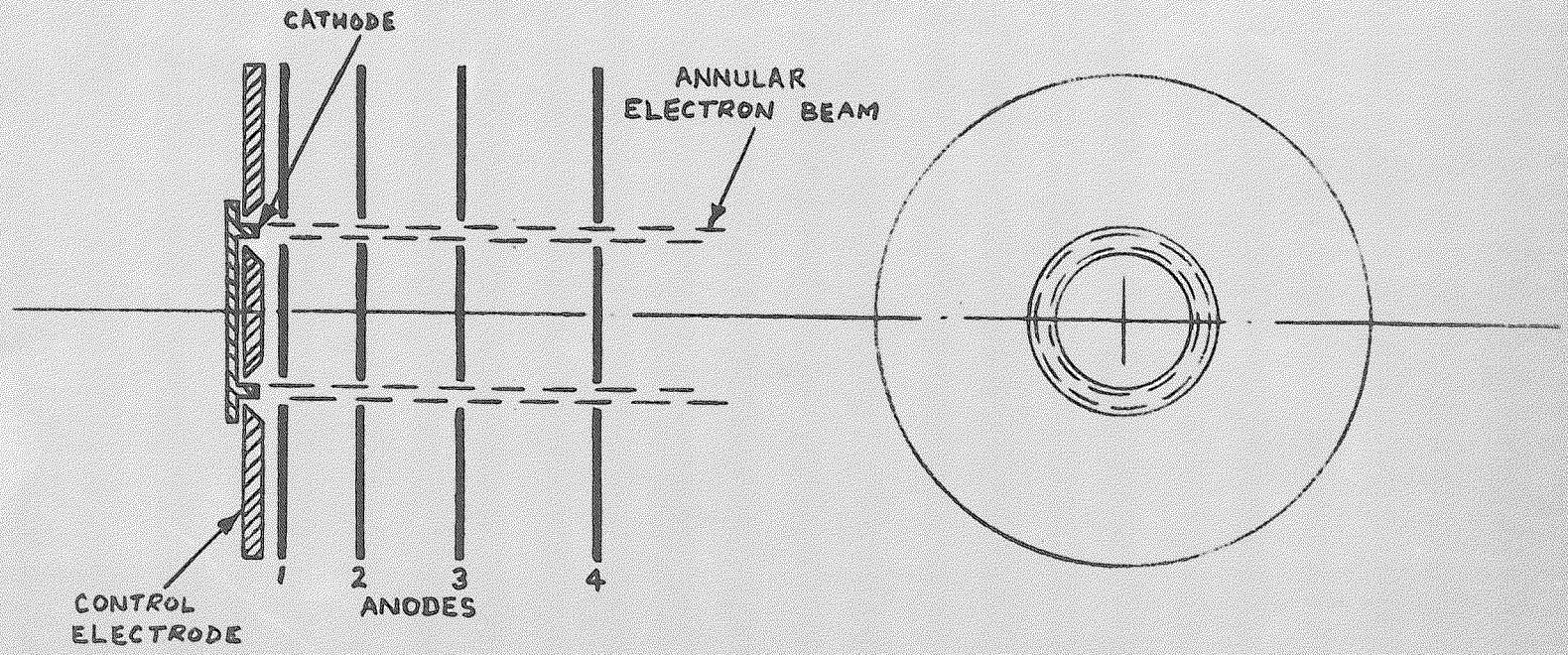


FIG.3.1 ELECTRODE ARRANGEMENT OF ELECTRON GUN

As the control electrode voltage was increased the beam, as observed on a fluorescent screen, was found to split up from a solid annulus to two concentric beams. The minimum noise figure occurred when the beam had just started to split up. The minimum noise figure also coincided with an abrupt change of slope of the anode 1 against control electrode voltage characteristic. Berghammer[28] attributed this change of slope to the '6L6 effect'* - a sudden drop and then limitation of the beam current as the current injected into the anode 1-2 region was increased by increasing the control electrode voltage. This limitation was due to the formation of a virtual cathode in the anode 1-2 region - a potential minimum of zero potential where some electrons entering the region were truned back and others passed through, according to their velocity.

Hysteresis in the beam current as the control electrode was altered was predicted by the one-dimensional analysis of virtual cathode formation by Salzberg and Haeff[29]. No such hysteresis was observed by Berghammer[28] in tests with a low-noise electron gun. Using a similar gun in later experiments, Eichenbaum and Hammer[30] were able to induce hystersis under certain conditions and believed it to be dependent on the trapping of positive ions. They also observed changes in

* So-called because it was first observed in the grid-anode region of a 6L6 beam power tube.

the electron beam profile on formation of the virtual cathode using a pinhole analyser.

It seems that there are two main features of the Currie gun which affect the beam noisiness:

a) The unique potential profile produced by the positive control electrode. This allows the electrons leaving the cathode to drift at a low velocity for a relatively long distance before they are accelerated.

b) The formation of a virtual cathode with the accompanying changes in d.c. beam current characteristics and beam profiles.

Measurements by various workers have shed some light on the way the beam noisiness is changed by these effects. Currie and Forster[22] found that as the control electrode voltage was increased (keeping the beam current constant by altering anode 1 voltage) the noise figure passed through a minimum which coincided with the formation of a virtual cathode. Zacharius and Smullin[31] used the double-cavity apparatus developed by Saito[32] to measure independently the beam parameters S and $\Pi/S$ for a Currie-type low-noise gun. They observed a similar minimum in the quantitity $S-\Pi$ (proportional to noise figure). They found that it was caused almost entirely by a change of S, $\Pi$ remaining negligibly small. Mueller[33] observed a rather different effect. He found that when the control electrode voltage

was increased (keeping all other voltages constant) a sudden drop in noise figure of up to 2dB took place. This drop corresponded to the decrease in beam current due to the formation of a virtual cathode. He also measured hysteresis in the noise figure corresponding to that in the beam current.

The most revealing measurements on the Currie gun were probably those made by Hammer[34]. He measured $F_{min}$, S and $\Pi$ over a wide range of control electrode voltages using a moving-helix tube. A similar dip in the noise figure to that found by Currie and Forster[22] was observed. The decrease in noise figure when the control electrode voltage was increased from a negative to a positive value was found to be brought about by a considerable increase of $\Pi$ and a slight decrease of S. These changes indicated that in the extended low-velocity region beam noisiness was reduced mainly by positive correlation between velocity and current fluctuations. When the control electrode voltage was further increased so that a virtual cathode formed S increased again but $\Pi$ remained unchanged. The virtual cathode therefore had a detrimental effect on the beam noise.

## 3.3 Theoretical Work on the Currie Gun

Most of the theoretical work on the noise-reducing processes in the Currie gun has been concerned with the effects of the low-velocity drift space. Birdsall and Bridges[35,36]

however, considered the effect of the virtual cathode. They carried out computer calculations on electron flow in a diode into which electrons were injected. When the injected current was sufficient for the formation of a virtual cathode the value and position of the potential mimimum were found to oscillate with large amplitudes. Electrons were thus let through periodically giving rise to a modulated transmitted current with an average value less than the injected current. The frequency of oscillation was near the plasma frequency corresponding to the electron density at the potential minimum. It seemed possible that in an electron gun the fluctuations at a lower frequency of a noisy injected current could be compensated by such an unstable potential minimum, resulting in a less noisy beam. Experiments to detect oscillations of the potential minimum showed these to be very much weaker than expected from the theory.

An analysis by Berghammer[37] took into account the low-velocity drift space and the virtual cathode. He considered a long, finite-diameter electron beam with a velocity spread (assumed rectangular) very much greater than the electron velocity. This condition is approximately satisfied in the region between the cathode and the potential minimum when there are electrons travelling in both directions due to the presence of a virtual cathode. He found that in addition to the usual fast and slow waves (equations 2.31 and 2.32) two reactively-

damped waves existed. One of these corresponded to a reflected wave which was excited only by discontinuities in the propagating medium. It was assumed that only the other wave, which had a decreasing amplitude away from the cathode, was excited by full shot noise. Reactive damping of this wave was found to bring about a considerable reduction of beam noise at frequencies below the plasma frequency.

Mueller and Currie[38] used Siegman's density function method[19] to analyse the change in S and $\Pi$ from the cathode through an extended low-velocity drift region with a linear potential profile (approximately true for a Currie gun). Depending on the slope of the potential profile, S was found to decrease with distance from the cathode and $\Pi$ to increase. The more gradual the slope of the potential profile the more S and $\Pi$ changed and the lower was the beam noise at the input to the single-velocity region. Hence, in theory, considerable noise reduction should be possible by extending the multi-velocity region in order to accelerate the electrons as gradually as possible away from the cathode.

Theoretical work by Berghammer[39] has shown the existence of spatial damping of the fast space-charge wave in a multi-velocity drift region by a process known as 'Landau damping'. Considering a beam with a Maxwellian velocity distribution, the phase mixing of different velocity classes was found to damp the fast space-charge wave. The slow wave remained unaffected. The current modulation thus took the form of a damped

sinusoid and approached a constant level over a distance of several plasma wavelengths. This damping process was observed experimentally by Caulton, Hershenov and Paschke[40] using a movable cavity to measure current modulation on a slowly drifting beam. A similar effect was observed by Mihran[41] who studied beams with velocity spreads of about 10%. It is possible that Landau damping could contribute twoards change of beam noisiness in multi-velocity flow.

3.4 Conclusions

The Currie gun and developments of it have shown that smoothing of high-frequency noise is possible by suitable gun design. The mechanisms which bring about the noise reduction are not yet clearly understood. Most of the evidence, however, points to the extended low-velocity drift region as being the main factor which contributes towards low noise. Practical and theoretical work indicate that both an increase of $\Pi$ from zero at the cathode, and a reduction of S, are brought about in such a region. The minimum obtainable noise figure which is proportional to $S-\Pi$ is thus reduced.

The effects of virtual cathode formation on beam noise are uncertain. In general, however, experimental results seem to indicate that the virtual cathode has a detrimental effect by increasing S, $\Pi$ being unaffected.

## 4. OUTLINE OF RESEARCH PROGRAMME

### 4.1 Objects of Research

The theory of electron-beam noise shows that the noise figure of a beam-type microwave amplifier depends on conditions in the multi-velocity region of the gun immediately in front of the cathode. Currie has shown that very low noise figures can be achieved by careful design of the electron gun. Also optimum adjustment of the electrode voltages is necessary to provide an extended low-velocity region in front of the cathode. The formation of a virtual cathode within the gun, with the accompanying hysterisis effects and changes of beam profile, appears to have an effect on the beam noise.

The objects of the research reported here were to investigate the factors leading to the production of a low-noise electron beam by the Currie gun. In particular the effects of a virtual cathode and changes of beam profile were to be studied.

### 4.2 D.C. Characteristics and Beam Profiles

The structure of the electron beam from a Currie gun has been found to show marked changes as the control electrode voltage is varied[22]. The beam current characteristic shows that a virtual cathode can form within the electron gun[28] and under certain conditions a hysteresis phenomenon has been observed[30].

In order to study these effects in detail two electron

tubes were used. They consisted of an envelope containing a Currie-type gun and a fluorescent screen as the collector. To observe any changes in the beam structure along the beam axis, the collector of the second tube could be moved along the beam axis.

The changes of beam current and its structure were noted for a wide variation of voltages on the control electrode and anodes 1 and 2. Particular attention was paid to the hysteresis effects accompanying the formation of the virtual cathode and to the effects of positive ions.

4.3 Noise Measurement

The beam noise parameters S and $\Pi$ can be measured by passing the beam through either a helix or two cavities. If a helix is used[34], S and $\Pi$ are derived from the maximum and minimum noise figures obtained when the distance between the gun and helix is varied. If cavities are used[32], the signal from one movable cavity is sufficient to measure S. A second movable cavity is required to measure $\Pi$.

Because of the limited facilities for tube construction, it was decided to keep the noise measuring apparatus as simple as possible to start with. A tube with a single cavity to measure S was designed and built, together with a radiometer microwave measuring system. Published work on the measurement of S and $\Pi$[31,34] has shown that the formation of a virtual cathode changes only S. Thus a single cavity

tube should be sufficient to observe the effect of a virtual cathode on beam noise. Up to the time of writing no results have been obtained from this tube.

The design of the S-measuring apparatus was such that it could be fairly easily adapted for the measurement of S and $\Pi$. The modification consists of replacing the single cavity by two cavities. Some addition to the microwave measuring apparatus is also necessary.

# 5. APPARATUS

## 5.1 Auxilary Equipment

In addition to the three electron tubes a considerable amount of auxilary equipment was necessary. This included a high-vacuum system with facilities for baking tubes and for vacuum measurement. A special power supply was necessary for the multi-electrode electron gun. Two solenoids for beam focusing were required together with a cooling system and a high-power current-stabilized power supply. None of this equipment was available commercially except at a prohibitive cost and so it had to be designed and built at the University. This part of the research programme took a little over two years to complete.

## 5.2 Vacuum System

The layout of the high-vacuum system is shown in fig.5.1, and fig.5.2 is a photograph of the system. The components used were as follows:-

| | |
|---|---|
| Backing pump | Metrovac DR1 |
| Magnetic valve | Edwards D11206 |
| Pirani gauge | Pye 11018 |
| Oil diffusion pump | Edwards F203 |
| Cold trap | Edwards NTM28 |
| All-metal valve | Edwards MCV4 |
| Ion gauge | Mullard EIP2 |
| Ion gauge control unit | Edwards Model 1 control unit and Model 1 amplifier |

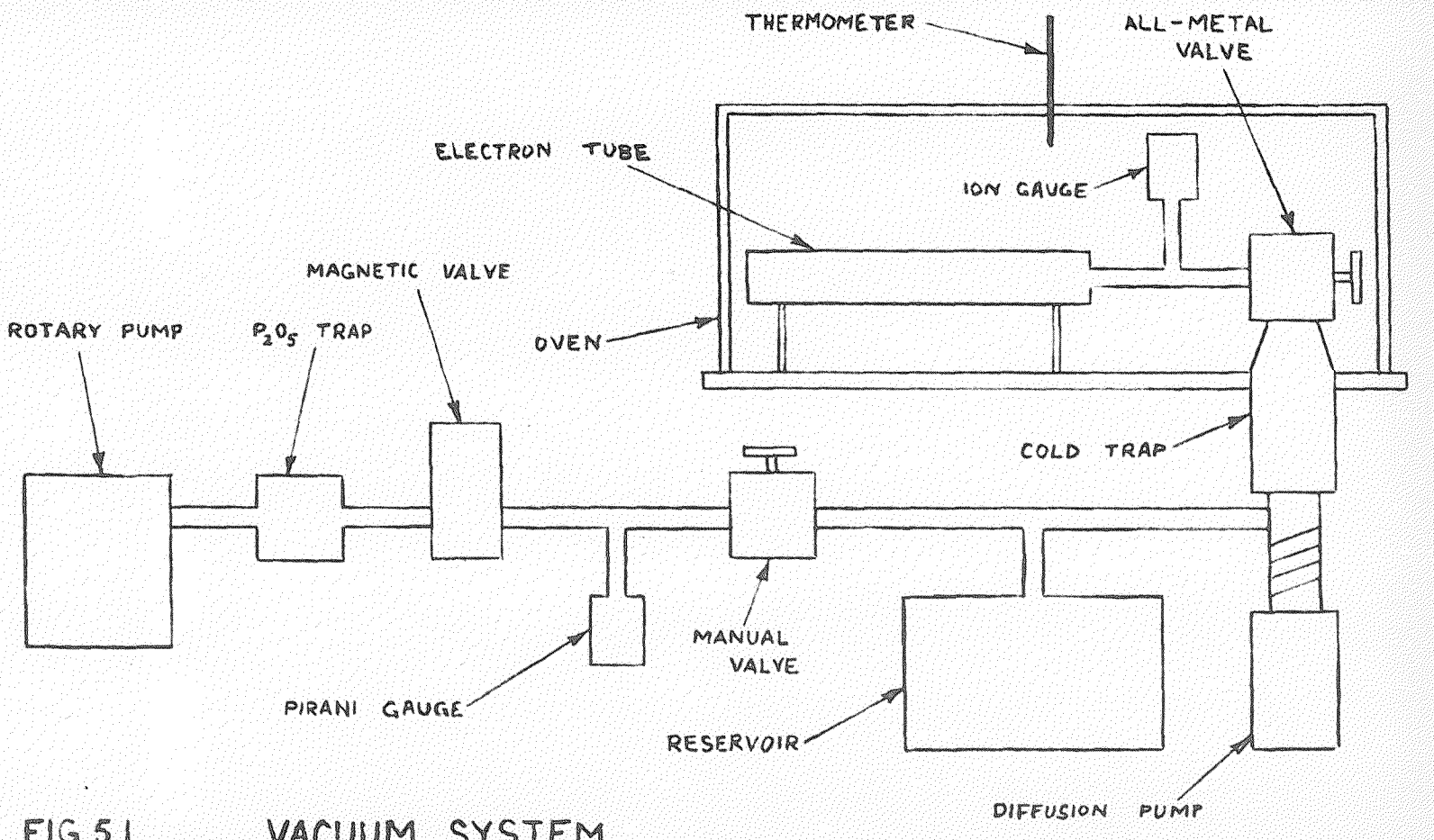


FIG. 5.1 VACUUM SYSTEM

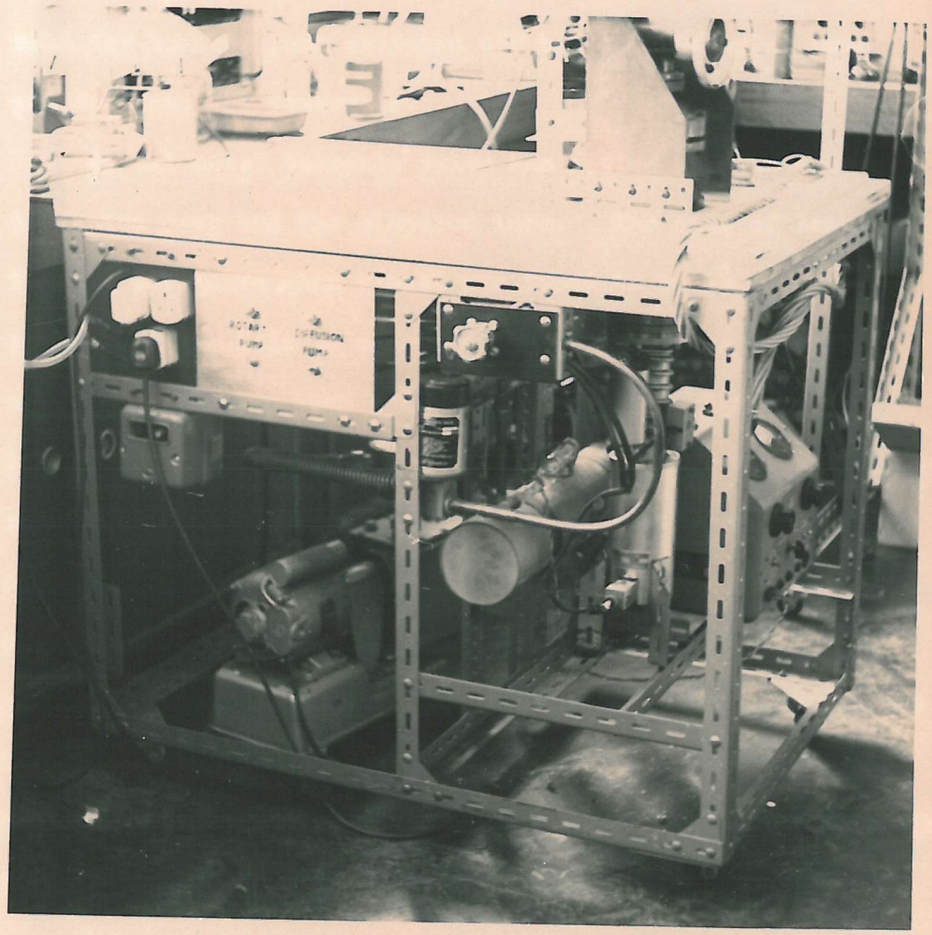

FIG.5.2 VACUUM SYSTEM

A reservoir of about 0.25 cu.ft. capacity, and a manual shut-off valve, were fitted between the pumps. It was possible to run the system for periods of up to a week with the backing pump switched off and the diffusion pump pumping into the reservoir.

An all-metal bakeable valve was fitted between the diffusion pump and the electron tube. The rate of leakage through the valve when closed was found to be so great that it was not possible to maintain a high vacuum in the tube with the diffusion pump switched off as was originally intended. To try and overcome this difficulty the stainless-steel valve seating was replaced by one made of O.F.H.C. copper. However, there was little improvement in the closed conductance.

Vacuum measurement was by means of a Pirani gauge on the backing-pressure side of the system and an ion gauge on the high-vacuum side. Using an Edwards Model 1 ion-current amplifier it was possible to measure pressures down to $10^{-9}$mmHg.

A 6 kw. controlled oven was made which could be lowered over the electron tube, ion gauge, all-metal valve and the top half of the stainless-steel cold trap. The maximum baking temperature was limited by the glass to 450°C. and with liquid nitrogen in the cold trap a vacuum of about $10^{-8}$mmHg could be attained in the electron tube. This figure could be further improved by isolating the electron tube and ion gauge from the

rest of the system with the all-metal valve and then pumping with the ion gauge running with a grid current of 10mA. Because of the poor closed conductance of the all-metal valve the diffusion pump could not be switched off during this operation.

Small leaks on the high-vacuum side of the system were detected using methyl alcohol. When drawn into the system through a leak this caused an increase in the ion gauge pressure reading. A hypodermic syringe was used to place one or two drops at a time on suspected areas and thus determine fairly accurately the position of the leak. The method proved to be rather slow at times because the methyl alcohol could take up to several minutes to get into the system if the leak was very small.

5.3 Note on Bakeable Vacuum Seals

Considerable difficulty was experienced with beakeable metal vacuum seals. It was proposed originally to use Mullard VMS series stainless-steel knife-edged seals[42]. These were to be used in the vacuum system between the cold trap and the metal closure valve, and for sealing the demountable flange of the moving-screen electron tube. Fig.5.3 shows the cross section of these seals. Copper washers are used as the sealing medium sandwiched between the knife edges and the flange faces. A slot between the knife edges provides the necessary elasticity in the seal to ensure good contact when

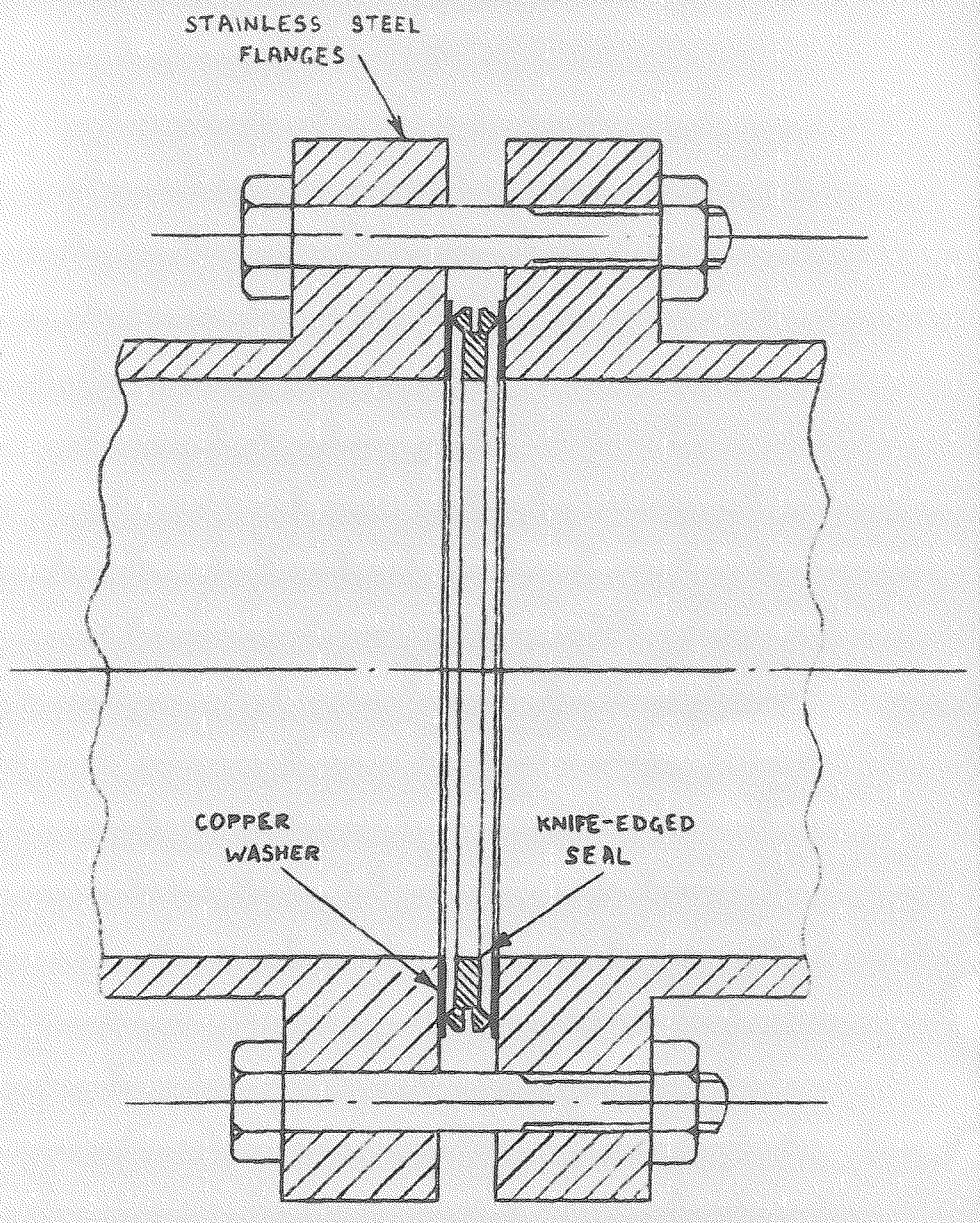


FIG.5.3 METAL VACUUM SEAL

the seal is baked.

In practice the seal used in the vacuum system (knife edges 3.625" diameter) repeatedly developed a leak after baking at 450°C. Finally, after increasing the flange thickness from $\frac{1}{2}$" to 1", a permanent seal was obtained and it seems likely that the main cause of the trouble was a slight bending of the flanges.

The experience gained, and the considerable time wasted, with this type of seal has shown that great care is necessary to make a successful leak-proof joint. The flanges should be thick enough to prevent bending, and their surfaces should be flat (perferably ground) and scratch-free. All dust must be removed from the mating surfaces. The bolts must be tightened evenly using a torque wrench by exactly the right amount (gap between knife edges reduced by 0.002" to 0.003").

The smaller seal (2.25" diameter) used on the electron tube was also found to leak and it was decided to use an aluminium wire seal[43] instead. This proved to be very much more satisfactory as the assembly procedure was much less critical. A length of 1mm diameter aluminium wire was welded to form a loop using an oxy-acetelene flame. The wire was clamped between the flange faces with sufficient pressure to considerably distort it. The assembly was then baked at 420-450°C for a sufficiently long time to enable the flanges to reach that temperature. The bolts, of high-

tensile steel, had a lower coefficient of expansion than the stainless-steel flanges and further compression of the wire took place on heating. The baking caused partial welding of the aluminium to the flanges giving a leak-tight seal which could only be broken by forcing the flanges apart. Holes were drilled and tapped in one of the flanges for this purpose.

Typical figures for a successful test seal were as follows:-

| | |
|---|---|
| Diameter of aluminium wire | 1mm |
| Diameter of wire ring | 2.25" |
| Bolts | 5 5/16"B.S.F. on 2.75" P.C.D. |
| Torque on bolts | 30lb.ft. |
| Flange thickness | 0.75" |
| Baking temperature | 450°C. |
| Baking time | 6 hours |
| Width of wire ring after baking | 0.2" |

This type of seal was also used on the moving-gun electron tube. To reduce the strain on each bolt, the number of bolts was increased to 12.

## 5.4 Electron Gun Power Supply

Because of their multi-anode construction the electron guns used required several voltages, all independently variable. A backward-wave oscillator power supply, which was conveniently

at hand, was modified to give the following outputs:

| | | | | |
|---|---|---|---|---|
| 1. | 2 O/P's | -25V to +25V | 1mA | anode supplies |
| 2. | 2 O/P's | 0 to 50V | 1mA | |
| 3. | 2 O/P'S | 0 to 50V | 1mA | |
| 4. | 2 O/P's | 0 to 100V | 1mA | |
| 5. | 2 O/P's | 0 to 400V | 1mA | |
| 6. | 1 O/P | 100 to 1500V | 50mA | collector supply |

All voltages are with respect to earth, the electron guns being run with a grounded cathode. The anode supplies were duplicated so that voltages on the inner and outer sections of the anodes could be varied independently. Provision was also made for linking each inner section to the corresponding outer one by moving one switch.

The output resistances of the anode supplies were 500 to 1000Ω. This figure was considered to be good enough because when operating correctly the anodes should draw no current. The ripple was less than 2mV.pk-pk. on all the supplies

## 5.5 Solenoids

Fig.5.4 shows a sectional view, and fig.5.5 is a photograph of the first solenoid built for beam focusing. Aluminium foil was used for the three windings. The turns were insulated by coating the foil on one side with a 0.0002" thick epoxy resin film and baking for 1 hour at 180°C after winding. The coils were of the following dimensions:

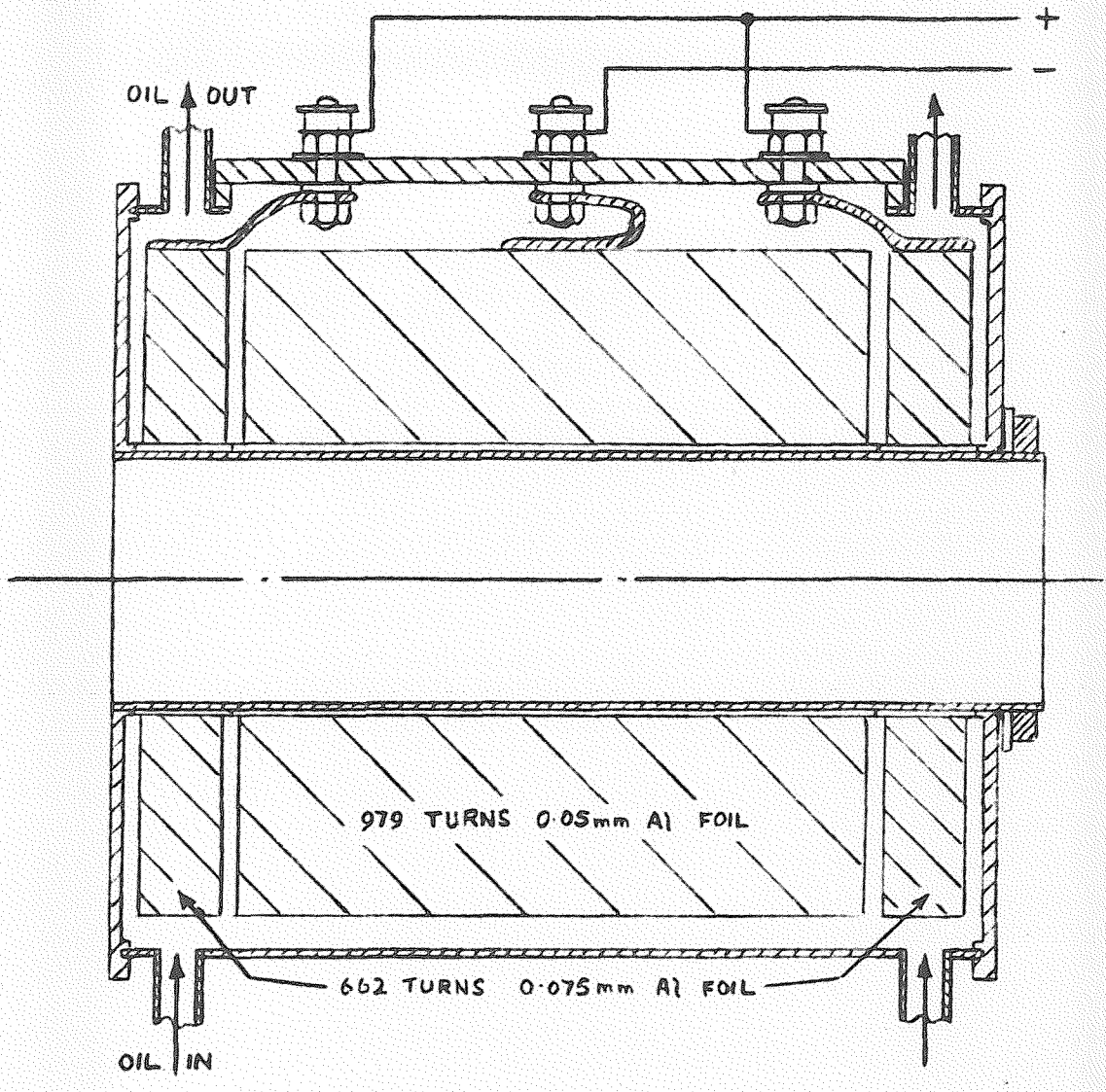


SCALE: HALF FULL SIZE

FIG.5.4 SOLENOID

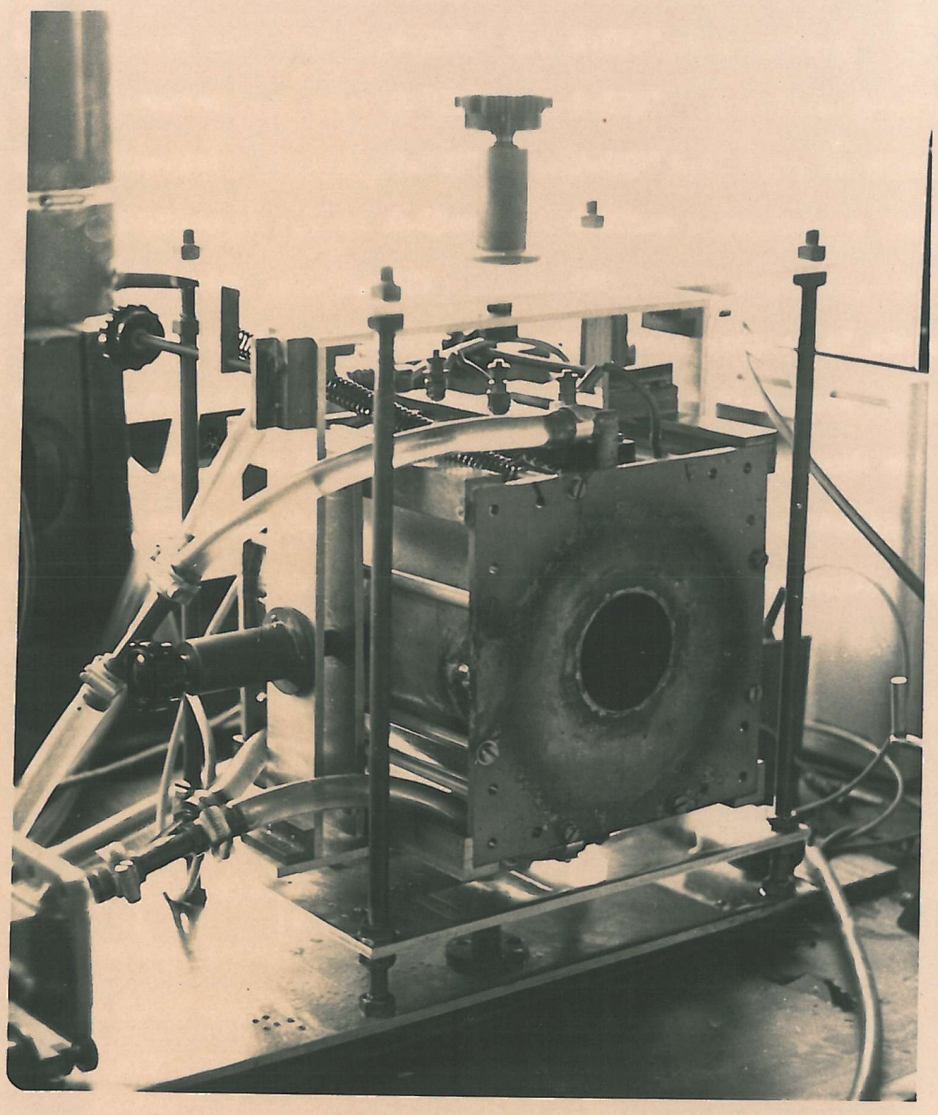

FIG.5.5 SOLENOID

| | Centre coil | End coils |
|---|---|---|
| Length | 6.75" | 0.875" |
| Inner diameter | 2.875" | 2.875" |
| Outer diameter | 7.125" | 7.125" |
| Foil thickness | 0.05mm | 0.075mm |
| Number of turns | 979 | 622 |

The end coils were positioned with their centres 4" along the axis from the centre of the centre coil. They were connected as shown in fig.5.4 so that the current in each end coil was one-half that supplied to the solenoid as a whole. The directions of the windings were such that the magnetic fields due to the centre and end coils aided one another.

The magnetic flux density B at a point on the axis of a coil distance d from its centre is given by:

$$B = \frac{1}{2}\mu_0 J\left\{(1+d)\ln\left[\frac{b+\sqrt{(1+d)^2+b^2}}{a+\sqrt{(1+d)^2+a^2}}\right] + (1-d)\ln\left[\frac{b+\sqrt{(1-d)^2+b^2}}{a+\sqrt{(1-d)^2+a^2}}\right]\right\} \qquad (5.1)$$

where $\mu_0$ = permeability of free space

$J$ = current density

$2l$ = coil length

$a$ = inner diameter

$b$ = outer diameter

The foil thicknesses and coil dimensions and connections were chosen such that the short end coils had a current density 2.61 times that of the centre coil. The flux density characteristics (calculated using equation 5.1) were as shown in fig.5.6. It can be seen that the total contribution from the three coils resulted in a substantially constant magnetic field over the centre 6" of the solenoid, and a drop of only 10% at the ends of an 8" length. The dotted line in fig.5.6 shows for comparison the characteristic of a single coil occupying the same space as the three coils used and having the same field strength at the centre. There is a considerably greater drop in magnetic field at the ends (30% at the ends of an 8" length). This curve shows the advantage of using the three-coil system.

Fig.5.6 shows that the theoretical field strength at the solenoid centre was $6.73 \times 10^{-3} Wb/m^2$ per amp of supply current. Measurements using a ballistic galvanometer showed that the actual field strength and distribution were within 3% of the calculated values as shown in fig.5.6. The measured flux density characteristic appeared, in fact, to be slightly more uniform over the centre portion of the coil than the calculated characteristic. The reason for this difference was probably that the centre of the coil was slightly hotter than the ends because the ends were cooled. The winding resistance at the centre was thus higher, and the current density lower, than at

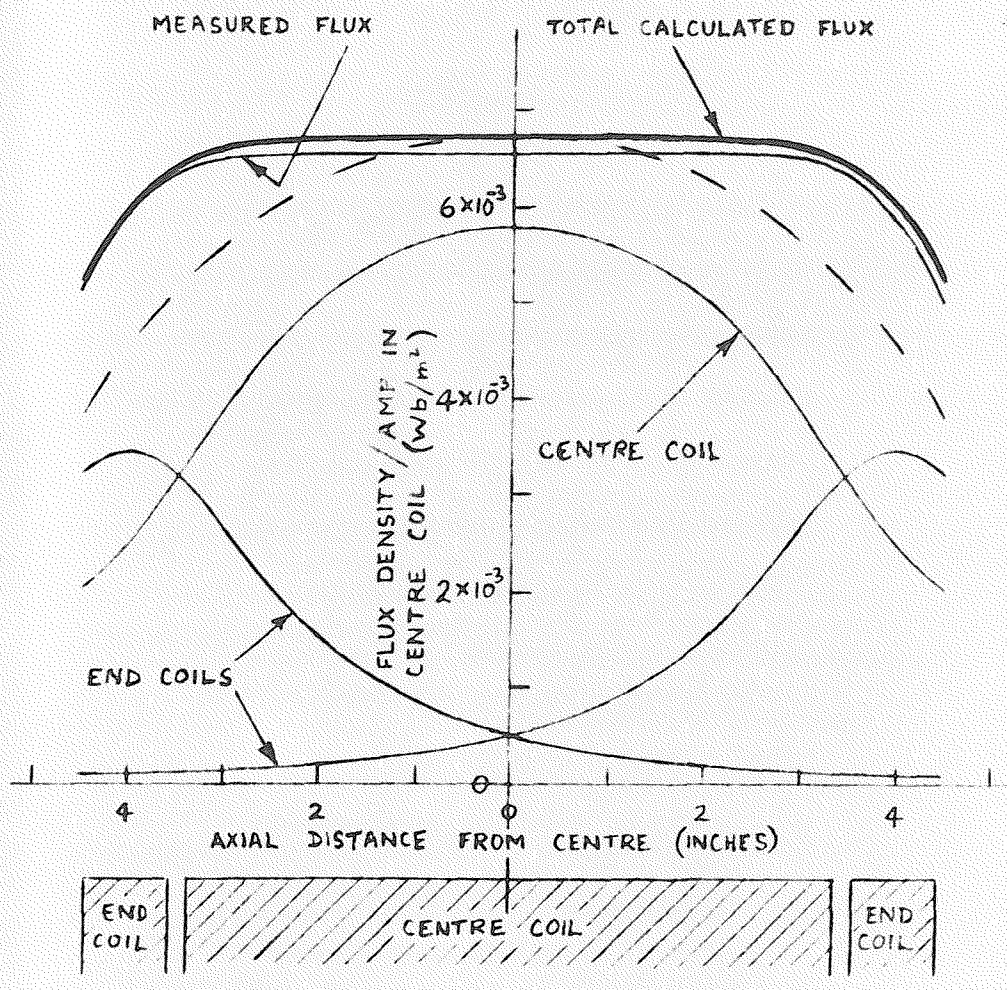


FIG.5.6 SOLENOID CHARACTERISTICS

the ends.

The total solenoid resistance was 3.56Ω, rising to 4.78Ω at the maximum operating temperature. Thus at the maximum field strength of 0.16Wb/$m^2$(24.8A) the power dissipation was 2.8kw.

The efficient cooling of such a solenoid is very important, particularly when it is supplied from a constant current source (which is necessary to maintain a constant field). With a constant current supply any increase of resistance due to heating causes an increase in the power dissipated and further heating. If the cooling is inefficient thermal runaway can occur. Using aluminium foil for the windings instead of the conventional round section copper wire greatly eases the cooling problems; in fact it is doubtful whether it would be possible to dissipate 2.8kw in a wire-wound solenoid of the size used. With foil the thermal resistance is relatively low in the axial direction due to the absence of any axial electrical insulation barriers which tend to be poor heat conductors. Efficient cooling can be achieved by circulating transformer oil around the ends of the coils. With a wire-wound coil the thermal resistance would be much higher in all directions and the centre of the coil would tend to get very hot. Copper foil was considered as this is more efficient than aluminium, having a lower specific resistivity. However, aluminium has the advantage of being lighter, cheaper and much easier to obtain.

The transformer oil was cooled in a heat exchanger. A spiral pipe through which the oil was pumped was surrounded by a tank through which tap water flowed. At the maximum power dissipation the rise in the solenoid resistance indicated a mean temperature of about 110°C.

The solenoid was mounted so that it could be turned independently about horizontal and vertical axes, and moved vertically and laterally. In this way fine adjustment of the electron beam direction was possible with a rigidly mounted tube.

A second, longer, solenoid for use with the moving-gun electron tube was designed on similar lines by Mr. G.R. Nudd, the specification being as follows:

| | Centre coil | End coils |
|---|---|---|
| Length | 12" | 2.25" |
| Inner diameter | 3" | 3" |
| Outer diameter | 9" | 9" |
| Foil thickness | 0.002" | 0.003" |
| Number of turns | 1365 | 940 |
| Overall length | 17.5" | |
| Total resistance | 2.73Ω | |
| Flux density at centre per amp | 5.77Wb/m$^2$ | |

## 5.6 Solenoid Power Supply

The solenoids required stabilized d.c. currents of up to 25A at about 3kw. It was not possible to obtain a commercial unit to give this output, except at a prohibitive cost and it

was therefore necessary to design and build such a power supply.

The supply was designed to the following specification:
Stabilized d.c. output current 5-30A continuously variable.
Output voltage 0-135V depending on the load.
Maximum output power 4.05kw.

Semiconductors, including silicon controlled rectifiers, were used throughout. As the circuit is particularly interesting it is described below (see also reference 44).

a) Introduction

Constant-current power supplies using d.c. machines have been described by Garwin[45], Johnson and Singer[46], and Garwin, Hutchinson, Penman and Shapiro[47]. In each case the series control element consisted of a bank of power transistors in parallel and the current was kept constant by reducing to zero the difference between the voltage drop across a series resistor and a reference voltage. Brog and Milford[48] and Richards[49] used a similar regulating system but obtained their d.c. supplies from rectifier circuits. It was found that with suitable precautions stabilities of better than 1 in $10^5$ could be obtained.

A similar type of current regulator was incorporated in the equipment described below. However, it was decided to use only semiconductor components and the d.c. source consisted of a bridge rectifier containing silicon controlled rectifiers.

This arrangement had the advantage that the voltage across the series transistors could be automatically limited to a safe value by means of an additional feedback loop.

b) General Principles

A schematic diagram of the final circuit design is shown in fig.5.7. Power was supplied to the load from the a.c. mains through a single-phase controlled bridge rectifier and a low-pass filter[50-52]. In series with the load was the series regulator consisting of five power transistors in parallel, and a stable reference resistor R.

The controlled bridge rectifier used two silicon controlled rectifiers 1 and 2, and two silicon rectifiers 3 and 4 as shown. By varying the time after the start of the half-cycle that the trigger pulse was applied to the controlled rectifiers the mean bridge output voltage could be varied from zero to the usual full-wave value. Fig.5.8 shows typical output voltage waveforms and the change of mean voltage with pulse firing angle is shown in fig.5.9. In this application the firing angle depended on the voltage across the series regulator and reference resistor.

One of the difficulties associated with transistors is that the collector-emitter voltage must not exceed a specified value, even momentarily, otherwise the transistor will be destroyed. In the circuit shown any change in load voltage, which may have been caused by a change in the load current or resistance, was followed by an appropiate adjustment of the output from the bridge so that the voltage across the series regulator and refer-

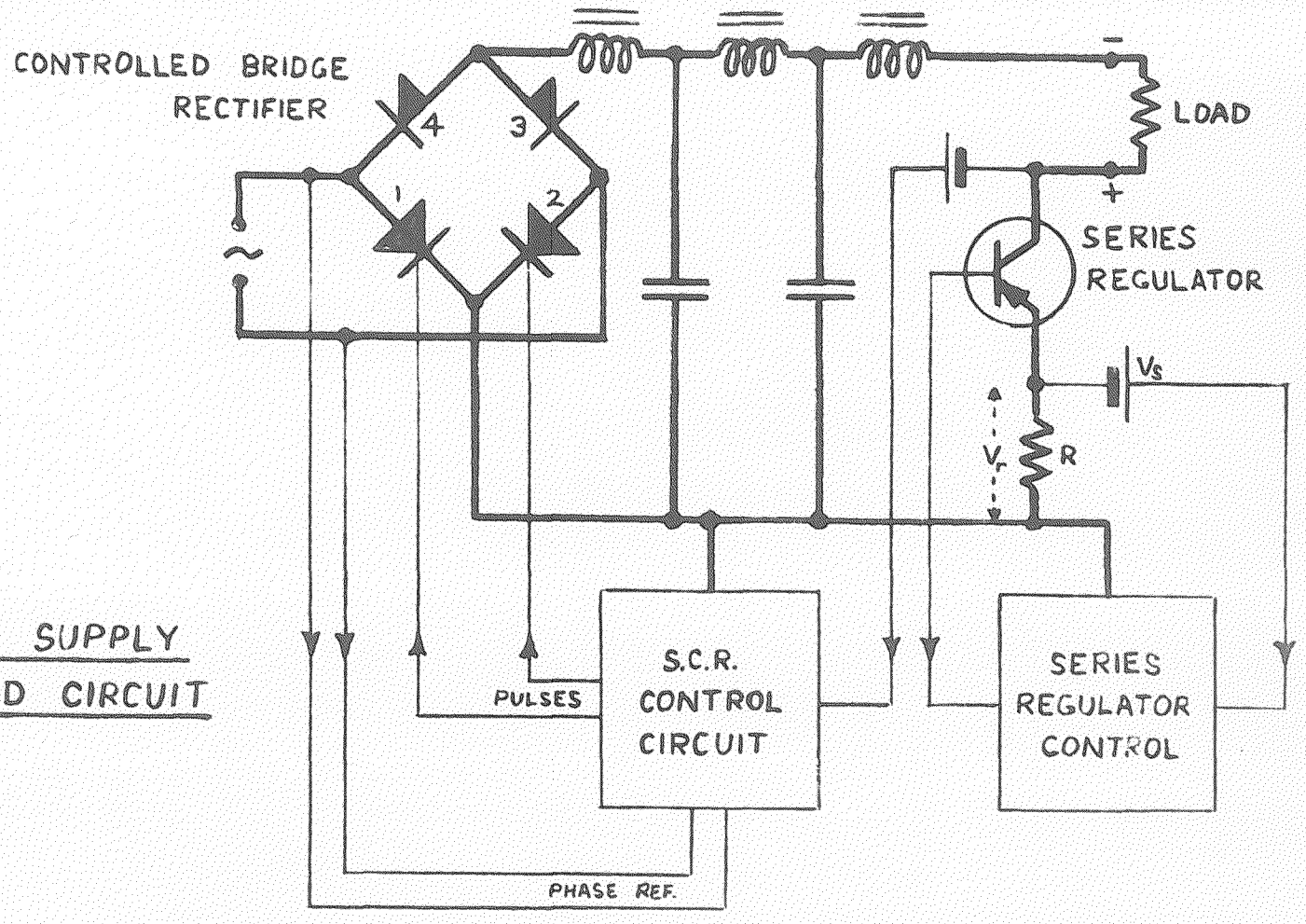


FIG.5.7

POWER SUPPLY

SIMPLIFIED CIRCUIT

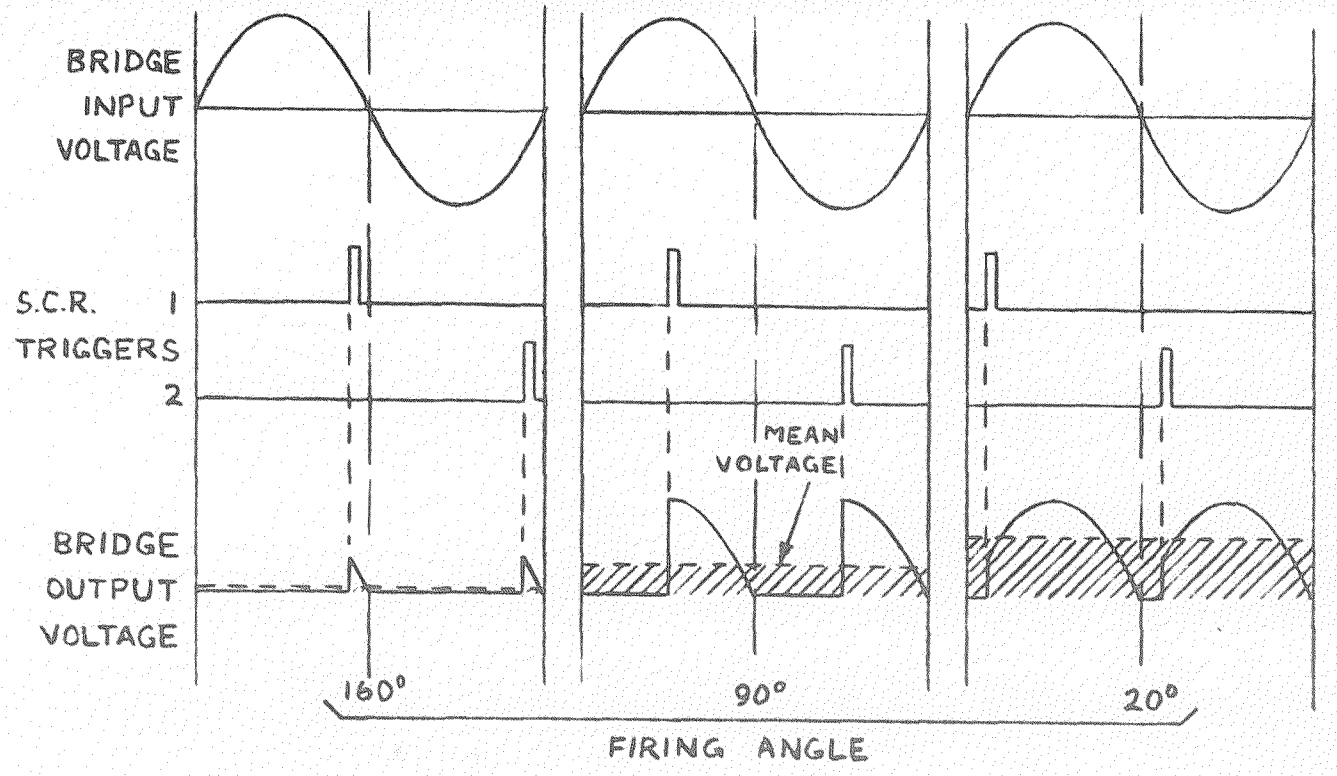


FIG.5.8 CONTROLLED BRIDGE RECTIFIER WAVEFORMS

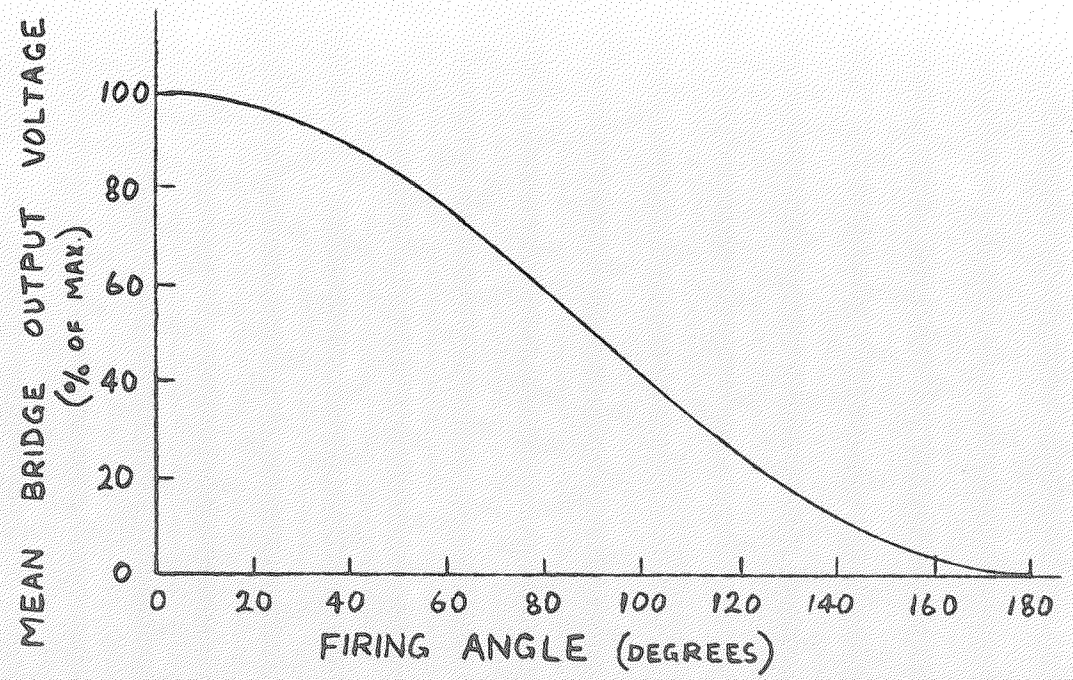


FIG. 5.9 BRIDGE OUTPUT CHARACTERISTIC

ence resistor remained approximately constant. The voltage across the transistors, and the power dissipated by them, were thus kept below the specified limits while the load current and voltage could be varied over a wide range. The load current depended mainly on the base current of the transistors and was virtually independent of the collector-emitter voltage. The difference between the voltage across the reference resistor $V_r$ and a stable reference voltage $V_s$ was applied to the input of a d.c. amplifier which supplied the base current for the series regulator transistors.

The feedback coupling was such that any difference between $V_s$ and $V_r$ caused a change in the base current, and hence in the load current, which reduced this difference (nearly) to zero.

A number of precautions must be taken in the design of such a circuit. For example, the d.c. output from the low-pass filter does not respond instantaneously to a change in the firing angle of the silicon controlled rectifiers. Consequently the response of the pulse generator must not be too rapid otherwise there is a danger of low-frequency oscillations occuring owing to positive feedback brought about by phase shift in the filter. It follows that if the load resistance or current is suddenly reduced it is possible that the rated collector-emitter voltage of the series transistors may be exceeded before a reduction in the output voltage from the filter takes place. It is essential, therefore, that a limiting circuit should be included

which, when a predetermined transistor voltage is reached, increases the load current sufficiently to transfer the excess voltage to the load.

Another factor is that if the load is inductive, as it is effectively with the low-pass filter, uncontrolled half-wave rectification may occur under certain conditions if the firing angle is increased to 180° (i.e. if the firing pulses are removed) too rapidly[52]. Suppose silicon controlled rectifier 1 (see fig.5.7) and rectifier 3 are conducting when the firing angle is increased to 180°. At the end of the half-cycle a forward voltage is applied to rectifier 4 which conducts and maintains the load current path through controlled rectifier 1. If this current is still above the minimum sustaining current at the end of the second half-cycle, controlled rectifier 1 will continue to conduct and the sequence will be repeated. This phenomenon occurred for small external load impedances even with the retarded response of the pulse generator and it is to be expected whenever the ratio of load inductive reactance to resistance is sufficiently high. The effect was prevented by so designing the pulse generator that the maximum possible firing angle was always less than 180°. An alternative, and sometimes preferable, remedy is to interchange rectifier 4 and controlled rectifier 2, although one controlled rectifier must now be transformer-coupled to the control circuit and it is more difficult to produce a rectangular driving pulse.

The above system gave the high degree of stabilization and low ripple associated with a series transistor regulator, while the problem of providing a wide range of output current and voltage without exceeding the voltage and power ratings of the transistors was overcome by using a controlled bridge rectifier. A readily adjustable power output of several kilowatts was possible with high efficiency and reliability. Slow changes of load impedance and input voltage were corrected by the controlled bridge rectifier. Rapid changes were corrected by the series transistors as long as the resulting change in voltage was not so large as to saturate the transistors or to bring the voltage limiter into operation. Under normal circumstances this limit was not exceeded.

c) Circuit Details

The complete circuit is given in fig.5.10. The type numbers of the semoconductors etc. are as follows:

Silicon transistors: $T_1$, $T_2$, $T_9$ OC465 ) Brush Crystal
$T_7$, $T_8$, $T_{10}$ OC465K) Co.Ltd.

Germanium transistors: $T_3$, $T_4$, $T_5$, $T_6$ OC72 Mullard Ltd.
$T_{11}$ CTP1736 ) Brush Crystal
$T_{12}$ 2N1147A ) Co.Ltd.

Silicon rectifiers: $D_1$, $D_2$, $D_5$, $D_6$, $D_7$, $BR_1$ S35) Brush Crystal
$BR_2$ OY5067 ) Co.Ltd.
$D_3$, $D_4$ DD716A Joseph Lucas Ltd.

Silicon controlled rectifiers: $S_1$, $S_2$ CS31M Westinghouse Brake and Signal Co.Ltd.

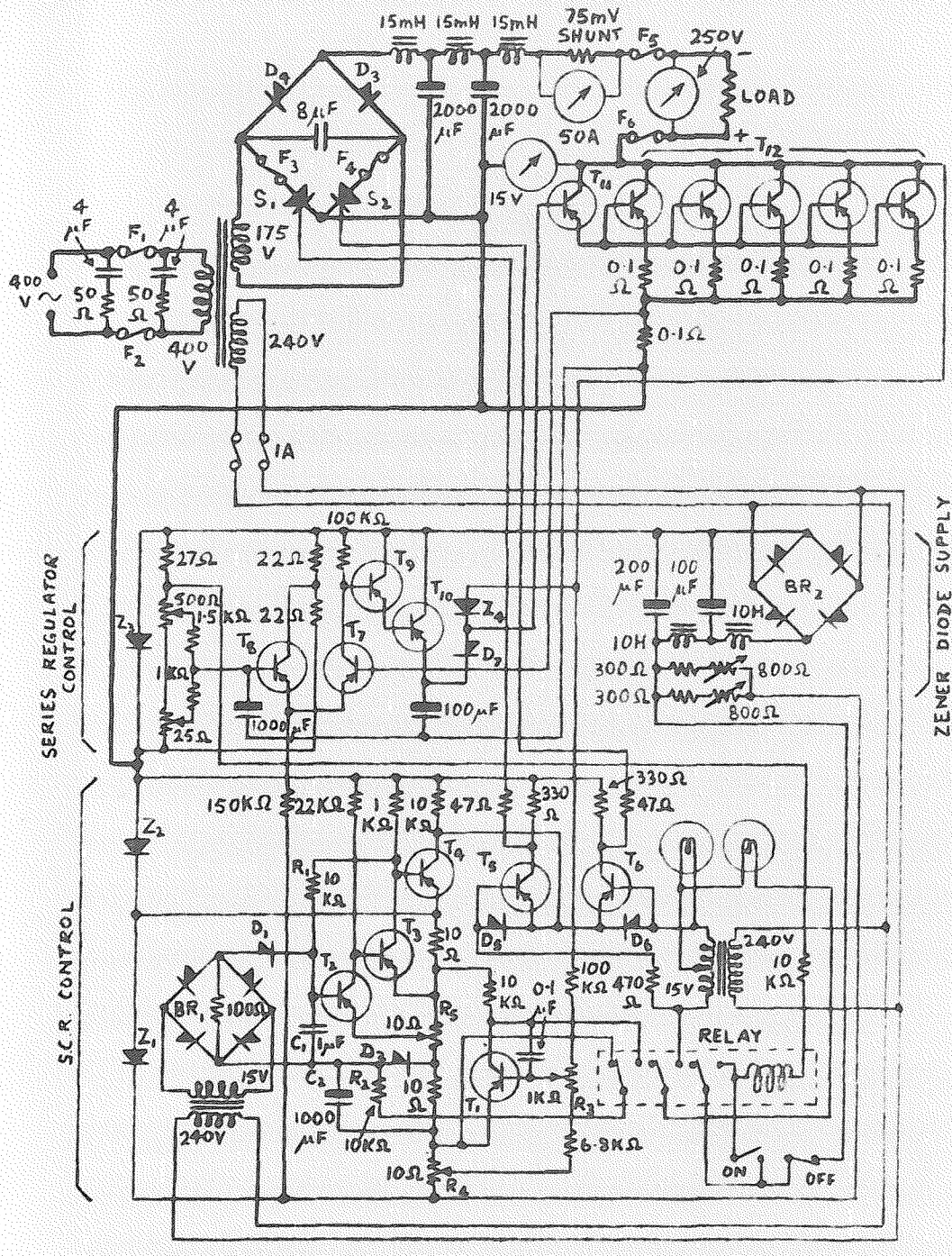


FIG.5.10 STABILIZED CURRENT POWER SUPPLY COMPLETE CIRCUIT

| | | |
|---|---|---|
| Zener diodes: $Z_1$, $Z_2$, $Z_3$, $Z_4$ | ZL8 | Brush Crystal Co.Ltd. |
| Fuses: $F_1$, $F_2$ | Y30RA | General Electric Co.Ltd. |
| $F_3$, $F_4$ | GS300/25 | English Electric Co.Ltd. |
| $F_5$, $F_6$ | GS300/50 | |

The circuit is most easily considered in three parts as follows:

(i) High-current circuit

The high-current circuit is shown by heavy lines and comprises the main input transformer, controlled bridge rectifier, power transistor series regulator and reference resistor.

The silicon controlled rectifiers (Westinghouse CS31M), of maximum mean current 26A and maximum peak voltage 350V, were each mounted on a heat sink of surface area $5ft^2$ and the silicon rectifiers (Lucas DD716A) on a common heat sink of area $5.5ft^2$. All the heat sinks were air-cooled by convection and were of black-painted aluminium. The five power transistors (Brush 2N1147A), together with the drive transistor (Brush CTP1736), were mounted on a common $12ft^2$ heat sink. This allowed a maximum total dissipation of 150W, thus limiting the continuous collector-emitter voltage to 5V at maximum current. The maximum peak collector-emitter voltage was 60V for both types of transistor. The high-power transistors had $0.1\Omega$ emitter resistors to ensure that each carried approximately the same current.

The $0.1\Omega$ reference resistor was constructed of eureka wire.

The maximum change of resistance on switching on to maximum current was 0.2%.

High-speed high-rupturing-capacity fuses (English Electric type GS) protected the circuit against current overload. A resistor-capacitor surge suppressor was necessary across the transformer primary to limit supply or transformer voltage transients which may have damaged the rectifiers[52].

(ii) Silicon controlled rectifier control circuit.

The stabilized voltages needed for both control circuits were obtained from three 8-9V Zener reference diodes ($Z_1$, $Z_2$, $Z_3$) connected in series. The silicon controlled rectifier control circuit consisted of a rectangular-wave pulse generator which produced positive pulses, the leading edges of which could be delayed by between $0^{\circ}$ and $160^{\circ}$ from the beginning of each half-cycle. To ensure that the controlled rectifier current had time to rise to the minimum sustaining level the pulses were made to last until the end of the half-cycle.

Transistors $T_2$ and $T_3$ formed a monostable switching circuit. At the end of each half-cycle capacitor $C_1$ was discharged through the diode $D_1$ so that $T_2$ was cut off and $T_3$ conducted. $C_1$ then charged at a rate determined by the time-constant $C_1R_1$. Switching began as soon as $T_2$ started to conduct and was accelerated by the increase in the current through $R_1$ caused by the decrease in the collector current of $T_3$. After switching $T_2$ conducted, $T_3$ was cut off and $T_4$ provided the necessary drive to fire the controlled

rectifiers. $T_5$ and $T_6$ were used as switches to apply the pulses alternately to the two silicon controlled rectifiers.

The firing angle was varied by altering the amount by which $C_1$ had to charge before switching occurred, by changing the voltage at the junction of $C_1$ and $C_2$, which in turn was controlled by the voltage across the series regulator. The time-constant $C_2R_2$ was sufficiently long to ensure stability under all operating conditions. The sensitivity was such that the firing angle changed from maximum to minimum with a decrease of 2V in the voltage across the series regulator. The voltage across the series regulator was adjusted to between 6 and 7V by the potentiometer $R_4$. Slight adjustments could be made if necessary when operating conditions were changed by means of the external control $R_3$.

The relay ensured that when the a.c. supply was switched on the firing angle was a maximum (preset by the potentiometer $R_5$). Switching on the relay brought the unit into normal operation.

(iii) Series regulator control circuit.

The series regulator control circuit used a long-tailed pair input stage ($T_7$ and $T_8$). The emitter-follower current amplifier ($T_9$ and $T_{10}$) supplied the necessary current to the series regulator. The difference between the base voltages of $T_7$ and $T_8$ was small at any load current. The latter therefore adjusted itself so that the voltage across the 0.1Ω reference resistor ($T_7$ base voltage) was very nearly equal to the reference

voltage ($T_8$ base voltage). Changes of load current were brought about by varying the reference voltage between 0.5 and 3V by coarse and fine controls $R_6$ and $R_7$ respectively.

The 8-9V Zener diode $Z_4$ limited the collector-emitter voltage of the series regulator transistors should the load resistance or current be suddenly reduced. If the voltage across the series regulator increased sufficiently for the $T_{11}$ base-collector voltage to equal or exceed the $Z_4$ Zener voltage, $Z_4$ conducted and reduced the dynamic impedance of the series regulator to a fraction of an ohm. Any further increase in voltage then appeared across the load.

d) Performance

The following tests were carried out using a resistive load:

(i) Load resistance change.

A suitable load resistance was connected and the output control was adjusted to give the maximum output of 30A at 135V. Without making any adjustments to the power supply the load resistance was gradually reduced to zero. The maximum change of load current was found to be less than 0.05%. This test was repeated at other, lower, load currents with the same result. The time of response to a step-function change in load resistance was 1 millisecond.

(ii) Mains voltage change.

A 10% reduction of mains voltage caused a reduction in the load current of about 0.1% at all load currents.

(iii) Drift.

During the first 10 minutes after initial switching on there was a load current increase of 1%. There was a further increase of about 0.1% in the next 20 minutes, after which the load current remained stable to within 0.06%.

(iv) Ripple.

Fig.5.11 shows how the maximum r.m.s. ripple current varied with load current. The maximum ripple was 0.1% and occurred at a current of 5A. At the maximum output current of 30A the ripple was 0.05%.

(v) Efficiency and power factor.

Fig.5.11 also shows typical curves of efficiency and input power factor against load current at constant values of load voltage. The maximum efficiency was 83% at maximum load power. The input power factor was lagging and varied between 0.85 and 0.38.

e) Conclusions.

The tests described above show that the performance of the power supply was very satisfactory. After an initial warming-up period the output current remained constant to about 0.05%. The initial drift was due mainly to temperature changes in the Zener reference diodes and to a lesser extent in the reference resistor. If necessary the stability could be greatly improved by obtaining the reference voltage from a mercury or standard

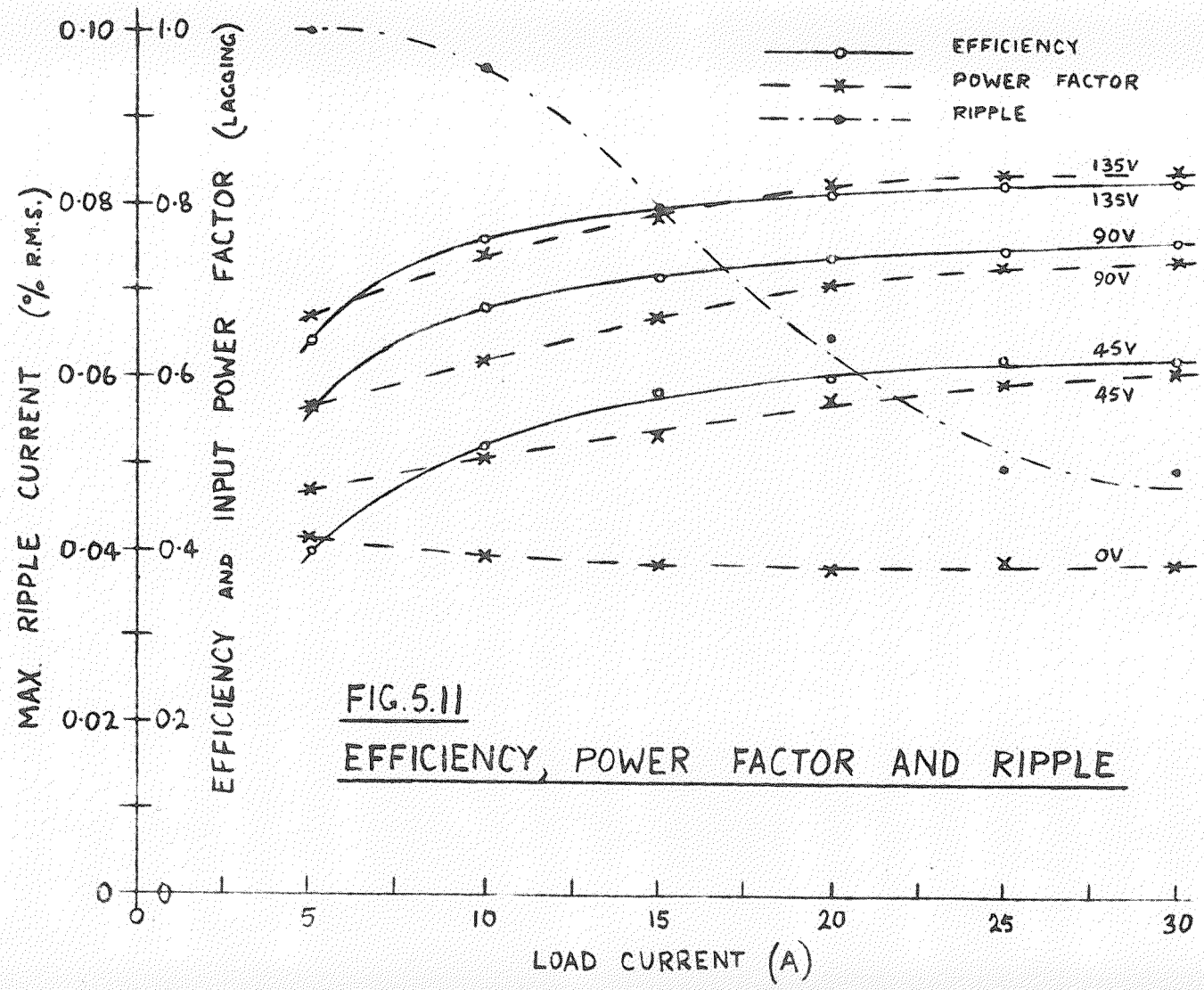


FIG. 5.11

EFFICIENCY, POWER FACTOR AND RIPPLE

cell and by cooling the reference resistor. The ripple could be reduced by increasing the amplifier gain, and by screening the chokes and transformers to reduce the effects of leakage flux. The requirements of the low-pass filter could be eased by operating from a three-phase a.c. supply, since the amount of ripple would be decreased and its frequency increased. However, a three-phase transformer and an additional rectifier and silicon controlled rectifier would be required, and the design of the controlled rectifier control circuit would become more complicated.

5.7 Electron Guns

The electron guns in the three vacuum tubes were almost identical and were similar to those used in Mullard experimental backward-wave amplifiers. The parts were supplied by the Mullard Research Laboratories through the courtesy of Mr. N.W.W. Smith and Mr. A.J. Gander.

The design was based very closely on that of Currie's original gun. The construction is shown in fig.5.12, and fig. 5.13 is a photograph of the gun. Oxide cathodes were used consisting of barium, strontium and calcium oxides in a nickel matrix. The cathode emitting surface was annular with a mean diameter of 8.52mm. and an annular width of 0.38mm. It was surrounded, outside and inside, by the control electrode as shown. In front of the cathode were a series of four or five accelerating anodes. Each consisted of an outer and inner

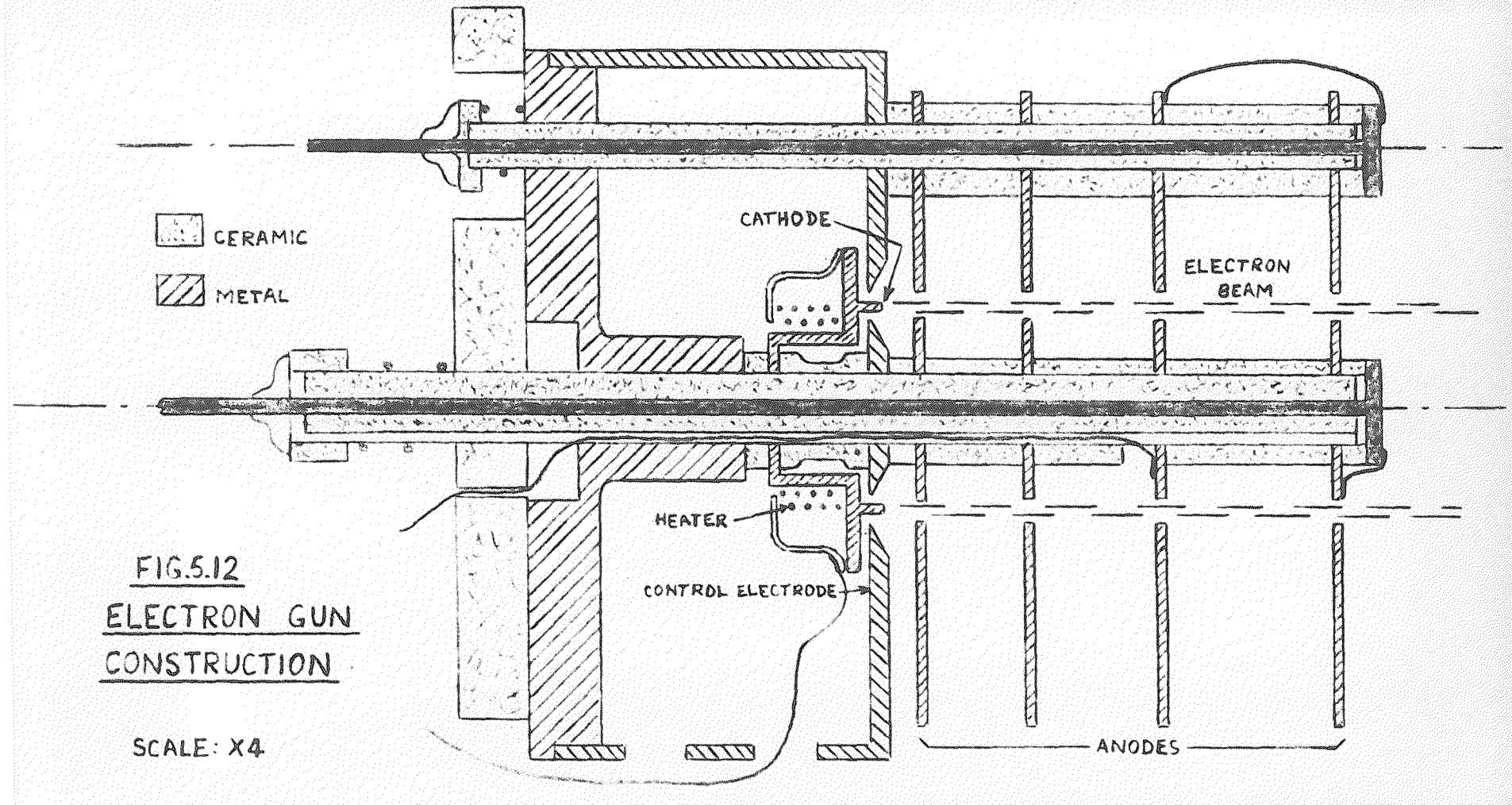


FIG.5.12
ELECTRON GUN CONSTRUCTION

SCALE: X4

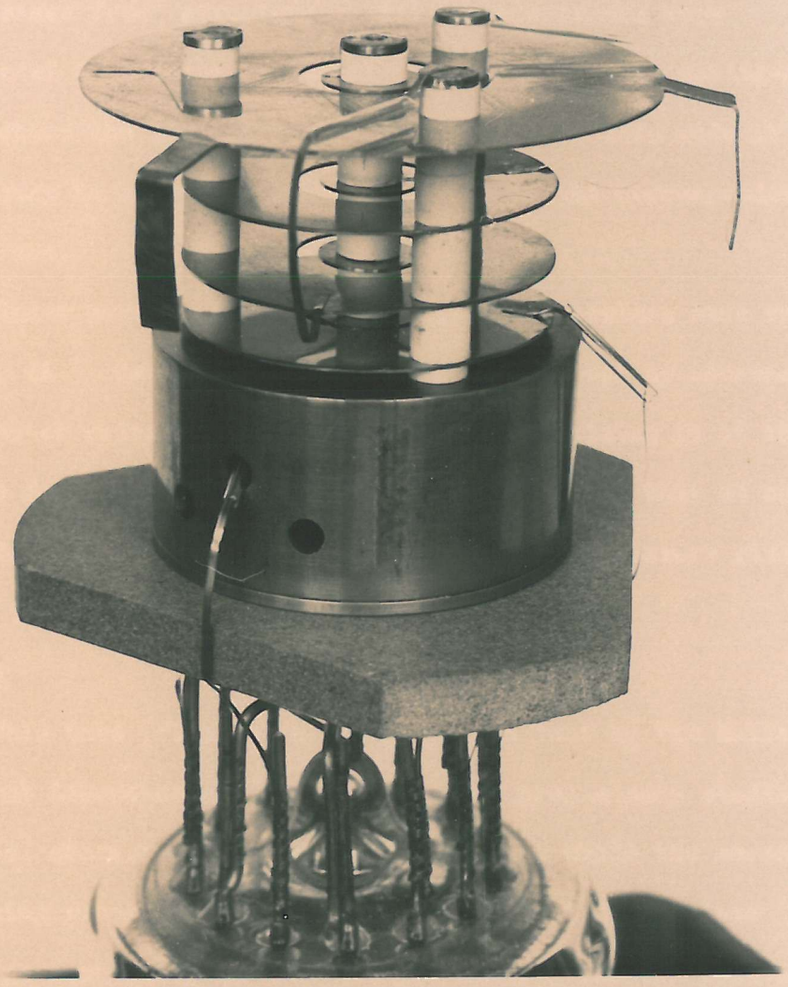

FIG.5.13 ELECTRON GUN

electrode surrounding an annular aperture through which the beam passed. The centre electrodes were supported by a ceramic pillar through the centre of the beam forming a 'Christmas Tree' structure. All the electrodes were connected to separate external pins except in the moving-gun tube where the limited number of sliding contacts made it necessary to link each inner electrode to the corresponding outer one.

Under normal operating conditions the heaters were run at 7V, 2A. Cathode activation was carried out by increasing the heater voltage gradually up to 8V and holding it at that figure for 1 minute. Care was taken to ensure that at no time during the activation procedure did the pressure rise above $10^{-4}$mmHg.

5.8 Tube 1

This tube (figs. 5.14 and 5.15) was lent by the Mullard Research Laboratores. It was used for preliminary studies of the d.c. characteristics and beam profiles while the second tube was being prepared. It consisted of a sealed-off glass envelope containing an electron gun and a collector positioned 8 inches from the final anode of the gun. The collector consisted of a glass screen with a conducting coating of tin oxide on which was deposited a layer of carbon. The carbon glowed red at points of high current density giving a visual picture of the beam current distribution. The sensitivity

SCALE: HALF FULL SIZE

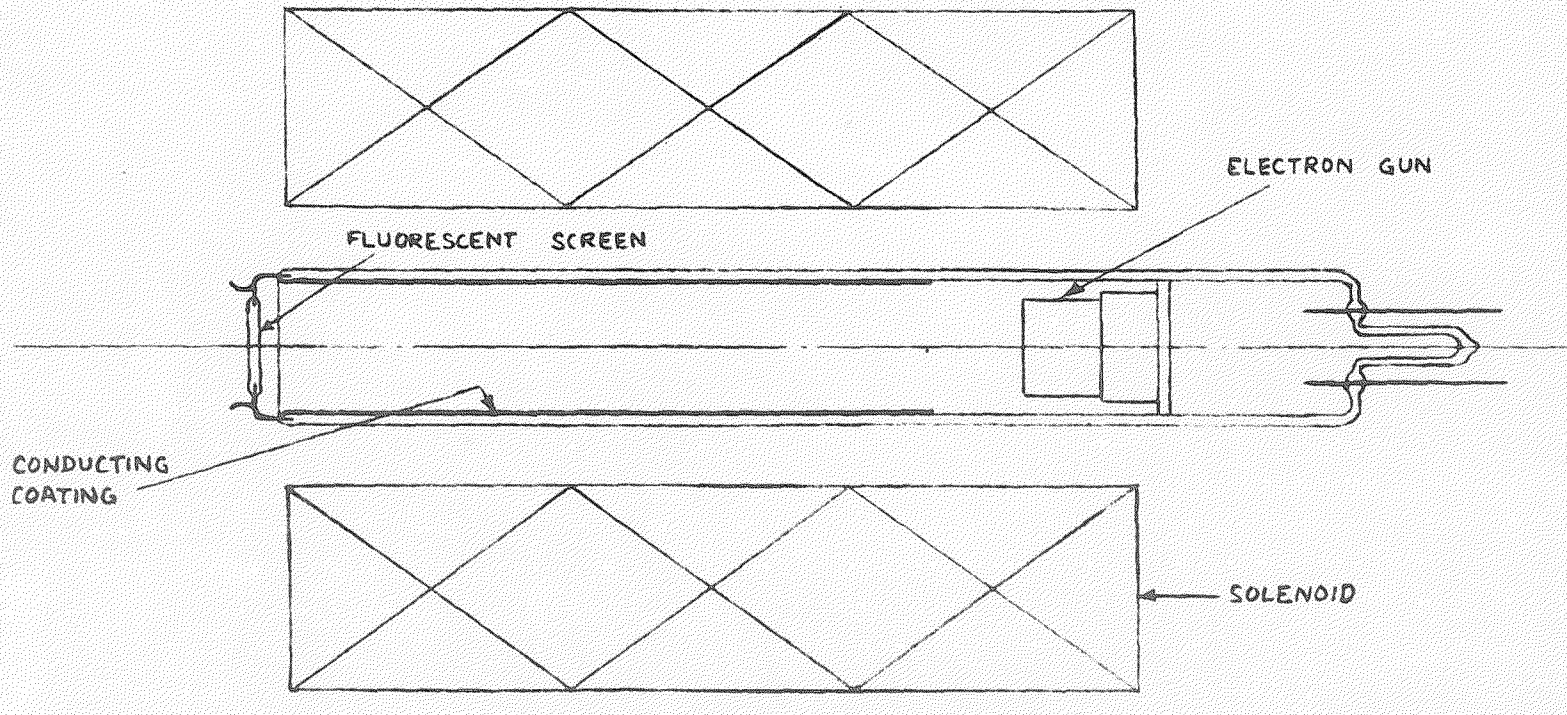


FIG. 5.14 FIXED SCREEN ELECTRON TUBE

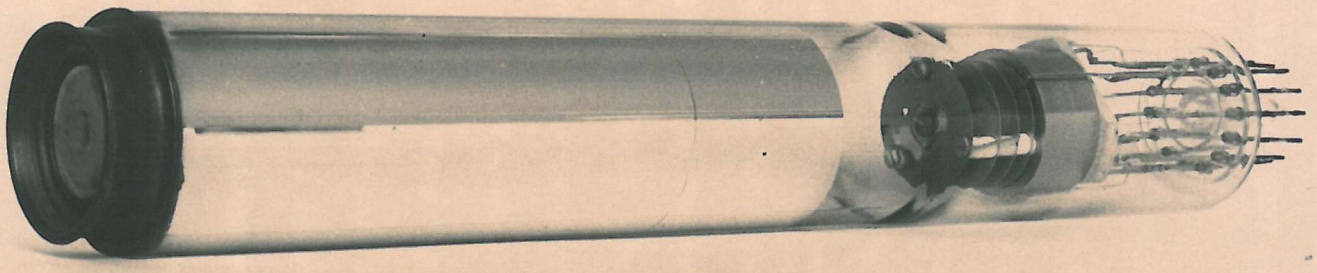

FIG.5.15 FIXED SCREEN ELECTRON TUBE

of the carbon was such that a beam current of about 4mA was necessary to get a clear image on the screen, working at a collector voltage of 1500V (the maximum available from the power supply).

5.9 Tube 2

This tube (figs. 5.16 and 5.17) also contained an electron gun and fluorescent-screen collector. In order to study any axial variations in the beam structure, the screen could be moved axially a distance of up to 6 inches from the final anode of the gun. Movement of the screen was by the action of an external magnet on a piece of iron attached to the screen. The carbon was deposited on the screen by holding it over the smokey flame from a wax taper. In order to get better sensitivity a thinner coating was deposited than in tube 1. At a collector voltage of 1500V a clear image was obtained with a beam current of about 1.5mA. This figure is typical of the operating beam current when the gun is used in a backward-wave amplifier.

The tube was made with a removable metal flange at one end for easy removal of the electron gun. An aluminium wire seal was used (see section 5.3). A conducting coating of aluminium was applied to the internal surface of the glass envelope using conventional evaporation techniques. This was connected to an external pin.

Although provision was made to seal this tube off, in fact it was left permanently connected to the vacuum system and

SCALE: THIRD FULL SIZE

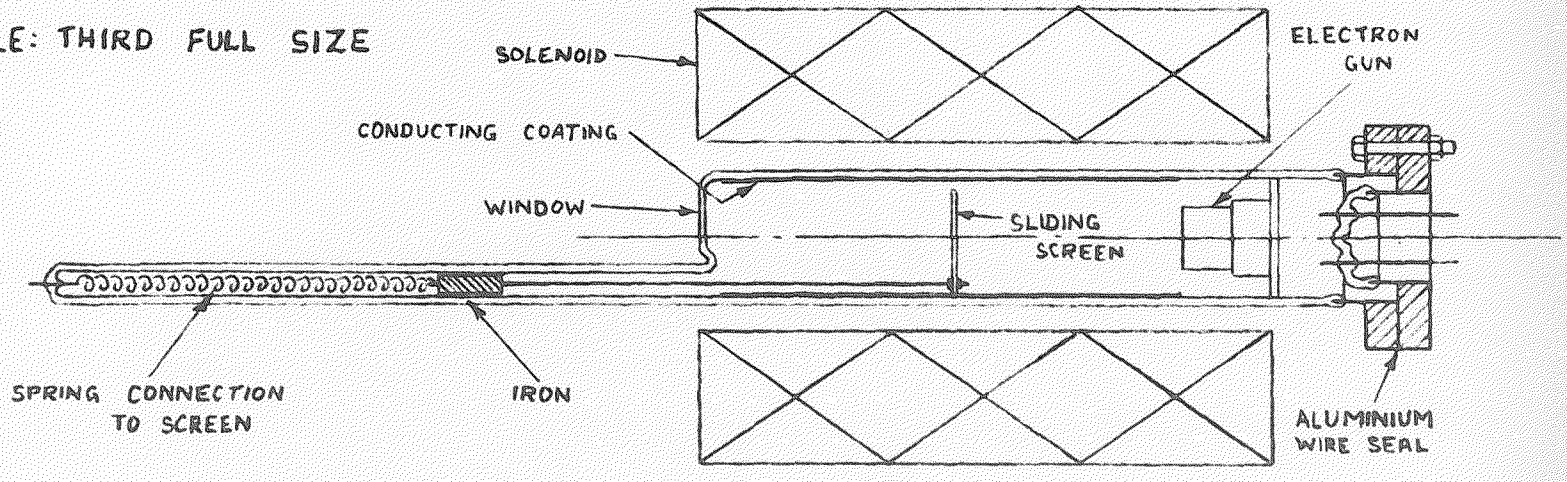


FIG. 5.16 MOVING SCREEN ELECTRON TUBE

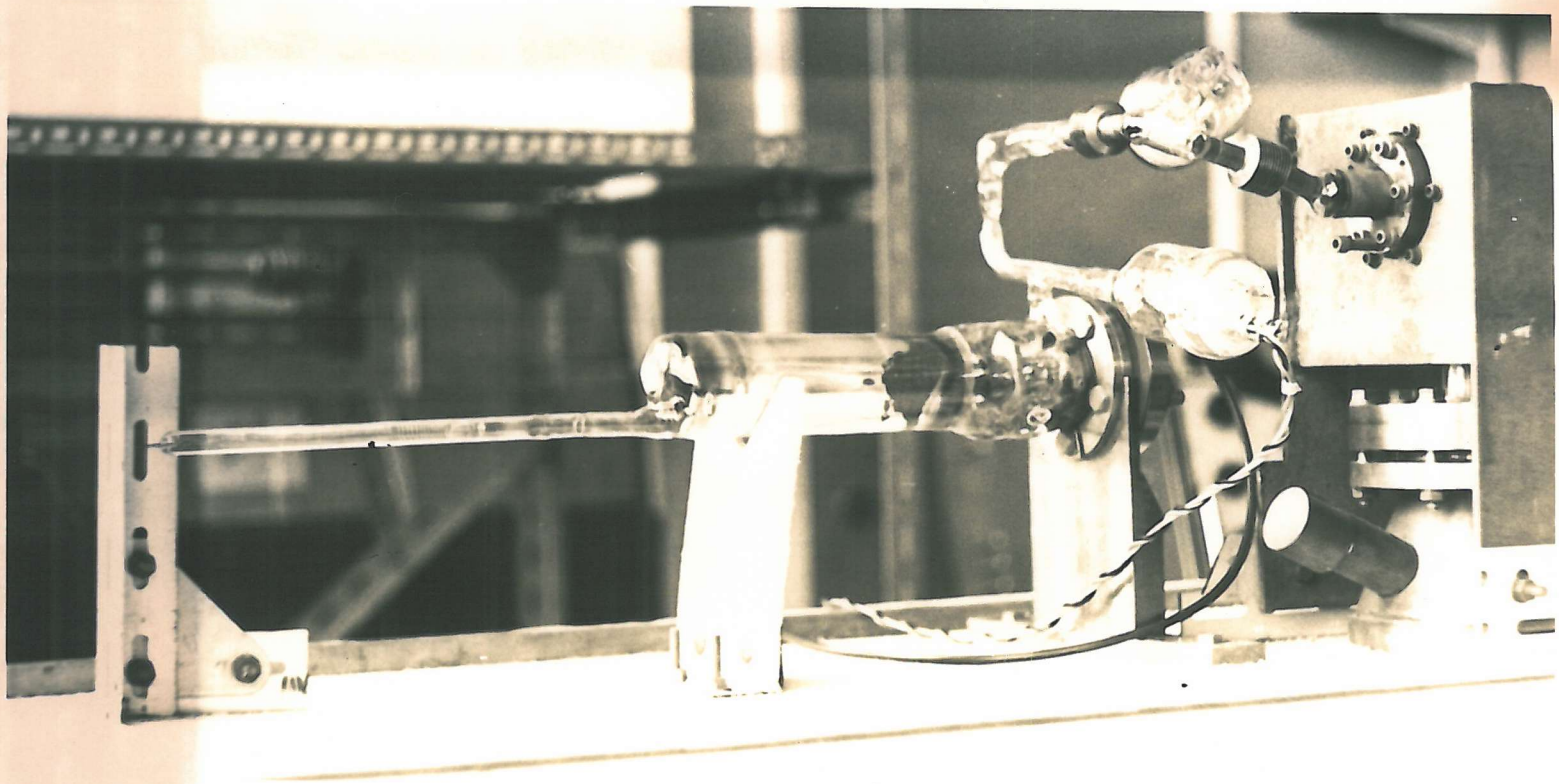

FIG.5.17 MOVING SCREEN ELECTRON TUBE

continuously pumped. It was thus possible to control the pressure and study the effects of pressure on the beam characteristics.

This tube had to be rebuilt several times due to trouble with the glasswork. The experience gained with the construction of this tube showed that with the limited facilities for carrying out glasswork at the University it would be best, in future, to keep glass structures as simple and robust as possible.

5.10 Tube 3

a) Description

Construction of this tube is complete but up to the time of writing no results had been obtained from it. The tube was built to measure the noise on the electron beam and at the same time to observe changes in the electron beam structure. To measure noise the electron gun is movable an axial distance of 10 inches relative to the re-entrant cavity through which the beam passes. A carbon fluorescent screen is to be used as the collector to observe the beam profile.

Fig.5.18 is a sectional view, and fig.5.19 is a photograph of the tube. It is demountable, being in two sections joined by flanges and an aluminium wire seal. Glass parts are as simple as possible. Most of the complex structures are made of stainless steel joined by argon arc welding.

It was decided that it would be easier to move the electron gun rather than the cavity because of the difficulty of making

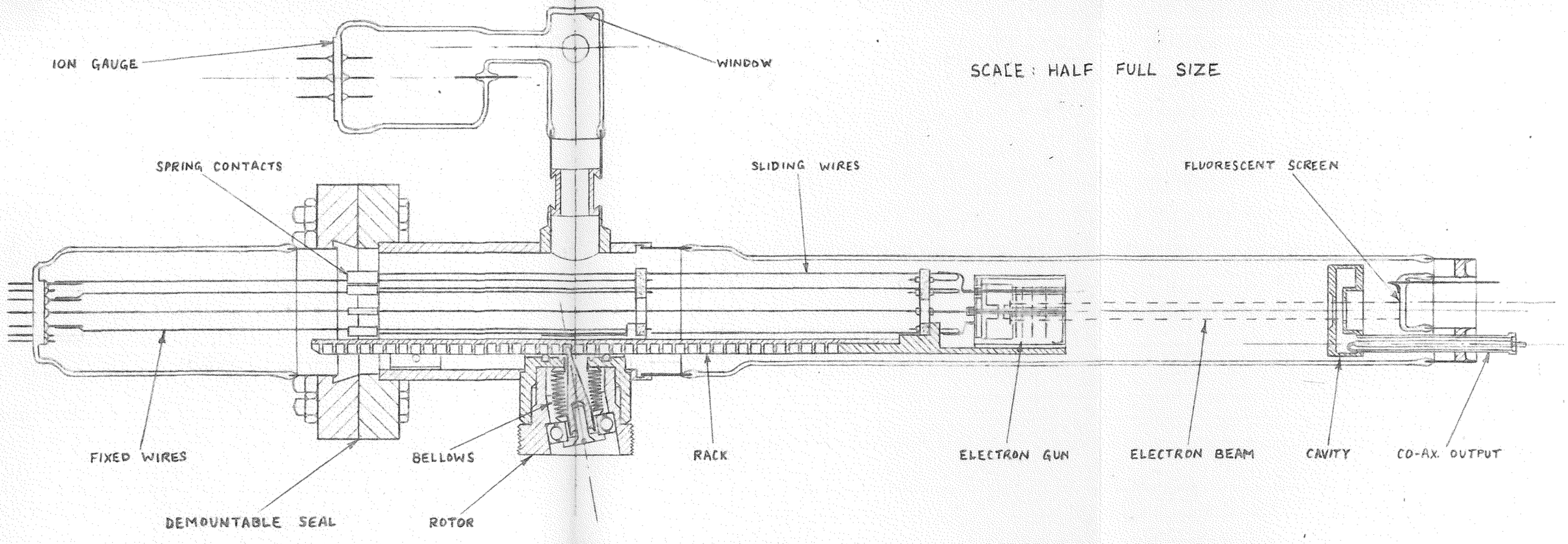


MOVING GUN ELECTRON TUBE FIG. 5.18

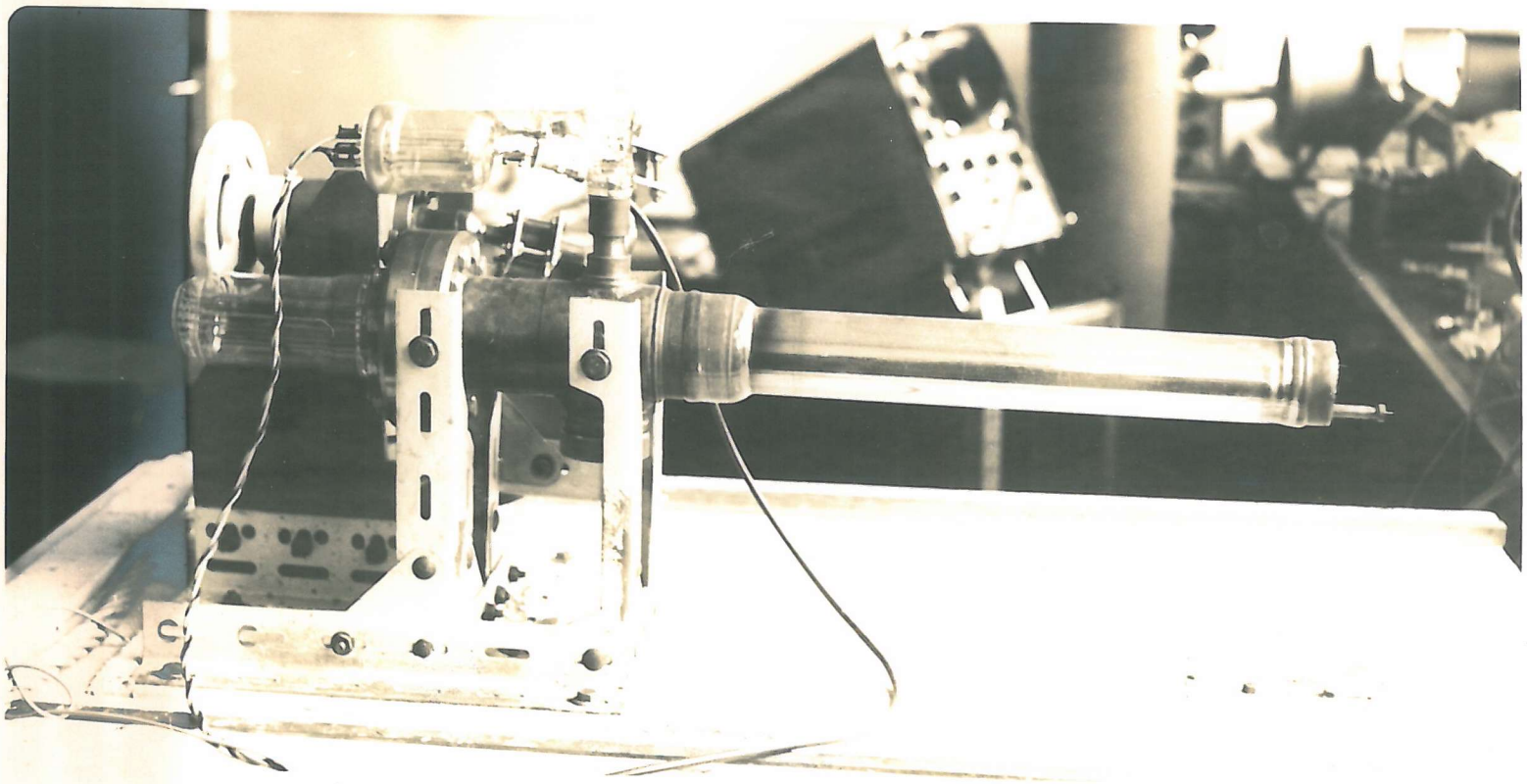

FIG.5.19 MOVING GUN ELECTRON TUBE

a sliding co-axial output from the cavity. Movement of the gun is achieved without sliding or rotating vacuum seals by means of the device shown in fig.5.20. A conical stainless-steel rod is mounted flexibily into the wall of the vacuum envelope by means of stainless-steel bellows. The free end of the bellows is screwed into the centre of a ball journal fitted into a rotor which can be turned about a vertical axis. The axis of the ball journal is inclined at $10^{\circ}$ to the vertical and the axis of the rod is held in this position, the free end of the bellows being pushed slightly sideways from its natural position. When the rotor is turned the axis of the rod (but not the rod) turns about a vertical axis while remaining at $10^{\circ}$ to the vertical. The free end of the bellows is pushed round in a circular path with a slight flexing of the walls. Because it is fixed into the bellows the rod cannot turn about its own axis. Relative rotation between the outer and inner of the ball journal allows the rotor to turn, but not the rod and bellows. The length of the rod and the position of the ball journal were chosen so that the small end of the rod rotates in a circle of diameter 0.30 inches and engages between the teeth of a rack machined as shown in fig.5.20. The rack is pushed forward 0.25 inches for every revolution of the rotor. This mechanism thus transforms rotary motion outside the vacuum envelope to linear motion inside it. The electron gun, attached to the rack, can be moved 10 inches along the tube axis by

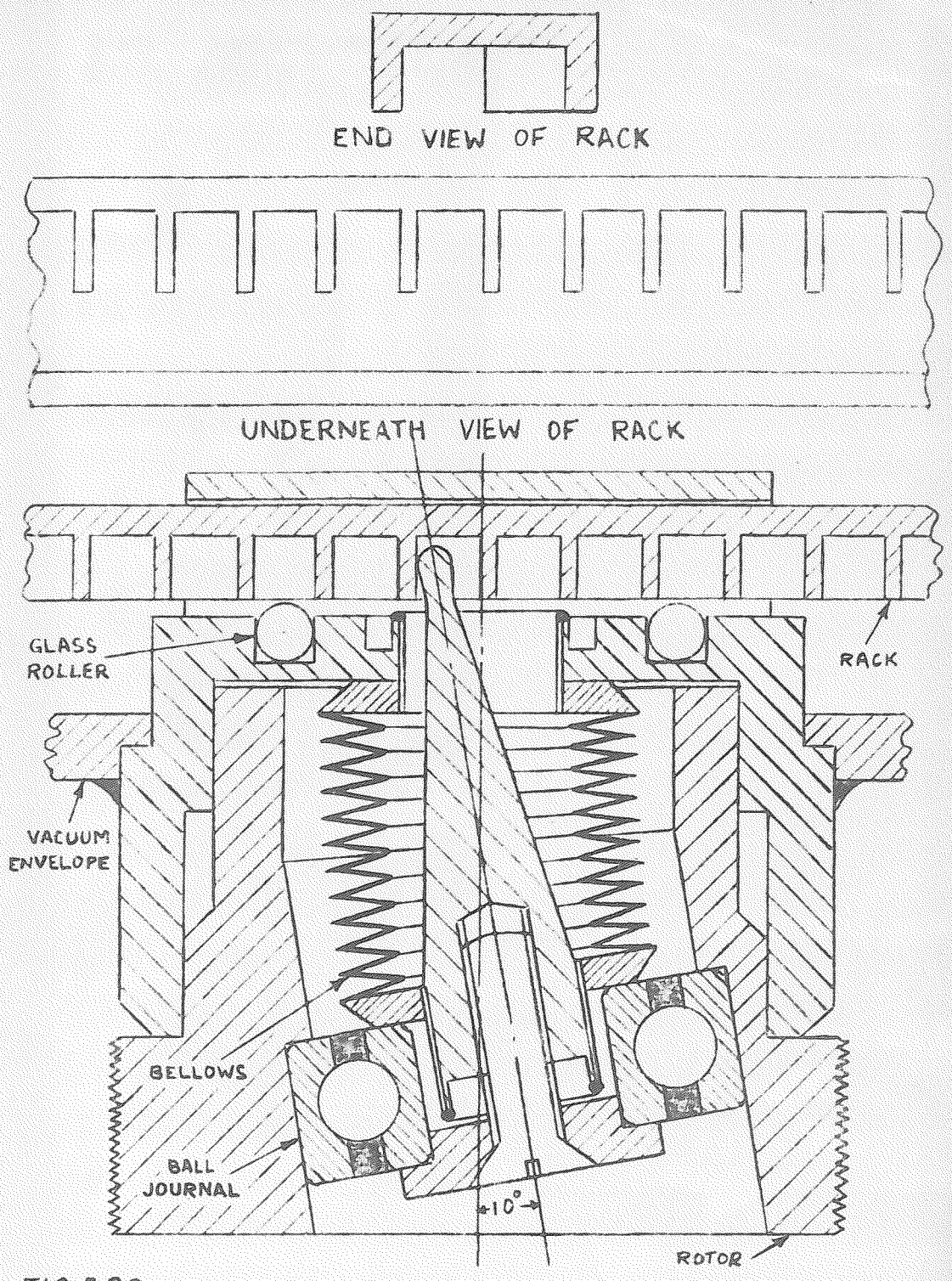


FIG.5.20 SCALE: X2

MECHANISM FOR MOVING ELECTRON GUN

turning the rotor 40 times.

The electrical connections to the gun anodes are by means of sliding spring contacts running along fixed stainless-steel wires. The connection to the cathode (earthed) is through the rack and main metal part of the tube. The cavity, and also the co-axial output and metal end of the tube, are at beam potential. A d.c. break, positioned as close to the tube as possible, is therefore necessary to allow for the potential difference between the cavity and the earthed waveguide system. The connection to the collector is via a separate pin.

The position of the gun is indicated by a scale on the rack viewed through a window in the exhaust stem. A conducting coating of aluminium was evaporated on to the inside of the glass tube. Connection to the coating is via the outer conductor of the co-axial output.

b) Cavity.

The re-entrant cavity was made using an electroforming process. A distrene mandrel was machined to the shape of the inside of the cavity as shown in fig.5.21(a). Copper was chemically deposited on its surface using the 'Sel-Rex Lectroless' process.[⌘] Once a conducting film had been formed the mandrel was transferred to a copper-plating bath. Sufficient copper was deposited to allow the final outside size as shown in fig.5.21(d) to be obtained by machining. To ensure a fairly even coating of copper the

⌘ Sel - Rex(U.K.) Ltd., Slough, Bucks.

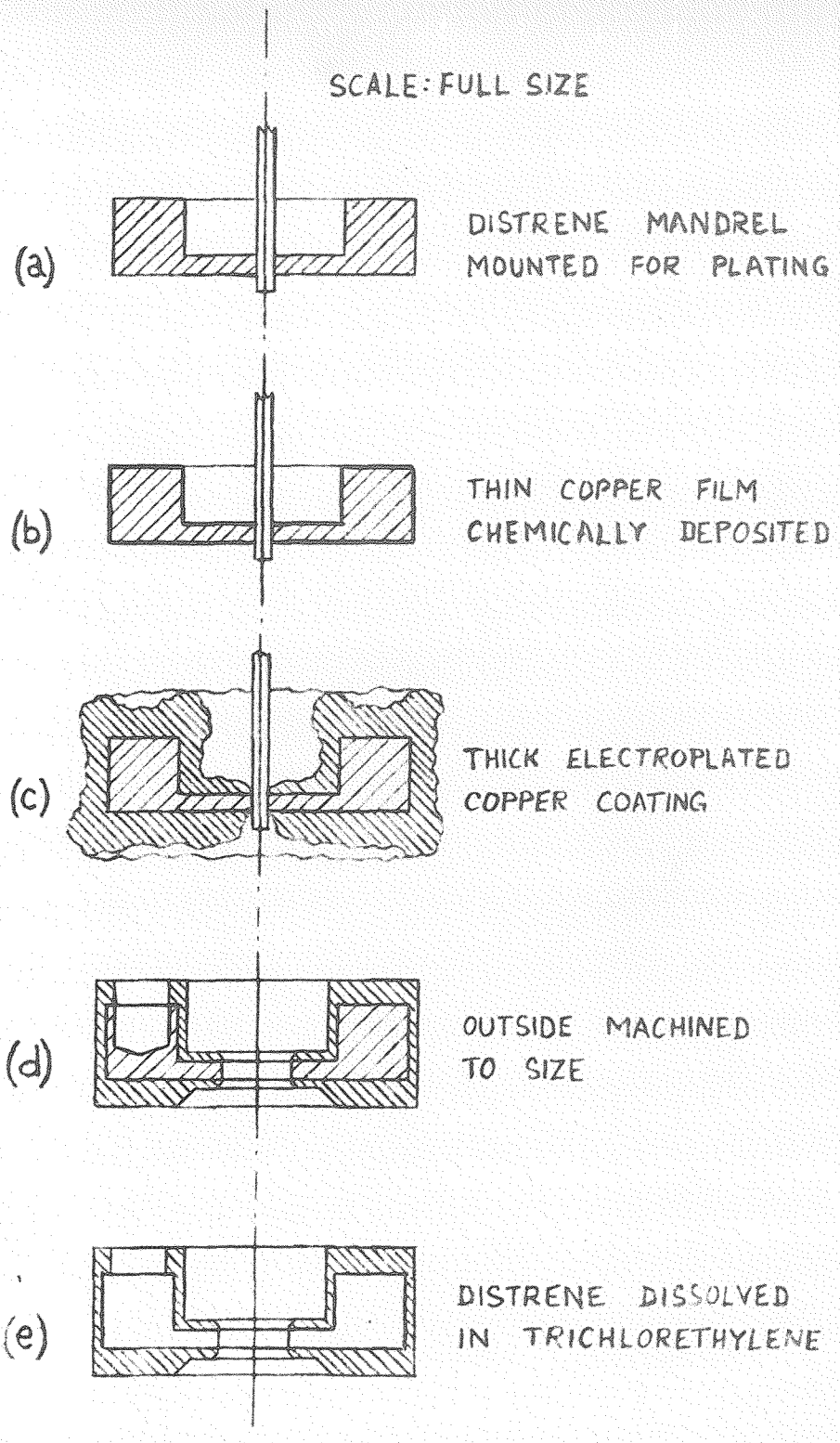


FIG. 5.21 ELECTROFORMING PROCESS

mandrel was rotated in the plating bath and its position relative to the axis of rotation was occasionally changed. After machining to size, holes for the electron beam and co-axial output were made. The distrene mandrel was then dissolved in boiling trichloretheylene, leaving a hollow cavity with a smooth internal surface and with no joins in the walls. Figs. 5.22 and 5.23 show the cavity before and after machining.

It was decided to make the resonant frequency as near as possible to 3Gc/s, this being a typical operating frequency of a backward-wave amplifier containing the type of electron gun under test. The cavity dimensions were calculated using design curves given by Moreno.[53] A re-entrant cavity consists essentially of a short length of co-axial transmission line terminated with a short-circuit at one end and with a capacitive load at the other. It was expected that the relatively large hole for the electron beam would reduce this capacitive load and give a higher resonant frequency than that calculated using the design curves where a negligibly small hole was assumed.

Because of the uncertainty of the resonant frequency, a test cavity was initially made having the dimensions shown in fig.5.24(a). According to the design curves the resonant frequency was 2.66Gc/s. Measurement showed the actual figure to be 2.70Gc/s, less of an increase than was expected. A correction derived from these two figures was applied to the calculations of the dimensions

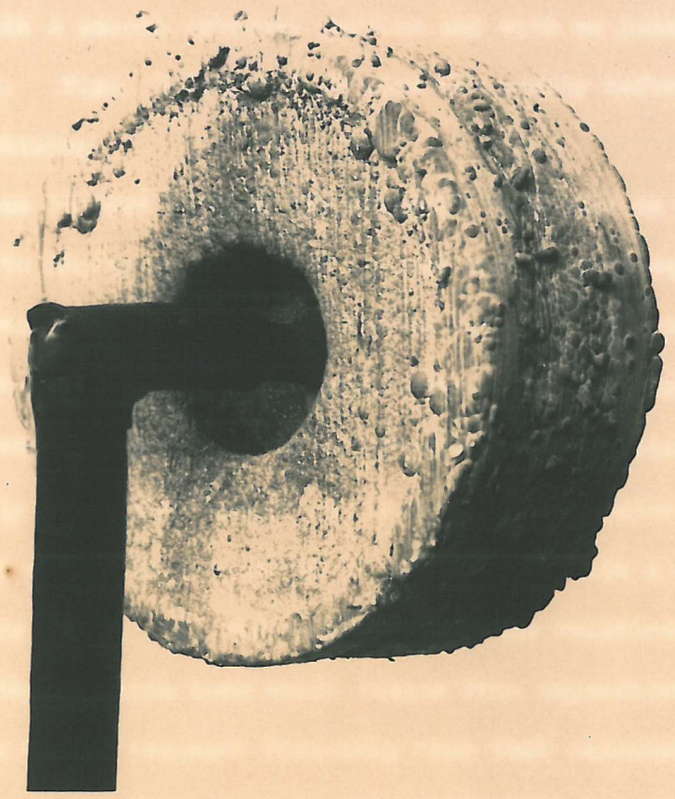

FIG.5.22 CAVITY BEFORE MACHINING

FIG.5.23 CAVITY AFTER MACHINING

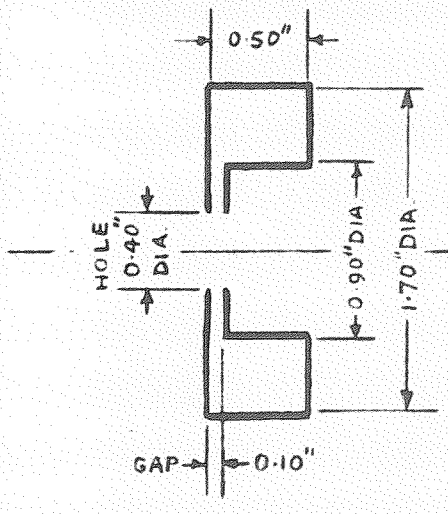


(a) TEST CAVITY
RESONANT FREQ.=2·66GC/S

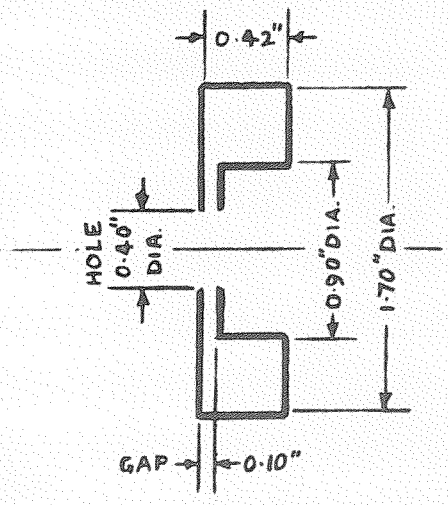


(b) FINAL DIMENSIONS
RESONANT FREQ=3·00GC/S

FIG.5.24 CAVITY INTERNAL DIMENSIONS

of the second cavity. The size for a theoretical resonant frequency of 3.00Gc/s worked out to be as shown in fig.5.24(b). The measured value for this cavity was, in fact, 3.00Gc/s.

The power from the cavity is taken out through the vacuum envelope by means of a short length of 50Ω copper co-axial line containing a matched glass/metal vacuum seal. This was supplied by the Services Electronics Research Laboratory through the courtesy of Mr. T.J. Bridges. The cavity is coupled to the co-axial output by means of a loop.

The cavity was matched to the output using the apparatus shown in fig.5.25. The klystron reflector voltage and the oscilloscope x - plates were swept at 50c/s and the y - plates were connected to the detector. The oscilloscope trace thus gave a direct indication of the power reflected from the cavity as the klystron frequency was swept across the mode. Resonance was indicated by a dip in this characteristic due to absorbtion of power by the cavity. The length of the coupling loop was adjusted to give the sharpest dip with total absorbtion of power at resonance. The wavemeter was used to measure the resonant frequency.

A triple-stub co-axial tuner was connected as close as possible to the cavity to provide rapid external correction for any slight mismatch occurring in the cavity coupling.

The equipment shown infig.5.26 was used to measure the unloaded Q-factor, $Q_0$, of the cavity. The method used was that described by Ginzton[54] where $Q_0$ is derived from the change of

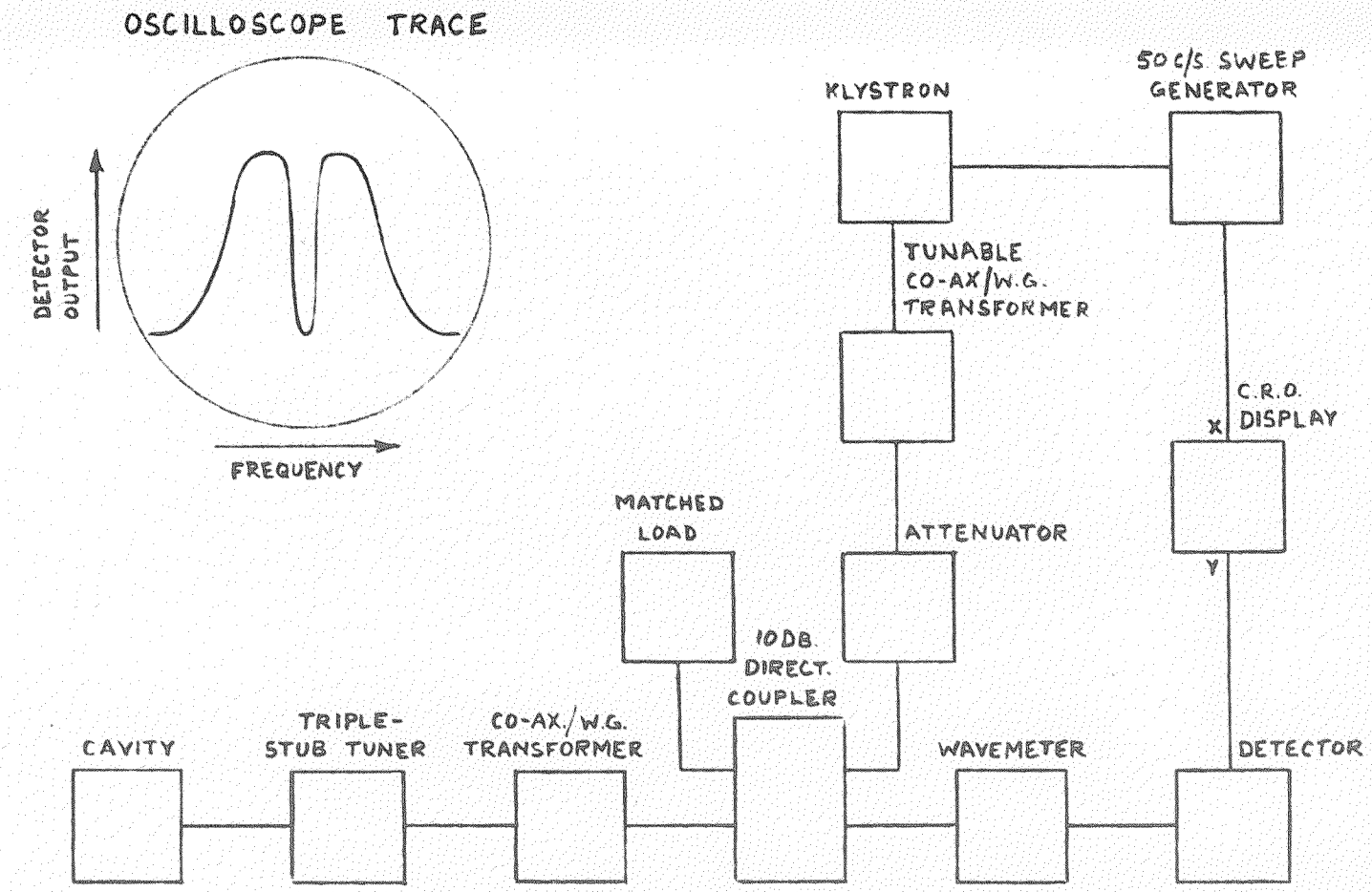


APPARATUS FOR SETTING UP CAVITY

FIG. 5.25

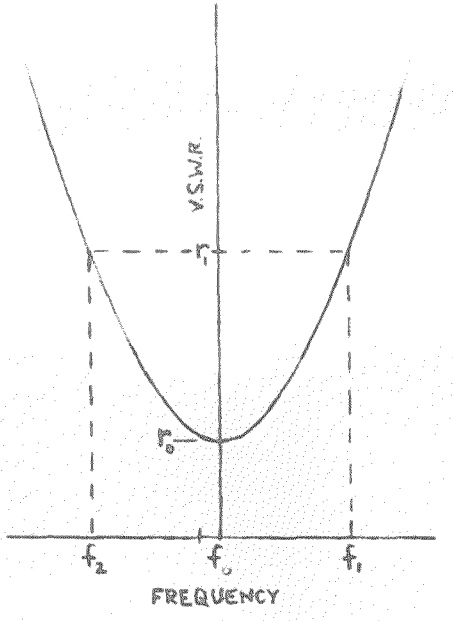


V.S.W.R. AGAINST FREQUENCY CHARACTERISTIC

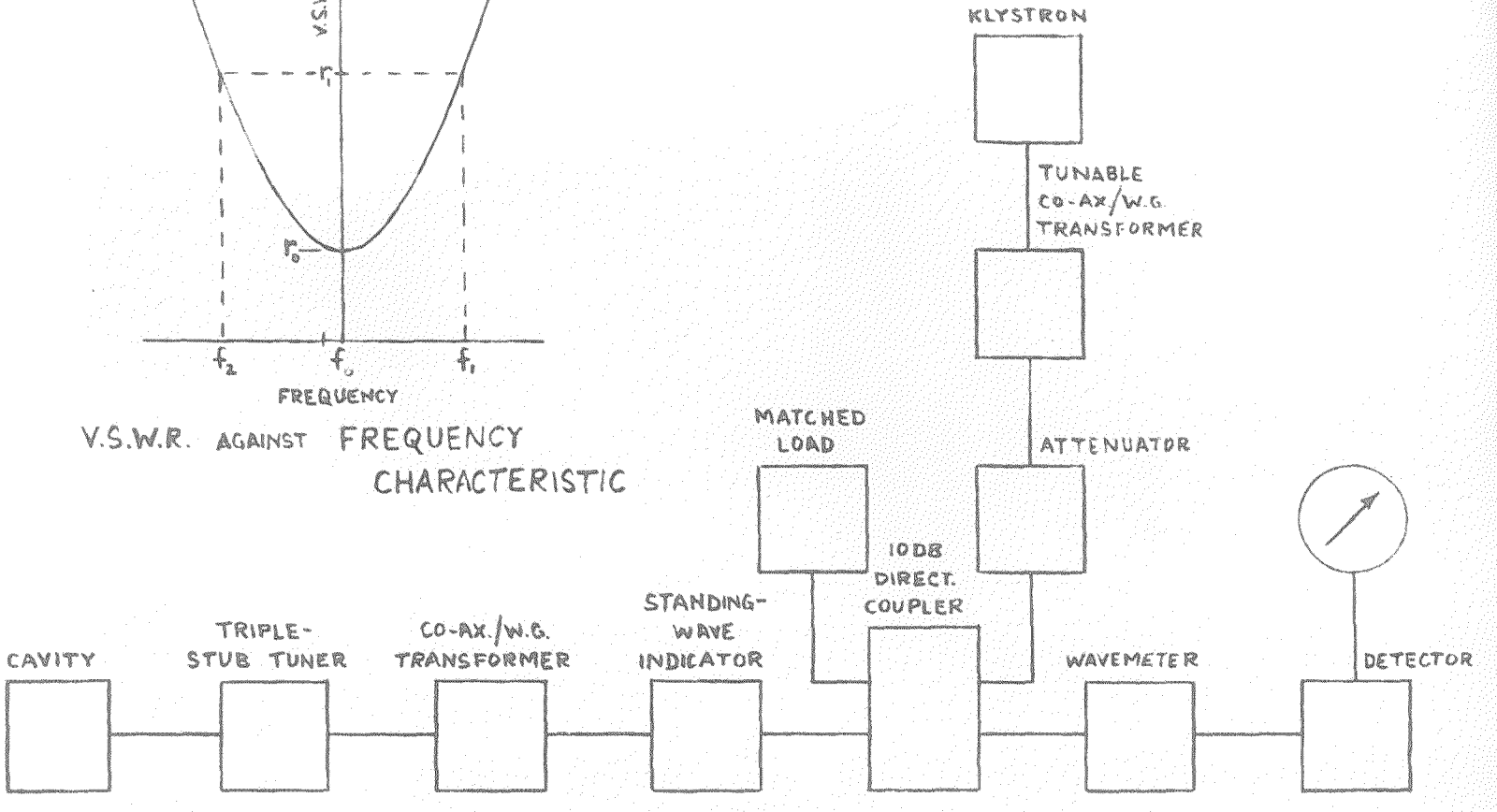


APPARATUS FOR MEASURING $Q_0$ OF CAVITY

FIG. 5.26

V.S.W.R. with frequency. First it is necessary to determine whether the cavity is overcoupled or undercoupled. If a voltage maximum occurs at the detuned short-circuit position it is overcoupled, and a voltage minimum indicates undercoupling. The detuned short-circuit is the position of the voltage minimum with the cavity detuned (in this case passing a piece of metal through the hole in the cavity detuned it adequately). The V.S.W.R. against frequency characteristic is as shown in fig.5.26. The V.S.W.R. at resonance $r_o$ gives the coupling coefficient $\beta$ by the relationship:

if the cavity is overcoupled $r_o = \beta$ (5.2)

if the cavity is undercoupled $r_o = \frac{1}{\beta}$ (5.3)

$Q_o$ is given by the expression:

$$Q_o = \frac{f_o}{f_1 - f_2} \qquad (5.4)$$

where $f_o$ is the resonant frequency.

$f_1$ and $f_2$ are frequencies at which the V.S.W.R. $r_1$ is:

$$r_1 = \frac{2 + \beta^2 + \sqrt{4 + \beta^4}}{2\beta} \qquad (5.5)$$

By this means the $Q_o$ of the cavity was found to be 2500.

## 5.11 Microwave Measuring Equipment

Fig.5.27 shows the layout of the equipment used for measuring the noise output power of the cavity. The components are as follows:

FIG. 5.27 MICROWAVE MEASURING APPARATUS

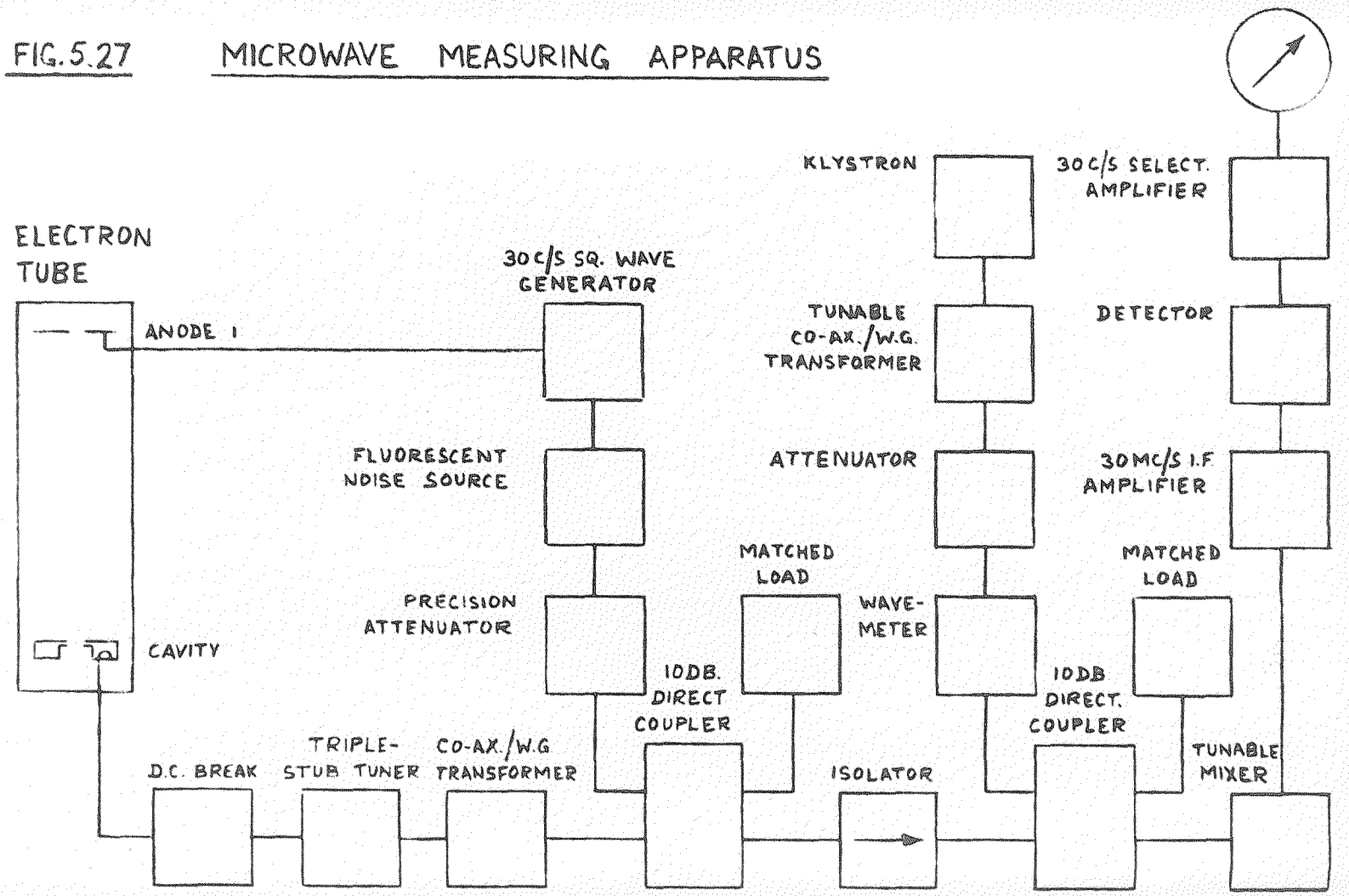

| | |
|---|---|
| D.C. break | Microlab HR-52N |
| Triple stub tuner | Microlab S3 - 15N |
| Co-ax. to w.g. transformer | Admiralty (on loan) |
| Fluorescent noise source | Bendix TD38 tube in Mid-Century MC10/32 mount. |
| Precision attenuator | Mid-Century MC10/3A |
| 10dB directional couplers | Mid-Century MC10/14 |
| Matched loads | Mid-Century MC10/20 |
| Isolator | Microwave Associates MA170 |
| Klystron | C.V.35 in Admiralty mount. |
| Tunable transformer | Mid-Century MC10/9 |
| Wavemeter | Mid-Century MC10/2 |
| Tunable mixer | Mid-Century MC10/17 |

The remainder of the equipment was made at the University.

The basis of the noise-measuring equipment is a radiometer system in which the electron beam and a reference noise source are pulsed at 30c/s. The phase of the pulses is such that when the beam is switched on the noise source is off, and vice-versa. The signal from the cavity and the attenuated signal from the noise source are fed into the measuring system. The difference between these two signals is indicated by the magnitude of the 30c/s square wave at the measuring system output. The power from the cavity can be determined from the amount of attenuation of the noise source necessary to reduce this 30c/s output to zero.

The noise tube has an output of 15.27dB above thermal noise

at the normal operating current of ~~20~~ 200mA and is specially designed for use under pulsed conditions. The power supply is a modified version of that described by Beam and Hughes[55]. The noise tube is switched on and off using a square-wave pulse generator which also supplies the voltage to anode 1 of the electron gun. When the noise tube is on, the beam is switched off by reducing anode 1 voltage to zero. When the noise tube is off, the gun works normally, anode 1 voltage being set by altering the height of the pulse supplied to it.

A 10dB directional coupler is used to feed the signals from the cavity and the noise source into the amplifying section of the apparatus. The superheterodyne system has a single-ended crystal mixer and a klystron as the local oscillator. The 30Mc/s i.f. amplifier consists of a pre-amplifier with a 5Mc/s bandwidth and a gain of 40dB, followed by an amplifier of 20Mc/s bandwidth with a gain of 60dB. It was found necessary to insert an attenuator of 30dB between the amplifiers to stop them oscillating.

Fig.5.28(a) shows the type of signal to be expected at the i.f. amplifier output where, for example, the contribution from the noise source is greater than that from the cavity. The feature of interest in this waveform is the difference between the mean noise amplitudes due to the elctron beam and the noise source. This difference is emphasized by first detecting the signal to give the waveform shown in fig.5.28(b). It is then

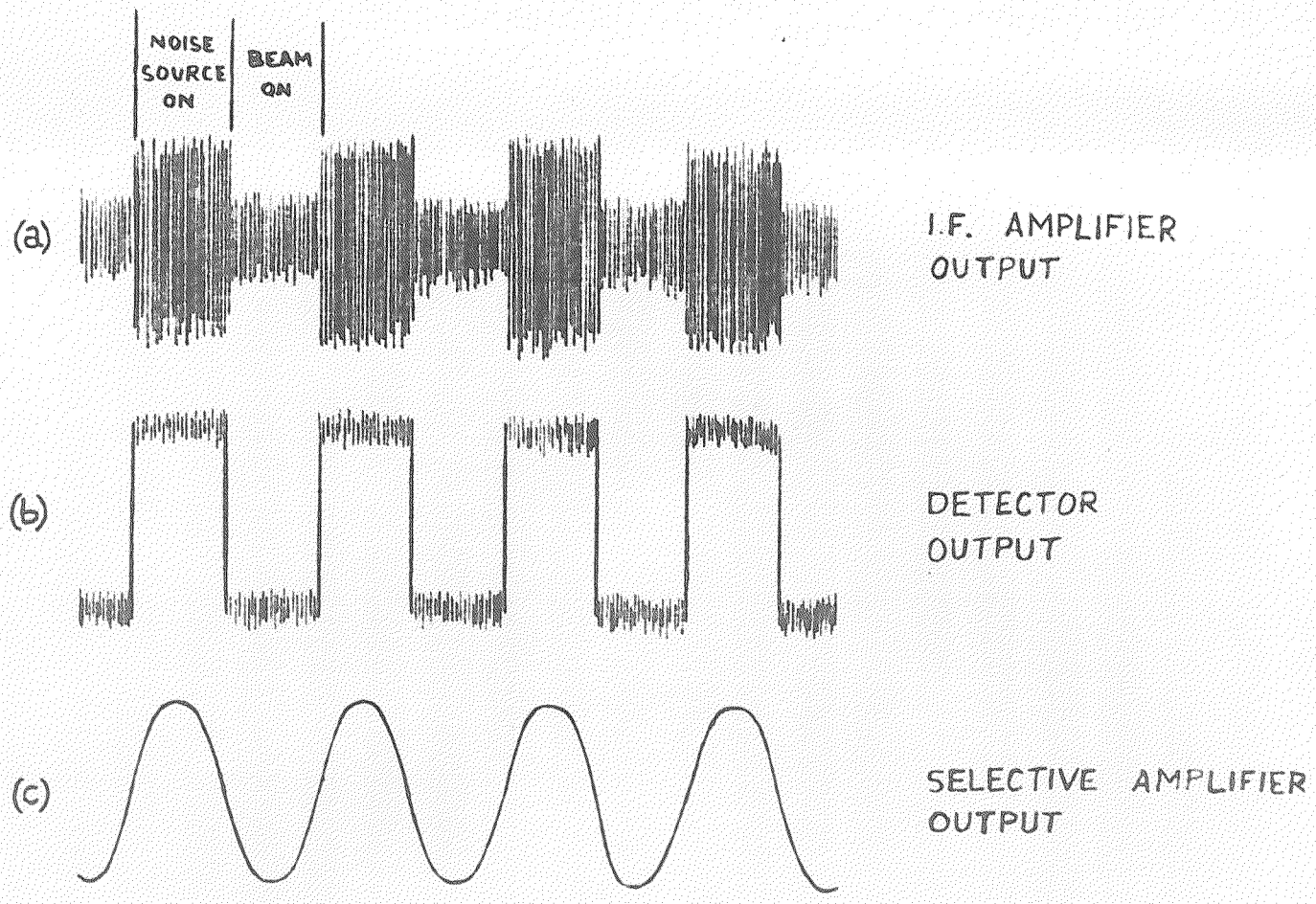


FIG. 5.28 MEASURING SYSTEM WAVEFORMS

passed through a selective amplifier with a gain of 30dB and Q factor of about 70 to select and amplify only the 30c/s component of interest.

To make a measurement of power output from the cavity, the attenuator in series with the noise source is adjusted to give as near zero output as possible from the selective amplifier. It is then known that the contribution from the cavity and from the noise source are equal at the input to the i.f. amplifier. A reading of relative power from the cavity can then be obtained from the reading of the noise-source attenuator.

The bandwidth of the cavity is less than that of the i.f. amplifier. The noise power from the cavity when the beam is switched on is therefore limited by its bandwidth. The noise source emits power over the whole of S- band. When the noise source is switched on, the signal at the i.f. amplifier output consists of contributions from the noise source at $f_o + f_1$ and $f_o - f_1$ ($f_o$ = l.o. frequency, $f_1$ = i.f.) at a bandwidth equal to that of the i.f. amplifier. In fact only relative readings of power from the cavity are required and the noise source is used only as a power reference. The actual amplitude and bandwidth of the noise source signal is therefore unimportant as long as the power level remains stable.

The main advantage of the radiometer system is that, in theory, noise from the local oscillator, mixer and i.f. amplifier do not affect the measurements. Noise from these

sources is present all the time but, as the system is sensitive only to changes of noise level at 30c/s, it has no effect. It is advisable, however, to keep these sources of noise to a minimum because the sensitivity of the system would be impaired if the signals being amplified were swamped by noise from the amplifying system. For this reason a low-noise klystron is used and the pre-amplifier was specially designed to have a low noise figure.

The microwave measuring system was tested using a signal generator to simulate the signal from the cavity. The sensitivity of the system was found to be such that a signal level of the order of $10^{-3}\mu W$ could be measured.

# 6. RESULTS

## 6.1 D.C. Characteristics

The d.c. characteristics of the electron guns of tubes 1 and 2 were almost identical. The results obtained using these two tubes are therefore grouped together.

The following symbols are used for electrode voltages etc. (see fig.3.1 for electrode arrangement). All voltages are quoted with respect to the cathode.

| | |
|---|---|
| Control electrode voltage | $V_c$ |
| Anode 1 voltage | $V_1$ |
| Anode 2 voltage | $V_2$ |
| Anode 3 voltage | $V_3$ |
| Anode 4 voltage | $V_4$ |
| D.C. beam current | $I_b$ |

Magnetic focusing field strength B

The inner section of each electrode was linked to the corresponding outer section

Only $V_c$, $V_1$ and $V_2$ affected $I_b$ under normal operating conditions. Anodes 3 and 4 form the transducer for optimum adjustment of the beam parameters for minimum noise when the gun is used in a low-noise amplifier. In the measurements of the d.c. characteristics the voltages on these electrodes were set at typical values of $V_3$ = 50V and $V_4$ = 200V.

Figs. 6.1 and 6.2 show how $I_b$ varied with changes of $V_c$, $V_1$ and $V_2$. To plot fig.6.1, $V_2$ was held constant at a typical value of 10V. Similarly in fig.6.2, $V_1$ was held at 10V.

It can be seen that two distinct modes of operation existed,

FIG. 6.1

VARIATION OF $I_b$ WITH $V_c$ AND $V_1$

$V_2 = 10$ VOLTS

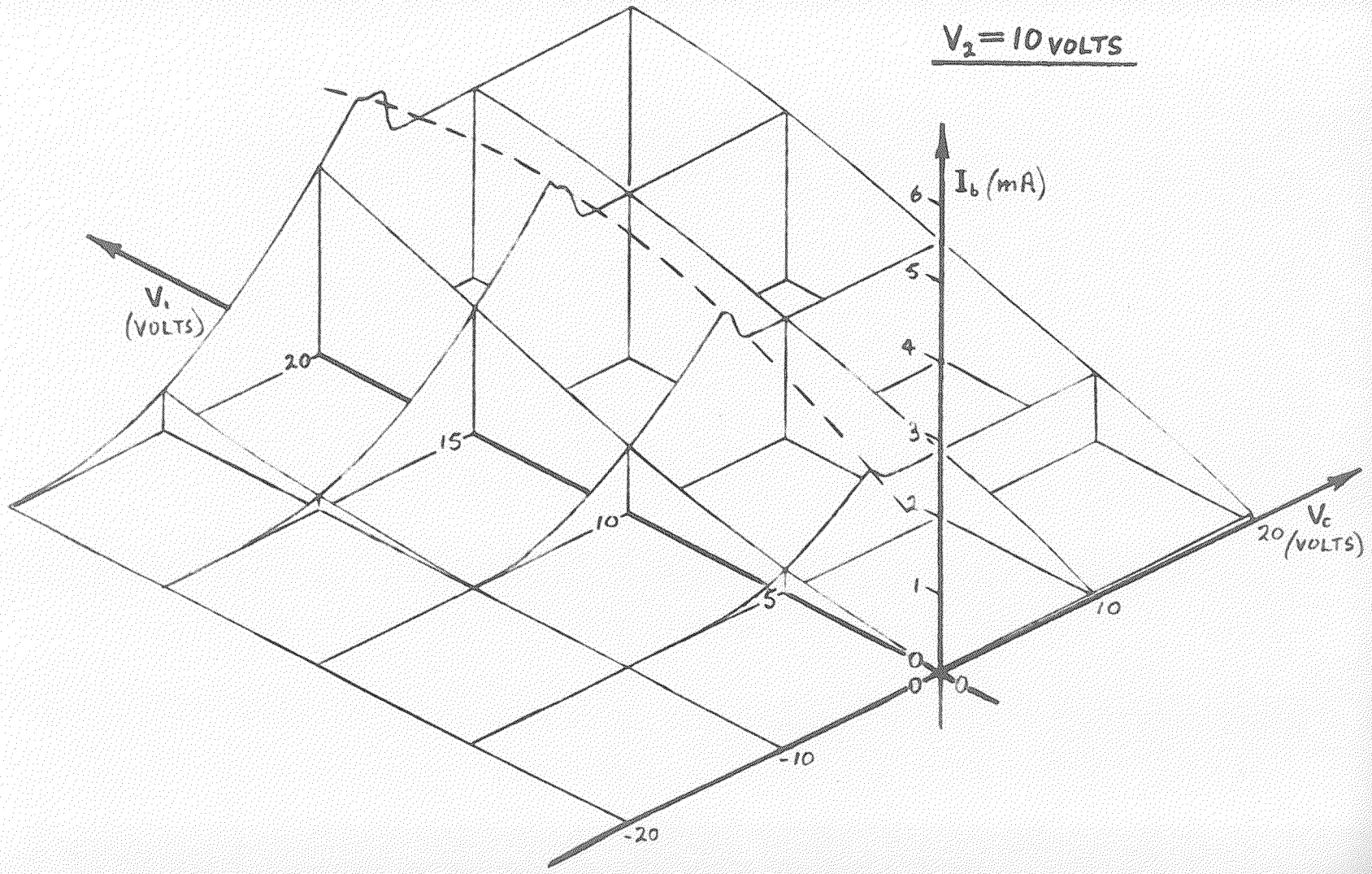

FIG. 6.2

VARIATION OF $I_b$ WITH $V_c$ AND $V_2$

$V_1 = 10$ VOLTS

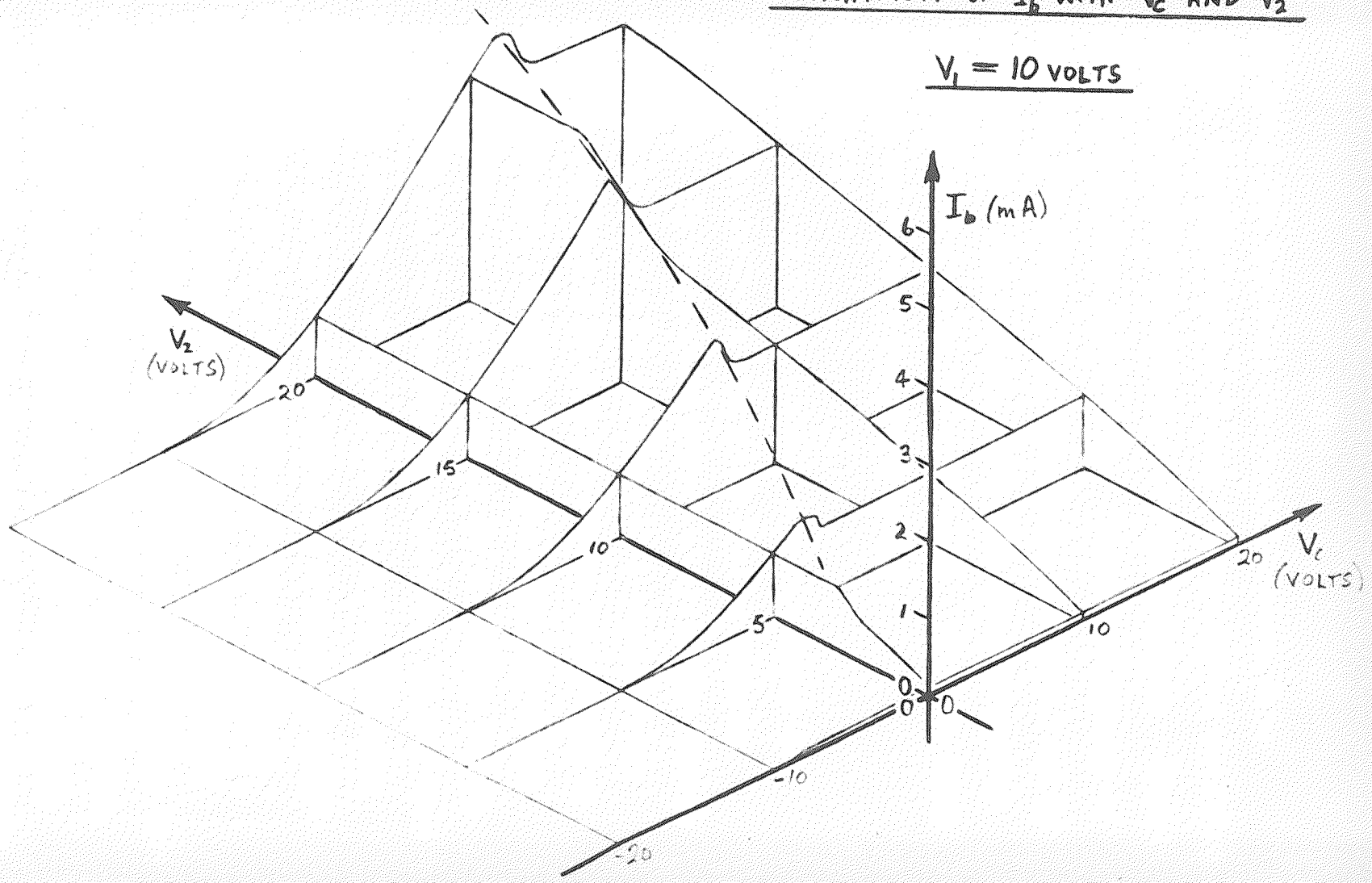

the dotted line indicating the transition between these modes. Fig.6.1 shows that in mode 1 (to the left of the dotted line) $I_b$ increased as either $V_c$ or $V_1$ were increased. Fig.6.2 shows that $V_2$ had no effect on $I_b$. In mode 2 an increase of either $V_1$ or $V_2$ increased $I_b$ as indicated in figs. 6.1 and 6.2 respectively. Increasing $V_c$ caused $I_b$ to decrease near the transition point from one mode to the next. At higher values of $V_c$, $I_b$ was virtually independent of $V_c$.

6.2 Beam Profiles

Figs. 6.3 and 6.4 are a series of photographs of the electron-beam profiles as seen on the fluorescent-screen collector. The bright areas indicate a high current density. These photographs show how the beam profile changed in the transition region from one mode of operation to the other as $V_c$ was increased. $V_1$ and $V_2$ were held constant at 30V and 14V respectively for fig. 6.3, and at 15V and 25V for fig.6.4.

Fig.6.3 shows the transition most clearly. In mode 1, at relatively low values of $V_c$, the current density was fairly uniform over the whole cathode surface as shown in fig.6.3(a). The brightness of the image increased as $I_b$ was increased. The transition into mode 2 took the form of a fairly sudden reduction of current in the centre of the annulus only (i.e. mid-way between the outer and inner edges). As $V_c$ was increased, the dark area caused by this current reduction spread rapidly round the annulus. Various stages in this transition are shown

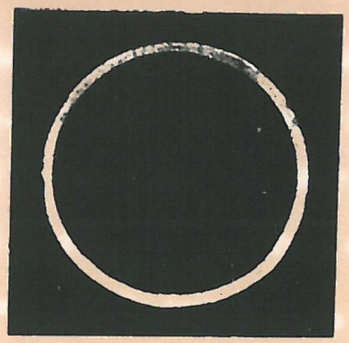

(a) $V_c = -3V$
$I_b = 4{\cdot}97mA$

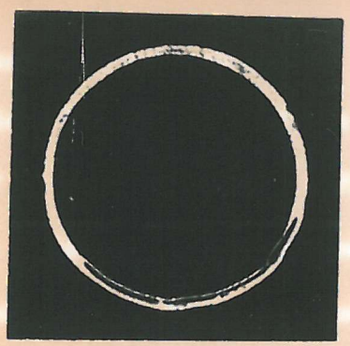

(b) $V_c = -0{\cdot}8V$
$I_b = 4{\cdot}92mA$

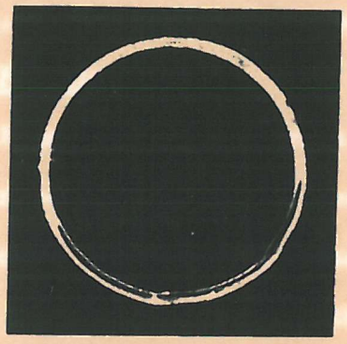

(c) $V_c = 0V$
$I_b = 4{\cdot}85mA$

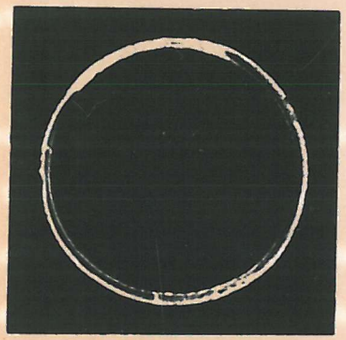

(d) $V_c = 0{\cdot}7V$
$I_b = 4{\cdot}22mA$

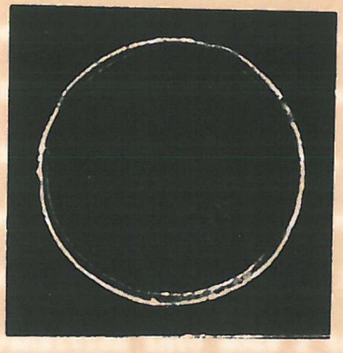

(e) $V_c = 3V$
$I_b = 3{\cdot}60mA$

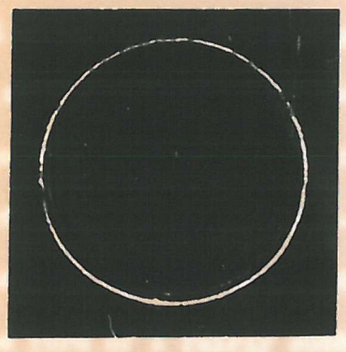

(f) $V_c = 2{\cdot}0V$
$I_b = 3{\cdot}25mA$

FIG. 6.3

BEAM PROFILES WITH $V_1 = 30V$ $V_2 = 14V$ $B = 0{\cdot}16\ Wb/m^2$

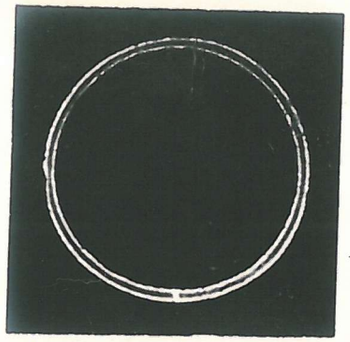

(a) $V_c = 10V$
$I_b = 4{\cdot}13mA$

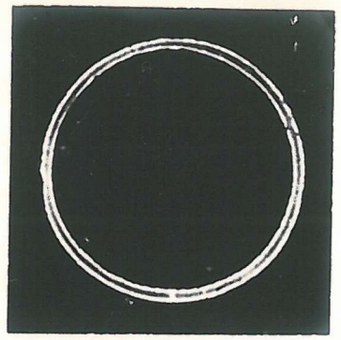

(b) $V_c = 14V$
$I_b = 4{\cdot}70mA$

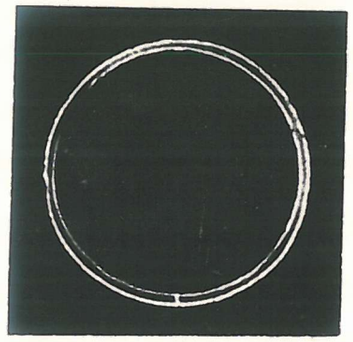

(c) $V_c = 15V$
$I_b = 4{\cdot}29mA$

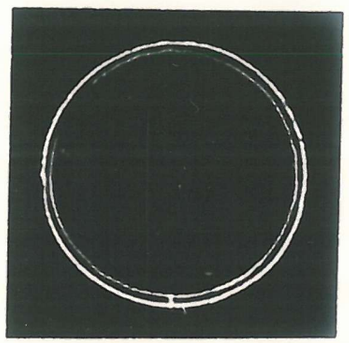

(d) $V_c = 17V$
$I_b = 3{\cdot}83mA$

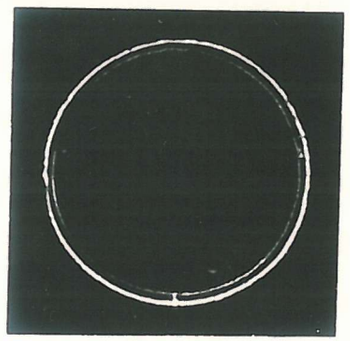

(e) $V_c = 20V$
$I_b = 3{\cdot}74mA$

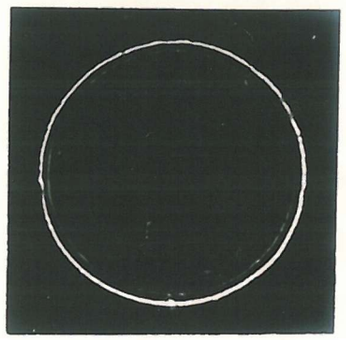

(f) $V_c = 30V$
$I_b = 3{\cdot}57mA$

FIG 6.4

BEAM PROFILES WITH $V_1 = 15V$ $V_2 = 25V$ $B = 0{\cdot}16 Wb/m^2$

in fig.6.3(b)-(d). Fig.6.3(e) and (f) show that in mode 2 there was little change in the beam structure as $V_c$ was further increased, except for a slight blurring of the image on the screen which can just be seen in fig.6.3(f). The reduced current in the centre of the annulus gave the beam the appearance of two concentric beams when operating in mode 2. In fig.6.3 the 'outer' beam is much more prominent than the 'inner'beam.

In fig.6.4 conditions were such that the transition from one mode to the other occurred at a higher value of $V_c$. Consequently the current density was higher at the edges of the annulus than in the centre when operating in mode 1, as shown in fig.6.4(a) and (b). The transition to mode 2 was again caused by a reduction of current in the centre of the annulus only (figs.6.4(c) and (d)). This change is not as clear as in fig.6.3 because of the bright edges of the annulus in mode 1. There was little change in the beam after transition to mode 2 as shown in figs.6.4(e) and (f).

Movement of the fluorescent screen along the beam axis showed no change in the beam structure or dimensions under all operating conditions. All the beam profile changes observed therefore took place within the gun itself as expected.

## 6.3 Hysteresis Effects

Under certain conditions hysteresis was observed in the beam current. Fig.6.5, an oscilloscope trace of the $I_b$ against

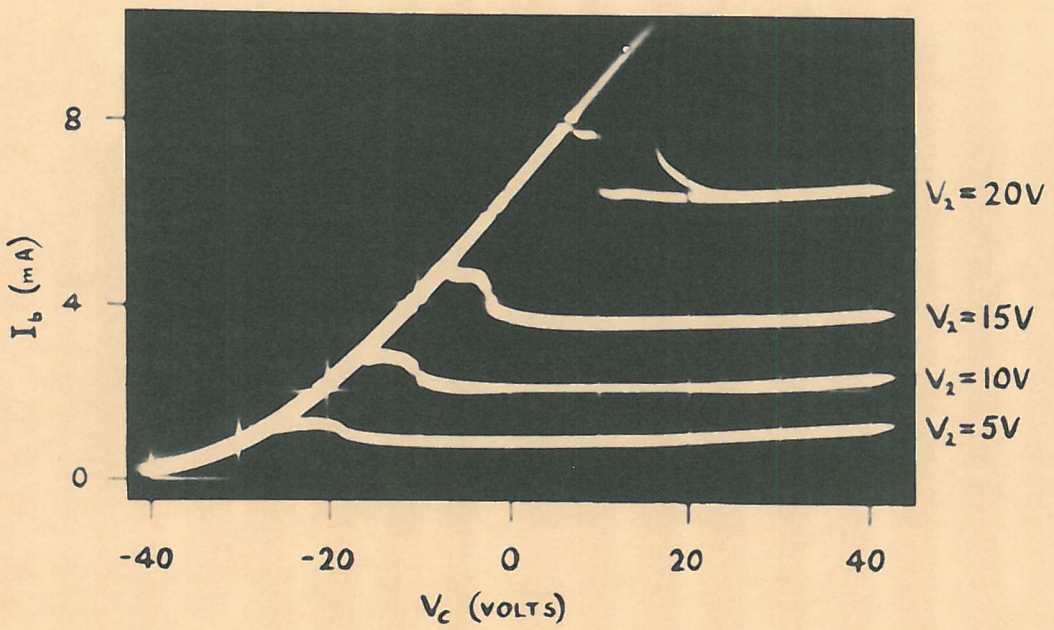


FIG.6.5 VARIATION OF $I_b$ WITH $V_c$ $V_1$ = 30V

$V_c$ characteristic obtained by sweeping $V_c$ at 50c/s, shows this effect when $V_2$ was adjusted to give a fairly high maximum value of $I_b$. When $V_c$ was increased the transition into mode 2 was delayed beyond the point at which the transition back into mode 1 occurred when $V_c$ was decreased again. $I_b$ therefore rose to a higher maximum value when $V_2$ was increased than when it was decreased and the $I_b$ against $V_c$ characteristic thus described a hysteresis loop. The delay, and hence the size of the loop, appeared to depend greatly on the speed at which $V_c$ was changed. If $V_c$ was changed at the rate of a few seconds per cycle, hysteresis could be induced at about 3mA beam current compared with 8mA in fig.6.5.

6.4 Explanation of D.C. Characteristics and Beam Profiles

Berghammer[28] first suggested the explanation of these characteristics by the '6L6 effect'. He made an analogy between the anode 1 - 2 region of the low-noise electron gun and the grid-anode region of the 6L6 beam power tube. In this tube limitation of the anode current is found to occur due to the formation of a virtual cathode.

Virtual cathode formation has been analysed in detail by Salzberg and Haeff[29], assuming an infinite one-dimensional electron beam. Because of this assumption the calculation is not directly applicable to the low-noise electron gun. It does give a good picture, however, of the type of processes involved in virtual cathode formation, and a summary of the

results of the analysis is presented here.

Consider a region of infinite extent in two directions bounded by two parallel ideal grids in the third direction. These grids, through which all electrons can pass, have potentials of $V_x$ and $V_y$ and are a distance a apart. Electrons from a cathode at zero potential are injected into the region through grid x. Electron flow is normal to the grids.

Suppose, for example, that $V_x = V_y$. In the absence of any injected current the potential distribution in the region is constant as shown in fig.6.6a.

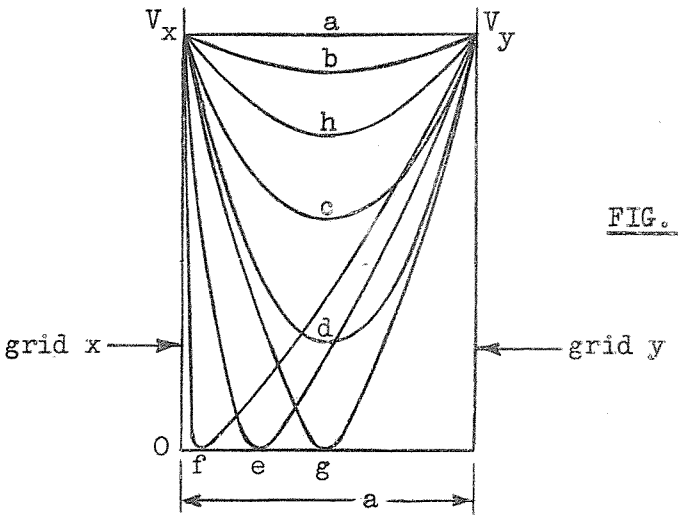


FIG. 6.6

As the injected current density $J_x$ is increased, the potential between the two grids is depressed by the effects of space charge as shown in fig.6.6b and c. As the minimum potential is greater than zero all the electrons entering the region pass through it and the transmitted current $J_y$ is equal to $J_x$. This mode of operation corresponds to the linear portion of the $J_y$ against $J_x$ curve, fig.6.7a-d.

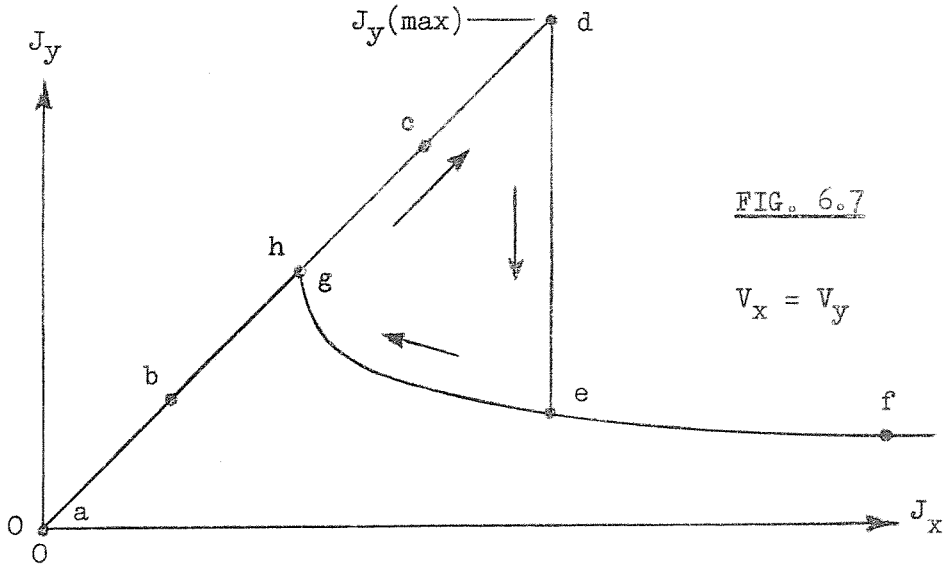


FIG. 6.7

$V_x = V_y$

When $J_x$ is increased sufficiently for the potential minimum to be depressed to the value shown in fig.6.6d, it suddenly decreases to zero and some of the electrons are turned back towards the cathode (the slower ones, assuming a small velocity spread). The space charge becomes stronger in the grid x - potential minimum region than in the potential minimum - grid y region because of the returning electrons and the potential minimum shifts instantaneously towards grid x to the position shown in fig.6.6e. In this position an appreciable number of electrons are turned back and the transmitted current density $J_y$ drops abruptly as shown in fig.6.7d-e. Further increase of $J_x$ shifts the potential minimum further twoards grid x with a slight decrease of $J_y$, as shown in fig.6.7e-f.

A rather different sequence of events takes place when $J_x$ is decreased again. Instead of changing abruptly as before, $J_y$ follows a smooth curve as shown in fig.6.7f-g. The potential

minimum moves away from grid x until it is mid-way between x and y in the position shown in fig.6.6g. Here $J_y = J_x$ and when $J_x$ is further decreased the potential minimum increases suddenly to the value shown in fig.6.6h. The original $J_y = J_x$ curve (fig.6.7h-a) is then followed.

A hysteresis effect in the $J_y$ against $J_x$ characteristic is thus predicted due to two theoretically possible solutions for $J_y$ over a range of $J_x$ values. Which solution is applicable appears to depend on whether $J_x$ is being increased or decreased.

Mathematically the linear part of the characteristic, where all injected electrons are transmitted (fig.6.7a-d), is given by the expression:

$$J_x = J_y \qquad (6.1)$$

The maximum transmitted current density (fig.6.7d) is given by:

$$J_y(\max) = K^2\left[V_x^{\frac{1}{2}} + V_y^{\frac{1}{2}}\right]^3 \qquad (6.2)$$

where $K = \frac{2}{3}\frac{\epsilon_o^{\frac{1}{2}}}{a}\left[\frac{2e}{m}\right]^{\frac{1}{4}}$ (6.3)

and $\epsilon_o$ = permittivity of free space

$\frac{e}{m}$ = electron charge/mass ratio

The curved part of the characteristic, where $J_y$ is limited

by returning electrons (fig.6.7f-h), is given by:

$$\left[\frac{V_y}{V_x}\right]^{\frac{3}{2}} = J_y\left[\frac{1}{KV_x^{\frac{3}{4}}} - \frac{1}{(J_x - J_y)^{\frac{1}{2}}}\right]^2 \qquad (6.4)$$

From equation 6.4, if the injected current is high compared with the transmitted current:

$$J_y \approx K^2 V_y^{3/2} \qquad (6.5)$$

This equation is identical to Child's Law, showing that for high degrees of space-charge limitation the potential minimum behaves like a space-charge limited thermionic cathode for changes of $V_y$. Thus the term 'virtual cathode' is used for a potential minimum which transmits only a fraction of the electrons reaching it.

Figs.6.8 and 6.9 are plotted from equations 6.1 - 6.4 and show how the $J_y$ against $J_x$ characteristic varies when $V_x$ is changed (fig.6.8) and when $V_y$ is changed (fig.6.9). Apart from the sharp peaks figs. 6.8 and 6.9 bear a resemblance to the measured characteristics shown in figs. 6.1 and 6.2. The similarity of these curves indicates that the formation of a virtual cathode is the cause of the observed beam current limiting.

Referring to the measured characteristics, mode 1 corresponds to the state where the current is insufficient to form a virtual cathode. Thus all electrons leaving the cathode region and reaching anode 1 pass through the anode 1 - 2 region

$J_y$ PLOTTED AGAINST $J_x$ FIG. 6.8

$J_x$ AND $J_y$ NORMALIZED WITH RESPECT TO $V_y$

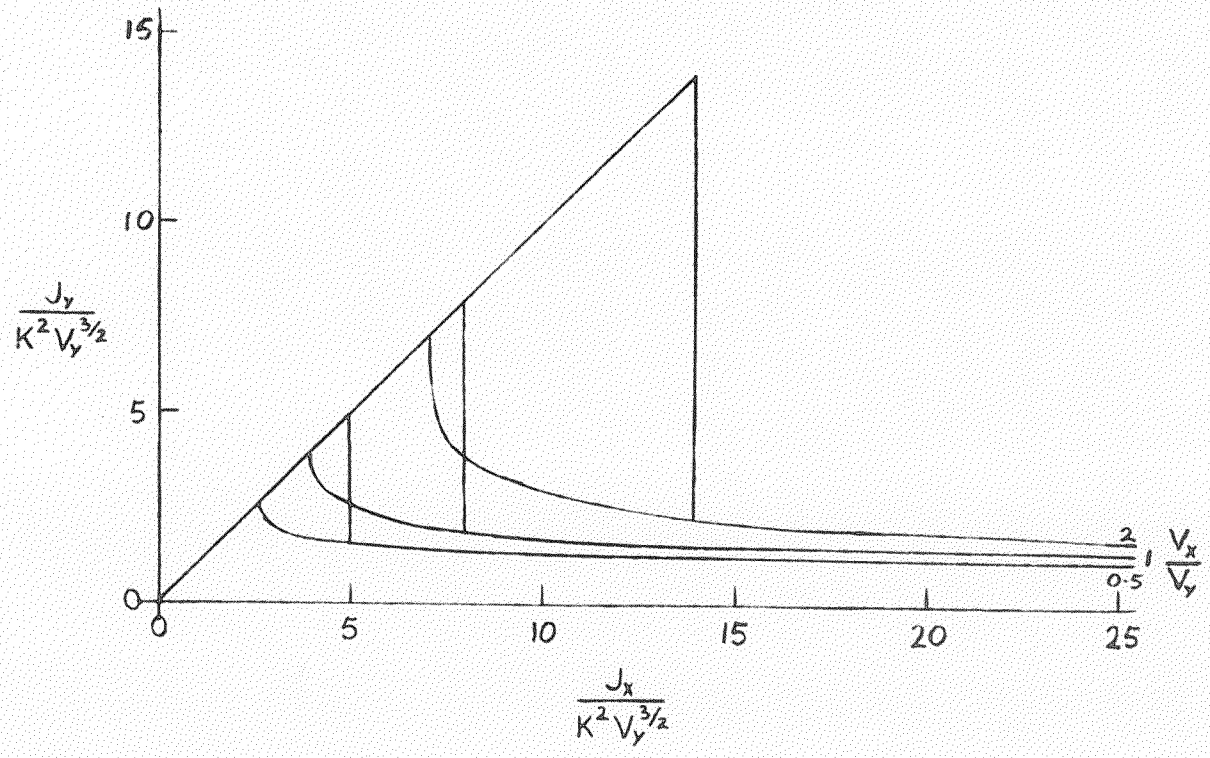

$J_y$ PLOTTED AGAINST $J_x$ FIG. 6.9

$J_x$ AND $J_y$ NORMALIZED WITH RESPECT TO $V_x$

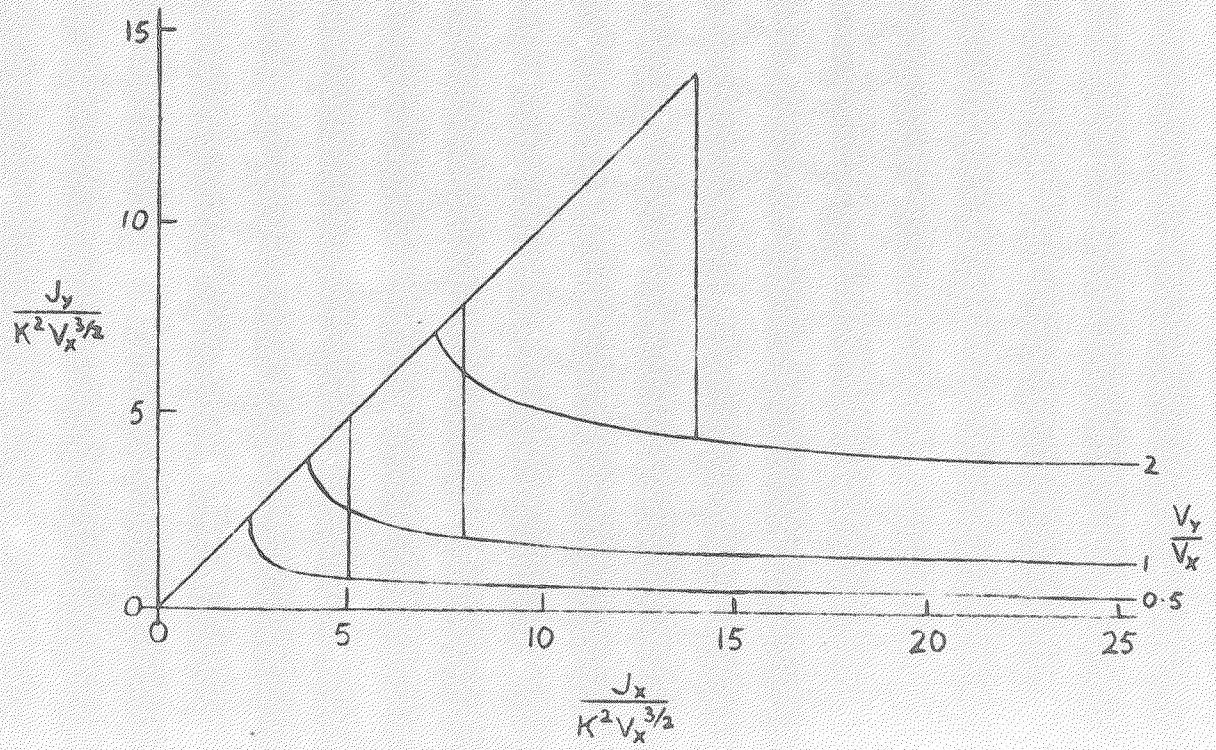

to the beam. Figs. 6.1 and 6.2 show that the beam current depends on both $V_1$ and $V_c$, but not on $V_2$, anode 2 being too remote from the cathode. At positive values of $V_c$ the beam profiles show that the emitted current density is higher at the edges of the annulus than at the centre, due to the proximity of the control electrode to the cathode edges.

The transition from mode 1 to mode 2 is due to the formation of a virtual cathode. The strong dependence of $I_b$ on both $V_1$ and $V_2$ indicates that the virtual cathode is situated between anodes 1 and 2. The beam profiles show that the decrease of the mean beam current accompanying virtual cathode formation is due mainly to a reduction of current in the centre of the annulus. The uneven current distribution makes it difficult to compare closely the theoretical and measured curves. However, the observed increase of $I_b$ with an increase of either $V_1$ or $V_2$ is consistent with the theoretical curves. Conditions in the centre of the annulus appear to be closest to the ideal one-dimensional assumption which predicts a gradual decrease of current density as $V_c$ is increased. At the edges of the annulus conditions are very different from the one-dimensional assumption. Using a pinhole analyser, Eichenbaum and Hammer[30] found that no virtual cathode limitation occurred at the edges. It seems likely, therefore, that the increase of current at the edges of the annulus balances any decrease at the centre and results in an almost constant mean beam current when $V_c$ is increased after virtual cathode formation.

The slight blurring of the edges of the observed beam profile when $V_c$ is increased is probably due to an increase of current density at the extreme edges of the annulus sufficient to cause noticeable space-charge repulsion of the electrons. Acceleration of the electrons away from the virtual cathode towards the edges of the beam as suggested by Atkinson[57] could also contribute towards blurring of the image at high degrees of space-charge limitation.

## 6.5 Explanation of Hysteresis

The hysteresis predicted by the one-dimensional analysis would seem, at first sight, to explain the observed effects. However, it does not explain why the size of the hysteresis loop varies with the rate of change of the injected current. The beam profiles show that the actual current density is far from uniform across the annulus and the one-dimensional analysis should be applied only with extreme caution. Eichenbaum and Hammer[30] suggested that the finite nature of the actual beam meant that no hysteresis should occur. No theoretical proof was given, however, and an attempt by the author to work out the theory of virtual cathode formation in a finite beam was unsuccessful. Eichenbaum and Hammer beleived the observed hysteresis to be an ion effect. In order to investigate further this idea the following experiments were carried out using tube 2.

The pressure in the tube was varied and the effect on the hysteresis was as shown in the oscilloscope traces of fig.6.10.

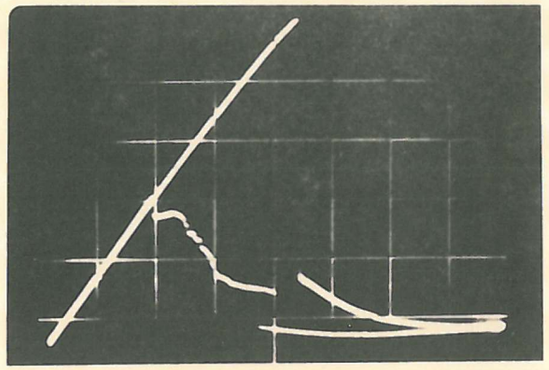

(a) PRESSURE = $10^{-6}$ mm Hg

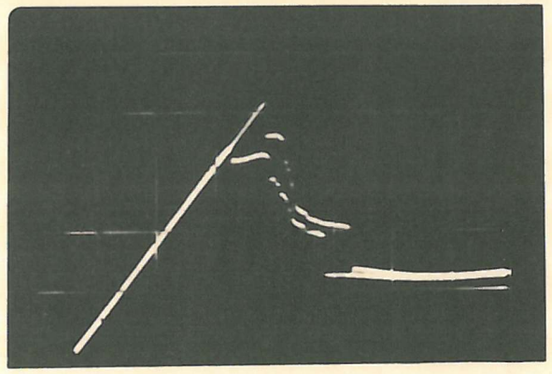

(b) PRESSURE = $10^{-7}$ mm Hg

FIG.6.10

HYSTERESIS LOOP

$V_1$ = 25V, $V_2$ = 20V

These were obtained by sweeping $V_c$ at 50c/s. It can be seen that at a pressure of $10^{-6}$mmHg the hysteresis loop was considerably larger than at $10^{-7}$mmHg, indicating that residual gas is almost certainly a major factor contributing to hysteresis.

The tube was next operated with the control electrode pulsed with various forms of triangular wave and the hysteresis in the beam current observed. When the waveform shown in fig.6.11(a) was applied it was found that at low pulse repitition frequencies the hysteresis loop was much larger than at high frequencies. Oscilloscope traces of hysteresis loops observed at 10c/s, 100c/s and 1kc/s are shown in fig.6.12(a), (b) and (c) respectively. At frequencies above about 1kc/s no hysteresis was observed. If the waveform was changed to that shown in fig.6.11(b) or (c), with the same rise-time as before, there was a slight reduction in the hysteresis. There was a slight increase in the hysteresis with the waveform shown in fig.6.11(d), again with the same rise-time. It does seem, however, that the most important feature of the waveform affecting hysteresis is the rate at which $V_c$ is changed.

It was not possible to induce hysteresis if $V_1$ was less than about 15V or $I_b$ less than about 3 mA. It was found that if the d.c. level of the waveform was altered so as to increase the maximum and minimum value of $V_c$ during the cycle the size of the hysteresis loop increased. Also, when hysteresis occurred, the value of $I_b$ in the virtual cathode

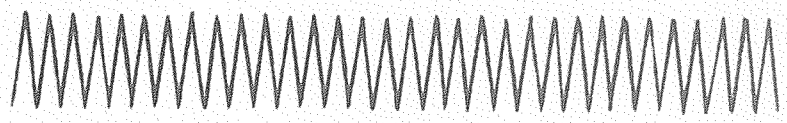

(a)

(b)

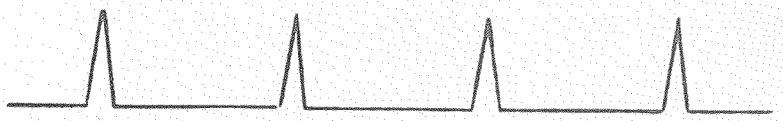

(c)

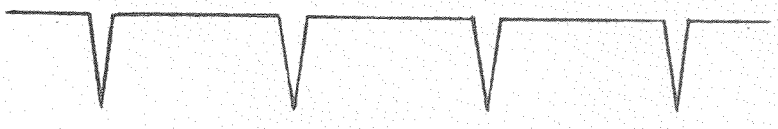

(d)

FIG. 6.11 WAVEFORMS APPLIED TO $V_c$

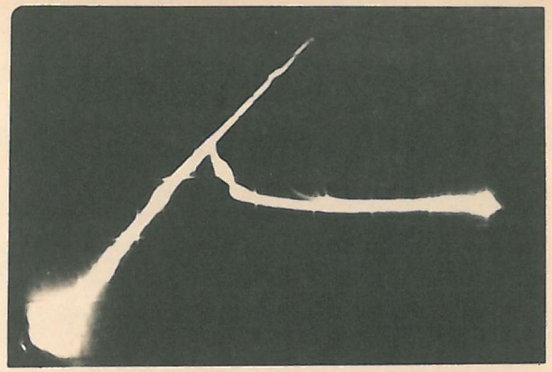

(a) $V_c$ PULSED AT 10C/S

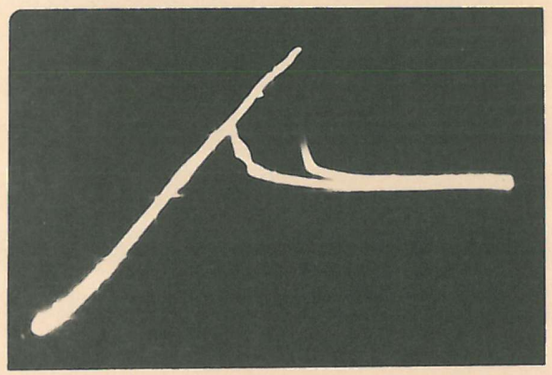

(b) $V_c$ PULSED AT 100C/S

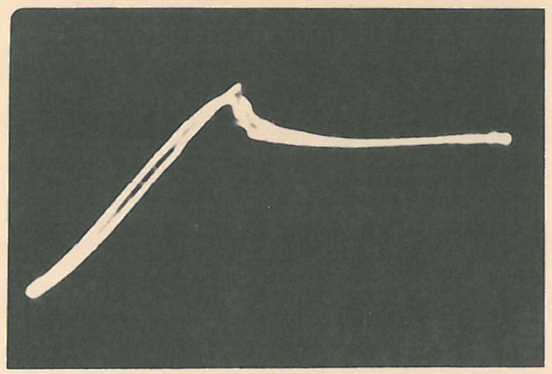

(c) $V_c$ PULSED AT 1KC/S

FIG.6.12 HYSTERESIS LOOP $V_1=32V$, $V_2=32V$

mode was slightly greater (about 10%) than when it was removed by increasing the rate of change of $V_c$.

These observations indicate that hysteresis occurs under the following conditions:

(a) $V_1$ greater than about 15V.

(b) $I_b$ greater than about 3mA.

(c) Pressure higher than about $10^{-7}$mmHg.

(d) Slow rate of increase and decrease of $V_c$.

(e) Maximum or minimum $V_c$ during cycle fairly high.

The absence of hysteresis under very high vacuum conditions shows that the one-dimensional analysis of virtual cathode formation is not directly applicable to the finite-beam case and that the observed hysteresis is almost certainly an ion effect. The theory can be used with great care, however, to obtain some idea of the movement of the potential minimum in the centre of the annulus where the situation appears to be closest to the ideal one-dimensional case. Comparing the theoretical and measured curves it would seem that, in the absence of ions, as the current injected into the anode 1 - 2 region is increased by increasing $V_c$, the potential minimum is depressed more and more. When the potential minimum reaches cathode potential the virtual cathode is formed. Further increase of the injected current results in first a decrease, and then a levelling off, of the transmitted current as the potential minimum shifts towards anode 1. Exactly the reverse happens when $V_c$ is decreased.

If gas molecules are present in the tube some of these are ionized by electrons having a potential higher than the ionization potential of the molecules (about 14V). Ions formed at a lower potential than $V_1$ on the opposite side of anode 1 to the cathode are unable to move past anode 1 and are trapped at the potential minimum. For ions to be trapped in this way $V_1$ must, of course, be greater than the ionization potention.

Consider again an increase of $V_c$. If this is slow enough, and the pressure in the tube is high enough, sufficient ions will be formed to neutralize partially the space charge. The potential minimum thus reaches zero voltage, bringing about the formation of the virtual cathode at a higher value of injected current than in the ion-free case. The formation of the virtual cathode is accompanied by a sudden reduction of transmitted current to a value only slightly higher than in the ion-free case indicating that the ion-neutralization effect is much less than before the virtual cathode formed. The most likely cause of this sudden drop is the depression of the potential between the outer and inner sections of anode 1. This potential is gradually depressed as the injected current is increased allowing some ions to drain out of the region. As soon as the potential minimum reaches zero a regenerative process sets in. The electrons returning from the virtual cathode cause further reduction of the potential at anode 1 and more ions drain out of the region. The space-charge neutralization is reduced and the number of returning electrons increases. The

reduction of transmitted current is thus as rapid as the ions can drain out of the potential minimum region.

Because of the sparsity of ions, when $V_c$ is reduced again the $I_b$ characteristic follows a path close to the ion-free one. The maximum beam current is therefore very much less than when $V_c$ is being increased. Hence when $V_c$ is pulsed with a triangular wave of sufficiently low frequency the beam current follows a hysteresis loop. There seems no obvious reason why an increase in the mean level of $V_c$ should increase the hysteresis effect.

Calculations of the approximate time scales involved in ion formation and drainage support the above explanation of hysteresis in the beam current.

To enable the time taken for ion formation to be calculated it is necessary to make some fairly drastic assumptions.

From reference 29 the infinite-beam theory gives the value of the potential minimum $V_{min}$ by the expression:

$$J_y^{\frac{1}{2}} = K\left[\frac{V_y}{V_x}\right]^{\frac{3}{4}}\left[\left(V_x^{\frac{1}{2}} - V_{min}^{\frac{1}{2}}\right)^{\frac{1}{2}}\left(V_x^{\frac{1}{2}} + 2V_{min}^{\frac{1}{2}}\right)\right.$$

$$\left. + \left(V_y^{\frac{1}{2}} - V_{min}^{\frac{1}{2}}\right)^{\frac{1}{2}}\left(V_y + 2V_{min}^{\frac{1}{2}}\right)\right] \qquad (6.6)$$

At the maximum value of $J_y$ given by equation 6.2, and for the special case of $V_x = V_y$:

$$V_{min} = \frac{1}{4}V_x \qquad (6.7)$$

According to the infinite-beam theory, therefore, for

equal anode 1 and 2 voltages, the virtual cathode forms when the voltage minimum is $\frac{1}{4}$ of the anode voltages.

For the analysis of ion formation the much simplified model shown in fig.6.13 is used.

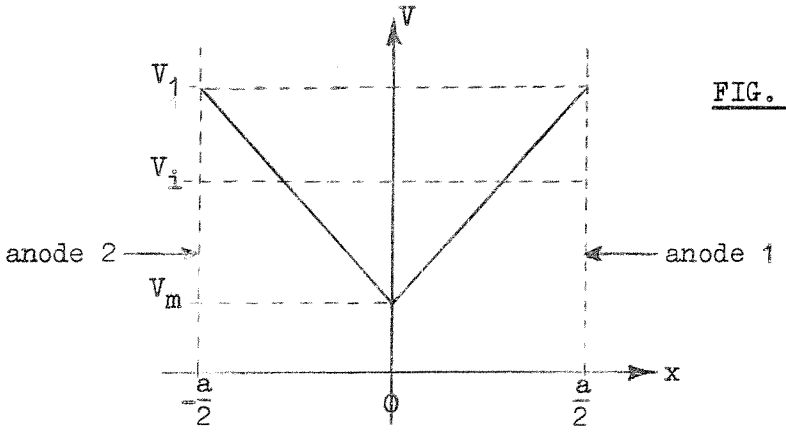


FIG. 6.13

Anodes 1 and 2 are considered to be at the same potential $V_1$. The potential distribution between the anodes and potential minimum is taken to be linear. The reduction of the potential minimum $V_m$ with increase in current I is also assumed to be linear. Using the infinite-beam theory as a basis, the virtual cathode is considered to be formed when $V_m = \frac{1}{4}V_1$. In addition the velocity spread is assumed to be small.

Obviously these assumptions are only approximate, but they have to be made otherwise the calculations are impossibly complex. The resulting calculations are sufficient to give the order of magnitude of the time factor involved in ion formation.

Firstly, the number of electrons present in the region at the maximum ion-free transmitted current is found. The additional number of electrons present at some higher current is then found and the time taken for sufficient ions to be formed to neutralize the charge of these additional electrons is calculated.

a) Number of electrons between anodes at maximum ion-free current (i.e. immediately prior to virtual cathode formation).

Consider a point distance x from the potential minimum. With the above assumptions the potential at this point is given by:

$$V = V_m + (V_1 - V_m)\frac{2|x|}{a} \qquad (6.8)$$

The electron velocity $v = (2V\frac{e}{m})^{\frac{1}{2}}$ (6.9)

If the maximum ion-free current is $I_1$ when $V_m = \frac{1}{4}V_1$, then the number of electrons in a short length dx is:

$$dN_1 = \frac{I_1}{e}\frac{dx}{v} \qquad (6.10)$$

From equations 6.8-6.10:

$$dN_1 = \frac{I_1}{e}\left[2\frac{e}{m}V_1\left(\frac{1}{4} + \frac{3|x|}{2a}\right)\right]^{-\frac{1}{2}}dx \qquad (6.11)$$

and $$N_1 = \frac{2I_1}{e}\left[\frac{m}{eV_1}\right]^{\frac{1}{2}}\int_{a/2}^{0}\left[\frac{1}{2} + \frac{3x}{a}\right]^{-\frac{1}{2}}dx \qquad (6.12)$$

By making the substitution $x = \frac{a}{6}\tan^2\alpha$, the solution

to equation 6.12 is found to be:

$$N_1 = \frac{4\sqrt{2}}{3}\frac{I_1 a}{e}\left[\frac{m}{eV_1}\right]^{\frac{1}{2}} \qquad (6.13)$$

b) Number of electrons with ions present.

If partial space-charge neutralization due to ions occurs so that the maximum transmitted current becomes $I_2 (> I_1)$, then the number of electrons becomes:

$$N_2 = \frac{4\sqrt{2}}{3}\frac{I_2 a}{e}\left[\frac{m}{eV_1}\right]^{\frac{1}{2}} \qquad (6.14)$$

c) Number of ions formed.

The current is increased linearly, hence at time t:

$$I = I_2 \frac{t}{t_{21}} \qquad (6.15)$$

where $t_{21}$ is the time at which the virtual cathode forms.

The potential minimum at time t is:

$$V_m = V_1\left[1 - \frac{3t}{4t_1}\right] \qquad (6.16)$$

An approximate expression for the number of ions formed per electron in length dx when $V \leq 2V_i$ is:

$$K_1 (V - V_i) P$$

where P = gas pressure

$V_i$ = gas ionization potential.

$K_1$ = a constant according to the gas (see reference 56)

Hence, in time dt the number of ions formed is:

$$dN_3 = \frac{K_1 PI}{e}(V - V_i)dxdt \qquad (6.17)$$

From equations 6.8 and 6.15-6.17:

$$dN_3 = \frac{K_1 PI_2 V_1}{et_1}\left[1 + \frac{3t}{4t_1}\left(\frac{2x}{a} - 1\right) - \frac{V_i}{V_1}\right]tdxdt \qquad (6.18)$$

Ions are formed only when $V > V_2$, hence integration is carried out in two stages:

(i) $V_m > V_i$ limits are $x = 0$ and $\frac{a}{2}$

$$t = 0 \text{ and } \frac{4}{3}t_1\left[1 - \frac{V_i}{V_1}\right]$$

(ii) $V_m < V_i$ limits are $x = \frac{a}{2}\left\{1 + \frac{4}{3}\frac{t_1}{t}\left[\frac{V_i}{V_1} - 1\right]\right\}$ and $\frac{a}{2}$

$$t = \frac{4}{3}t_1\left[1 - \frac{V_i}{V_1}\right] \text{ and } t_1$$

$$N_3 = \frac{2K_1 PI_2 V_1}{et_1}\left\{\int_{\frac{4}{3}t_1\left[1 - \frac{V_i}{V_1}\right]}^{0}\int_{\frac{a}{2}}^{0}\left[1 + \frac{3t}{4t_1}\left(\frac{2x}{a} - 1\right) - \frac{V_i}{V_1}\right]tdxdt\right.$$

$$\left. + \int_{t_1}^{\frac{4}{3}t_1\left[1 - \frac{V_i}{V_1}\right]}\int_{\frac{a}{2}}^{\frac{a}{2}\left\{1 + \frac{4}{3}\frac{t_1}{t}\left[\frac{V_i}{V_1} - 1\right]\right\}}\left[1 + \frac{3t}{4t_1}\left(\frac{2x}{a} - 1\right) - \frac{V_i}{V_1}\right]tdxdt\right\} \qquad (6.19)$$

Evaluation of this integral gives:

$$N_3 = \frac{2K_1 PI_2 V_1 t_1}{27e}\left[1 - \frac{V_i}{V_1}\right]^2\left[5 + 4\frac{V_i}{V_1}\right] \qquad (6.20)$$

The ions formed neutralize the effect of the additional electrons present when the higher current flows.

Hence $N_3 = N_2 - N_1$ (6.21)

i.e. from equations 6.13, 6.14 and 6.20:

$$t_1 = 18\left[\frac{2m}{eV_1}\right]^{\frac{1}{2}} \frac{I_2 - I_1}{K_1 PI_2 V_1\left[1 - \frac{V_i}{V_1}\right]^2\left[5 + \frac{V_i}{V_1}\right]} \qquad (6.22)$$

Taking the hysterisis loop shown in fig.6.12(b) as an example the following values are substituted into equation 6.22:

$\frac{e}{m} = 1.76 \times 10^{11}$ C/kg

$V_1 = 32$V

$I_1 = 12$mA

$I_2 = 16$mA

$K_1 = 25$ ions/electron/m/V/mmHg pressure for oxygen and nitrogen (from reference 56)

$P = 10^{-6}$ mmHg

$V_i = 14$V for oxygen and nitrogen

These figures give $t_1 = 1.6$msec

This figure compares favourably with fig.6.12(b) where the time from the start of the cycle to the formation of the

virtual cathode is 3msec. this agreement of measured and calculated values to within an order of magnitude supports the above explanation of neutralization of space charge by ion formation.

For an estimate of the time taken for ion drainage consider an accelerating potential of, say, 1V.

The time taken for an ion of mass M to move from rest through a distance $a_1$ under the effect of an accelerating potential $V_a$ is given by:

$$t_2 = \left[\frac{2a_1^2 M}{eV_a}\right]^{\frac{1}{2}} \qquad (6.23)$$

Substituting typical values into equation 6.23:

$a_1$ = 4mm (length between anodes 1 and 2)

M = $2.6 \times 10^4$ times the mass of an electron m (for nitrogen)

$V_a$ = 1V

$\frac{e}{m} = 1.76 \times 10^{11}$ C/kg

$$t_2 = 2.2\mu\text{sec}$$

This figure is the maximum time taken by an ion to move out of the anode 1 - 2 region if the accelerating potential is 1 volt. In fact this potential is likely to be higher and the ions will drain out more rapidly. Ion drainage can therefore occur in a time relatively short compared with the rest of the hysteresis-loop cycle. It could, therefore, account for the formation of the virtual cathode with the accompanying rapid reduction of transmitted current.

Atkinson[57] studied the effects of positive ions on an electron beam in a drift tube with a longitudimal magnetic field of 0.050 to 0.085 $Wb/m^2$ and at a pressure of about $10^{-6}$mmHg. The results were similar to those described above. When the beam was pulsed rapidly (at about 10kc/s) to eliminate the effects of positive ions only a very small hysteresis loop was observed in the beam current. At a pulse repetition frequency of 100c/s, which allowed sufficient time for ions to be formed, a large hysteresis loop was observed. The higher beam current when positive ions were present was undoubtedly due to the partial neutralization of space charge by the positive ions. The formation of the virtual cathode was believed by Atkinson to be due to instability in the beam current brought about by electrostatic two-stream interaction between the electron beam and the ions.

## 6.6 Oscillations and Noise in Beam Current

Fig.6.14(a) is an oscilloscope trace of apparent oscillations in the beam current which occurred under certain conditions. If $V_c$ was carefully decreased from a value corresponding to the virtual cathode mode, $I_b$ appeared to break into oscillations of up to 2mA pk-pk. Fig.6.14(b) shows these oscillations in relation to the hysteresis loop.

No discrete frequency of oscillation could be detected on the oscilloscope. Using a receiver a signal was detected over the whole of the band 15kc/s to 30Mc/s (the limits of the receiver

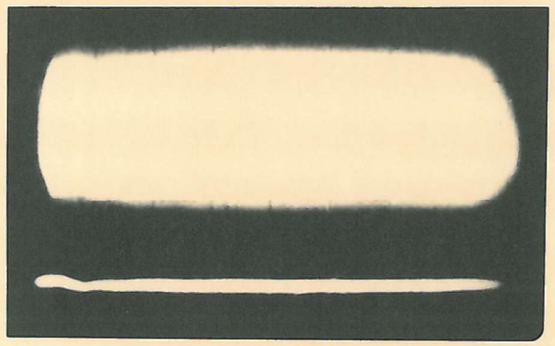

(a)

OSCILLATING CURRENT

NORMAL CURRENT

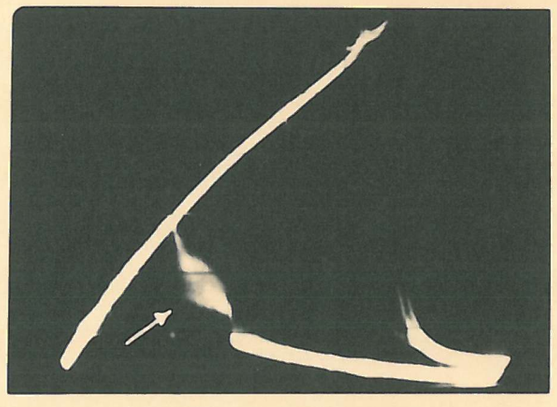

(b)

HYSTERESIS LOOP
SHOWING OSCILLATIONS

FIG.6.14 BEAM CURRENT OSCILLATIONS

used). It can therefore be assumed that the oscillations were of random frequency, in fact noise.

The noise occurs just as conditions are changing from the virtual-cathode to the non-virtual-cathode mode. The rather irregular $I_b$ against $V_c$ characteristic in this region (particularly clear in fig.6.10), and the beam profiles of fig.6.3, indicate that the change from one mode to the other does not occur over the whole annulus at once, presumably because of uneven emission or a slight misalignment of the gun. The noise appears to be due to a rapid change into and out of the virtual-cathode mode over only part of the beam area. When a virtual cathode exists over only a section of the annulus it is possible that an unstable condition could be set up at the division between the areas where the two different modes exist. Ions are trapped at a potential minimum but tend to drain out of the region when a virtual cathode is formed. It seems possible that the position of the division between these areas oscillates in a random manner due to ion formation and drainage, causing a variation of the mean beam current.

It is obvious that such noise could have a serious effect on tube performance by causing noisy modulation of the gain. It is doubtful whether such noise, if caused by ions, extended into the microwave region. To prevent such undesirable effects occurring uneven cathode emission should be avoided, all gun parts should be carefully aligned and the tube should have a

high vacuum.

Relaxation oscillations observed by Cutler[58] and Sutherland[59] appear to be of a similar nature. Cutler observed these oscillations in a magnetically-focused t.w.t. electron beam and Sutherland in a klystron beam. They were thought to be triggered by positive ions and, unlike the observations reported here, were of discrete frequencies ranging from 10c/s to 100kc/s under certain conditions. Cutler found that the oscillations did not affect the beam noise but did cause unwanted modulation of the gain.

## 6.7 Gun Characteristics at Normal Beam Currents

The hysteresis and oscillation phenomena described above were found to occur at beam currents higher than the normal operating values of 0.5 to 2mA. They would not therefore normally affect the operation of a tube using the type of electron gun under examination.

Figs. 6.15 and 6.16 are typical iso-current curves for normal operating beam currents of 0.5 to 2.0mA. These were plotted by adjusting $V_c$ and $V_1$ to give constant values of $I_b$, with $V_2$ held constant. These curves show how the operating conditions near the cathode could be changed without change of mean beam current. One of these curves would be followed when adjusting the noise figure of a tube to a minimum without change of other operating parameters. In addition, the voltages on the transducer section of the gun would have to be optimized but these voltages would have no effect on the beam current.

FIG. 6.15 ISO-CURRENT CURVES

$I_b = 0.5$ mA AND 1.0 mA

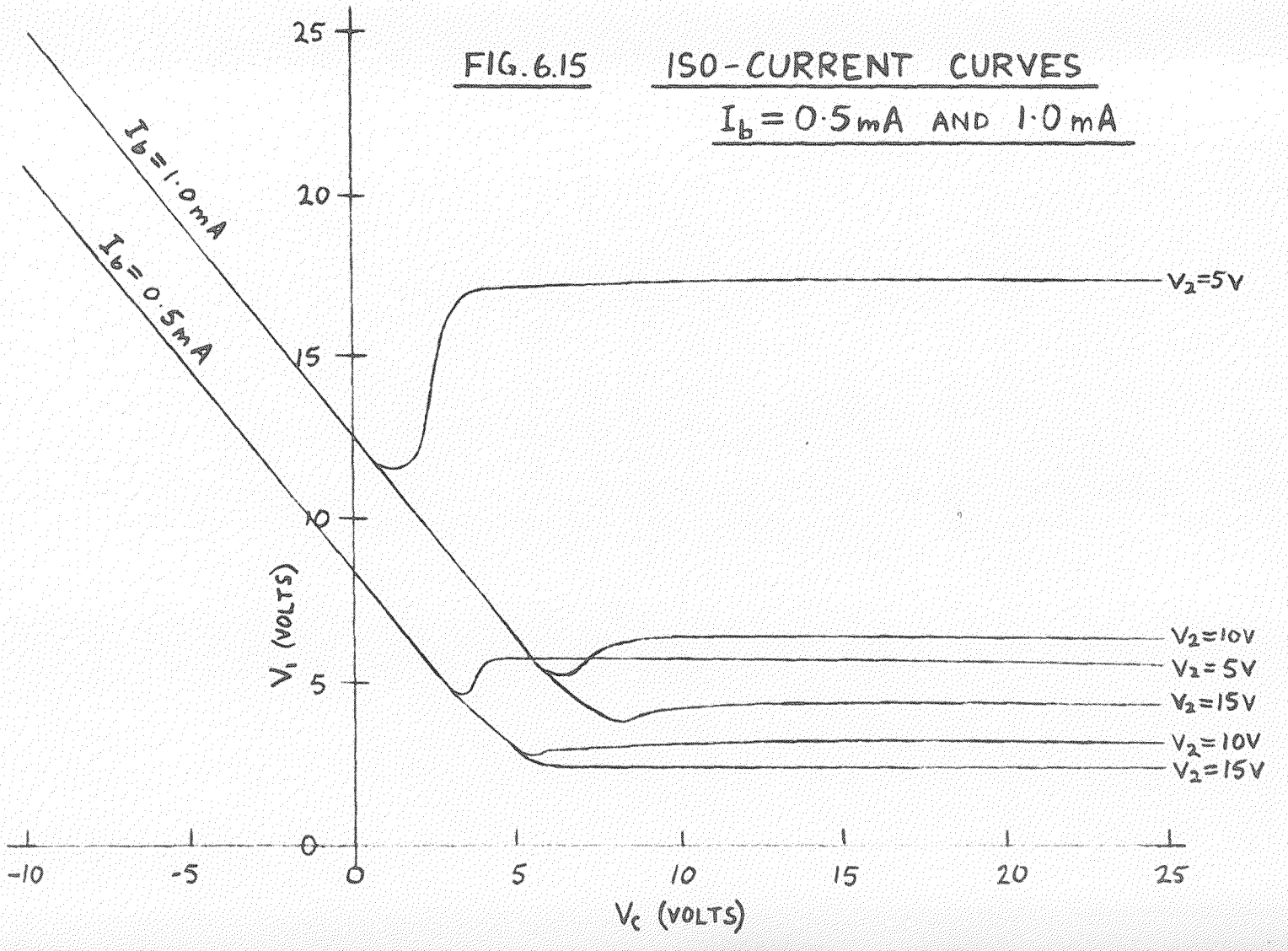

FIG.6.16 ISO-CURRENT CURVES

$I_b$ = 1·5 mA AND 2·0mA

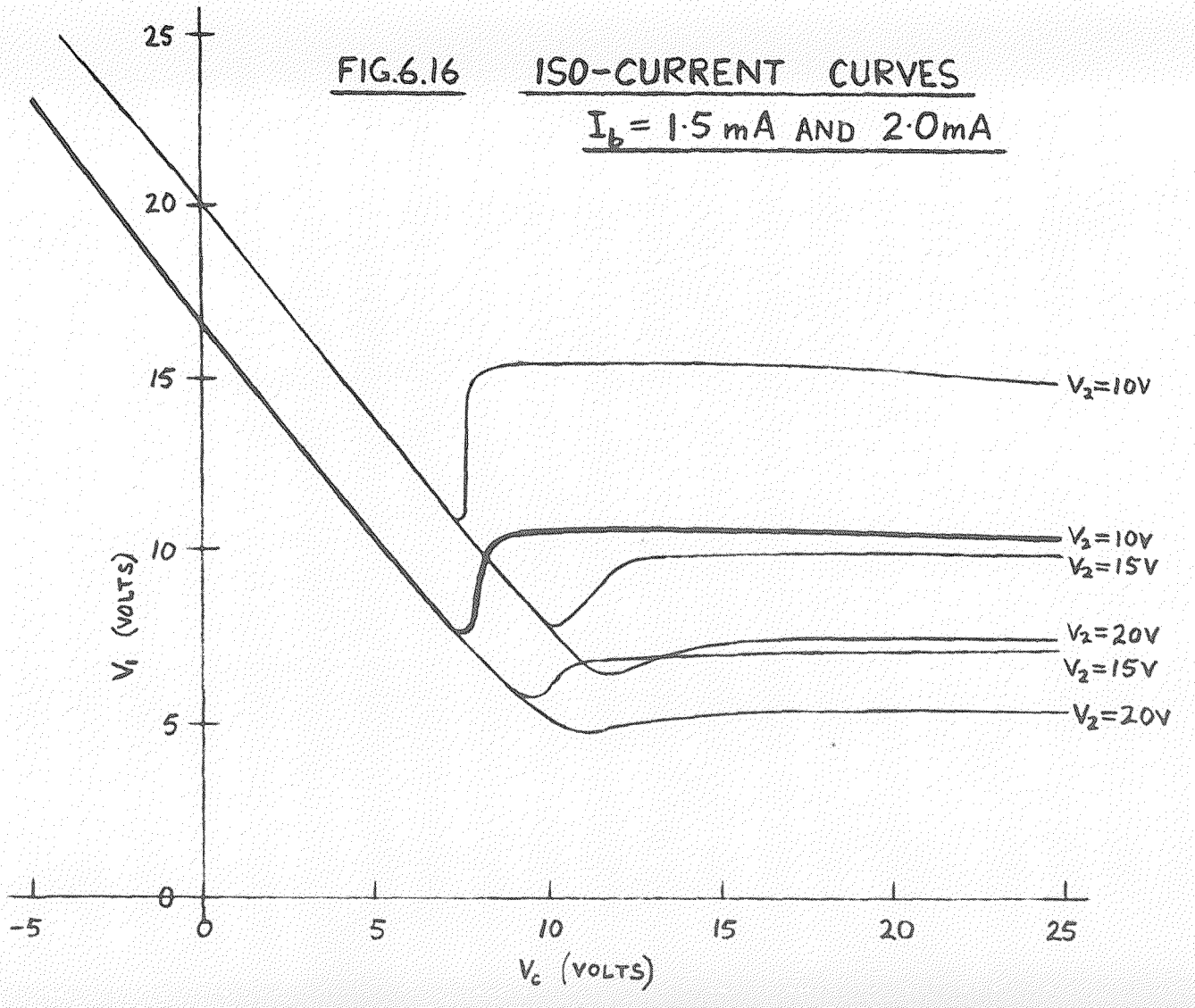

The formation of the virtual cathode is clearly indicated by the sudden change of slope of the characteristics. The sloping parts of the curves represent conditions where no virtual cathode existed and $V_2$ had no effect on the beam current. Formation of the virtual cathode was accompanied by a sudden increase in the value of $V_1$ necessary to maintain a constant $I_b$, especially at low values of $V_2$. In the virtual cathode state very little change of $V_2$ was necessary.

The beam profiles at various points on the $I_b$ = 1.5mA, $V_2$ = 10V curve (heavy line in fig.6.16) are shown in fig.6.17. Splitting of the beam occurred on formation of the virtual cathode as was observed at higher beam currents. Also the edges of the annulus were slightly blurred at high values of $V_c$ (fig.6.17(f)). Fig.6.18 shows the effect of reducing the magnetic field confining the beam when $V_c$ = 0V(solid beam) and fig.6.19 when $V_c$ = 15V (split beam). It can be seen that the solid beam depended less upon the magnetic field than the split beam which was severely distorted at a field of 0.05Wb/$m^2$. At high values of $V_c$ the radial electric field near the cathode was greater, and the electron density at the beam edge higher, making the magnetic field more essential for beam stability.

Fig.6.20 shows the effects of poor emission on the beam structure. The heaters were normally operated at 7V. If, in the case of tube 2, this voltage was reduced to 6.3V, the distortion shown in fig.6.20(a) was observed when the beam was

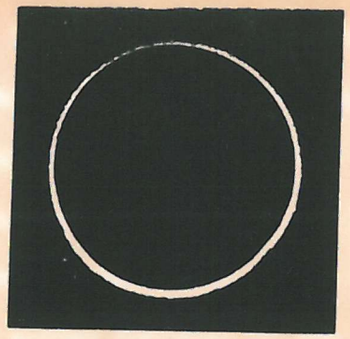

(a) $V_c = -5V$
$V_1 = 22{\cdot}6V$

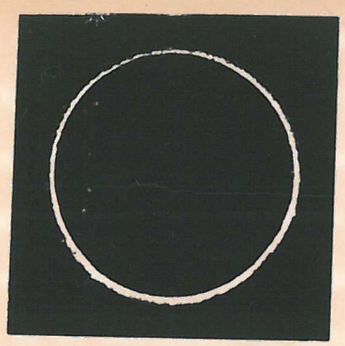

(b) $V_c = 0V$
$V_1 = 16{\cdot}0V$

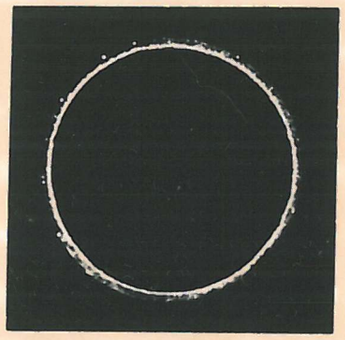

(c) $V_c = 5V$
$V_1 = 9{\cdot}9V$

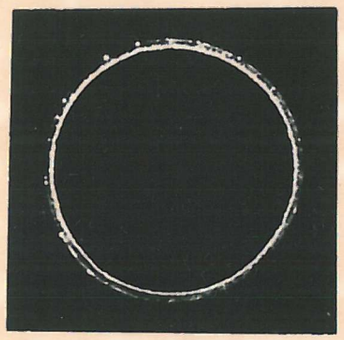

(d) $V_c = 6{\cdot}9V$
$V_1 = 7{\cdot}7V$

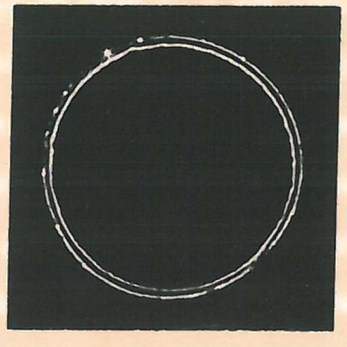

(e) $V_c = 15V$
$V_1 = 10{\cdot}1V$

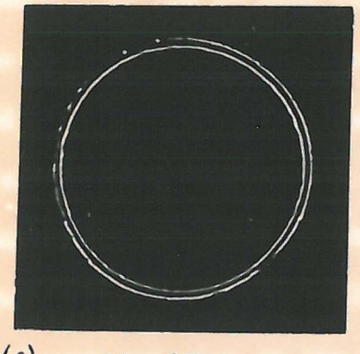

(f) $V_c = 25V$
$V_1 = 10{\cdot}0V$

FIG. 6.17

BEAM PROFILES WITH $I_b = 1{\cdot}5mA$ $V_2 = 10V$ $B = 0{\cdot}15 Wb/m^2$

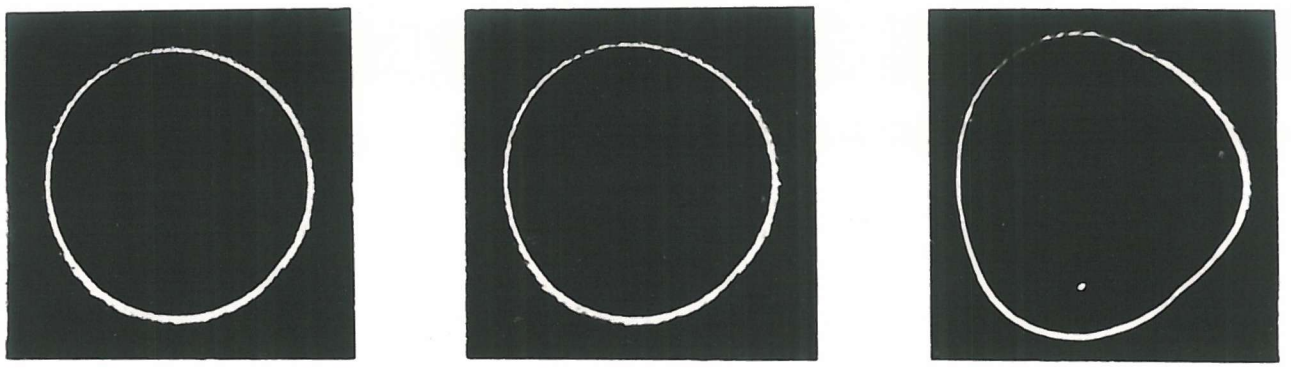

(a) $B=0{\cdot}1\,Wb/m^2$ (b) $B=0{\cdot}05\,Wb/m^2$ (c) $B=0{\cdot}02\,Wb/m^2$

FIG.6.18 BEAM PROFILES WITH $I_b=1{\cdot}5mA$ $V_c=0V$ $V_2=10V$

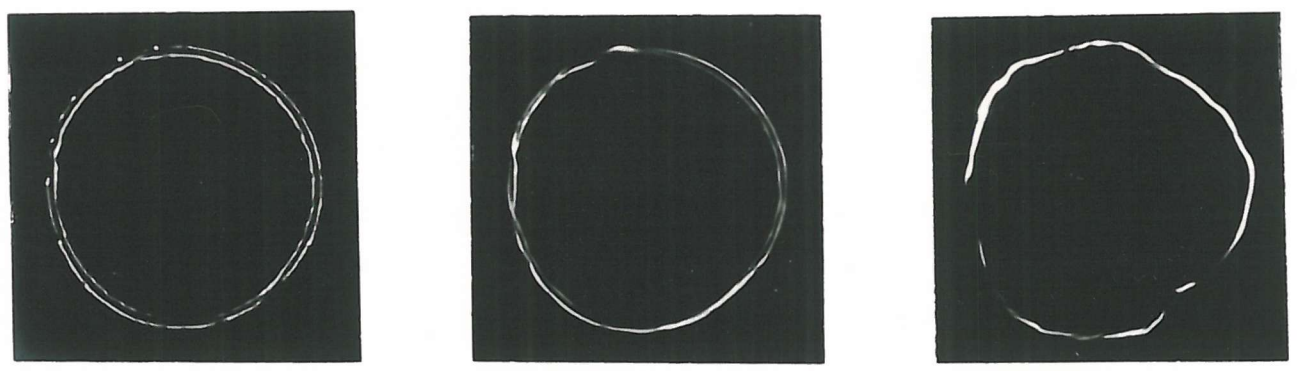

(a) $B=0{\cdot}1\,Wb/m^2$ (b) $B=0{\cdot}05\,Wb/m^2$ (c) $B=0{\cdot}02\,Wb/m^2$

FIG.6.19 BEAM PROFILES WITH $I_b=1{\cdot}5mA$ $V_c=15V$ $V_2=10V$

split due to high Vc (compare with fig.6.17(e)). This distortion was enhanced at reduced magnetic fields as shown in fig.6.20(b) and (c) (compare with fig.6.19(a) and (b)). No distortion occurred at lower values of Vc when the beam consisted of a solid annulus.

The shapes of the disturbances were similar to the vortex formations observed in thin hollow beams by Kyhl and Webster[60,61]. They show that a localized increase of charge density in the beam gives rise to circumferential components of electric field which are oppositely directed on either side of the disturbance. The magnetic focusing field brings about radial movement of the electrons, outwards on one side of the disturbance and inwards on the other side as shown in fig.6.21(a). The smooth curvature of the thin beam thus develops into an S-curve as shown in fig.6.21(b) and then into the type of vortex formation observed (fig.6.21(c)). Vortices are more likely to form with thin beams and at high current densities. Such conditions existed in the type of gun under test with a high value of Vc which produced a split beam.

The vortices were caused by uneven emission at the reduced heater voltage. Emission over parts of the cathode was probably temperature limited, giving rise to patches of reduced current density which initiated the process described above. Movement of the fluorescent screen showed that no change in the shape or size of the vortices took place beyond the final anode of the

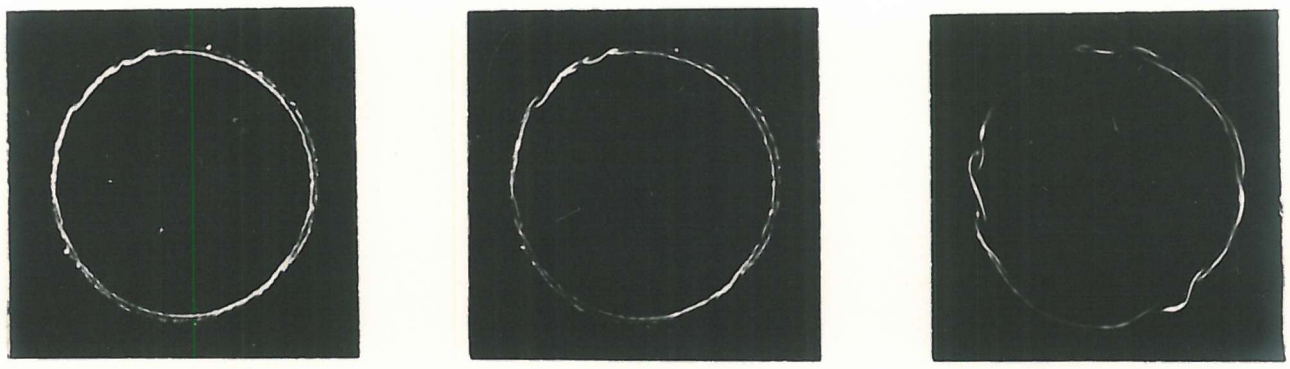

(a) $B=0.15\,Wb/m^2$ (b) $B=0.1\,Wb/m^2$ (c) $B=0.05\,Wb/m^2$

FIG. 6.20 BEAM PROFILES WITH $I_b=1.5mA$ $V_c=15V$ $V_2=10V$ AT REDUCED HEATER VOLTAGE

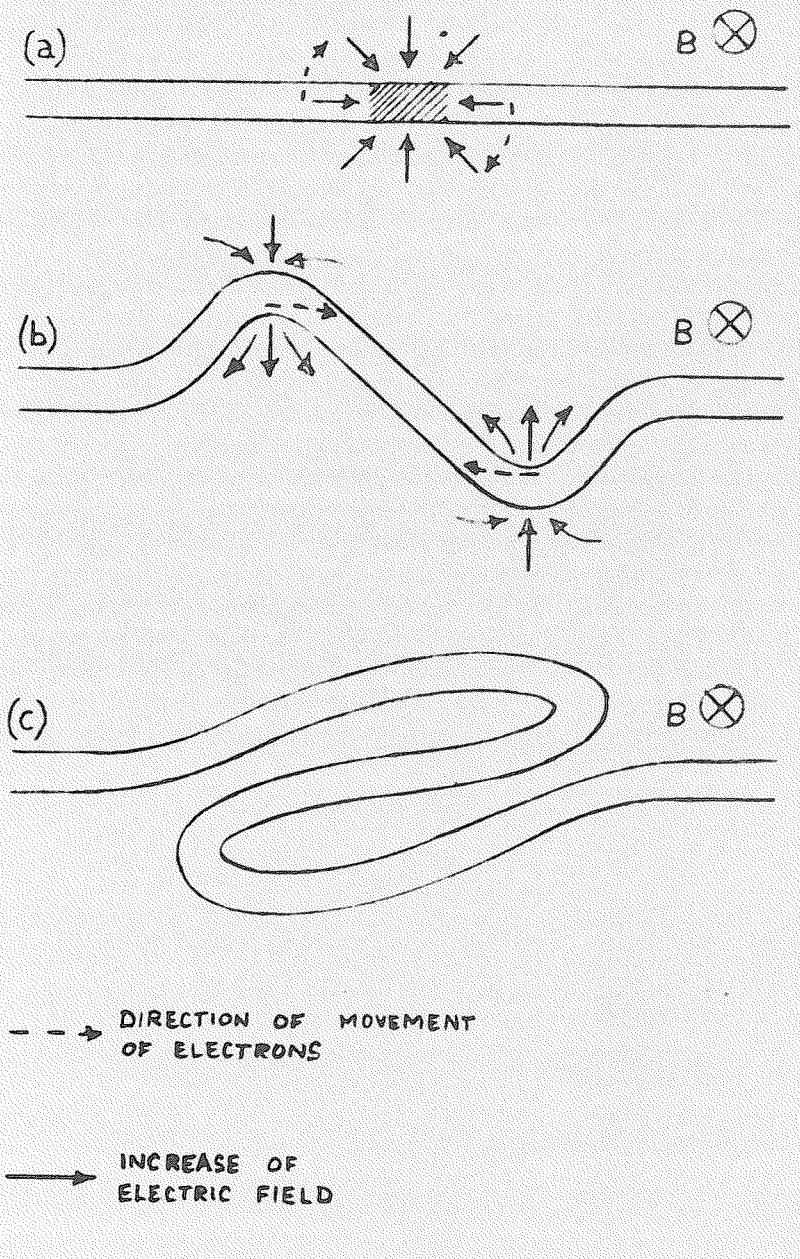


FIG. 6.21 FORMATION OF VORTICES

electron gun. It seems, therefore, that the formation of the vortices took place within the gun itself.

It is not clear what effect vortex formations have on beam noise. Khyl and Webster[60] remark that a direct contribution to microwave beam noise is unlikely. It is obvious, however, that if the disturbances develop to such an extent that beam interception occurs the noise figure of the tube is increased. If, as suspected, the vortices are initiated by temperature-limited emission over part of the cathode, a beam in which these disturbances occur would anyway be noisy. Formation of these disturbances can be minimized by avoiding non-uniform emission, and from fig.6.19 it can be seen that beam distortion is reduced by using a strong magnetic focusing field.

## 7. MEASUREMENT OF NOISE PARAMETERS S AND Π

### 7.1 Measurement of S

No results were obtained from the S-measuring tube up to the time of writing. However it seemed likely that the tube would be successful and the microwave apparatus worked satisfactorily.

To obtain relative measurements of S the electron gun is moved along the beam axis and the cavity output plotted as a function of gun position. The final anode of the electron gun, the cavity and the conducting coating on the inside of the tube are all held at the same voltage so that the beam is essentially in a drift space. The cavity is excited by the beam current and its output current $I_1$ is proportional to the beam current. Hence from equation 2.32:

$$I_1 = K_1\left[a_1 e^{j\beta_q z} + a_2 e^{-j\beta_q z}\right]e^{-j\beta_e z} \qquad (7.1)$$

where $K_1$ is a constant

$a_1$ and $a_2$ are the normalized wave amplitudes

(see section 2.6)

The microwave apparatus measures power from the cavity $P_1$ which is proportional to $|I_1|^2$, hence:

$$P_1 = K_2\left[|a_1|^2 + |a_2|^2 + \overline{a_1 a_2^*}\, e^{2j\beta_q z} + \overline{a_1^* a_2}\, e^{-2j\beta_q z}\right] \qquad (7.2)$$

where $K_2$ is a constant.

From equation 2.52:

$$A_{11} = \lim_{T\to\infty} \frac{2\pi}{T} \overline{|a_1|^2} \qquad (7.3)$$

$$A_{22} = \lim_{T\to\infty} \frac{2\pi}{T} \overline{|a_2|^2} \qquad (7.4)$$

$$A_{12} = \lim_{T\to\infty} \frac{2\pi}{T} \overline{a_1 a_2^*} \qquad (7.5)$$

$$A_{21} = \lim_{T\to\infty} \frac{2\pi}{T} \overline{a_1^* a_2} \qquad (7.6)$$

Substituting these equations into equation 7.2:

$$P_1 = K_3\left[A_{11} + A_{22} + A_{12}e^{2j\beta_q z} + A_{21}e^{-2j\beta_q z}\right] \qquad (7.7)$$

where $K_3$ is a constant.

The variation of $P_1$ with z is therefore sinusoidal as shown in fig.7.1.

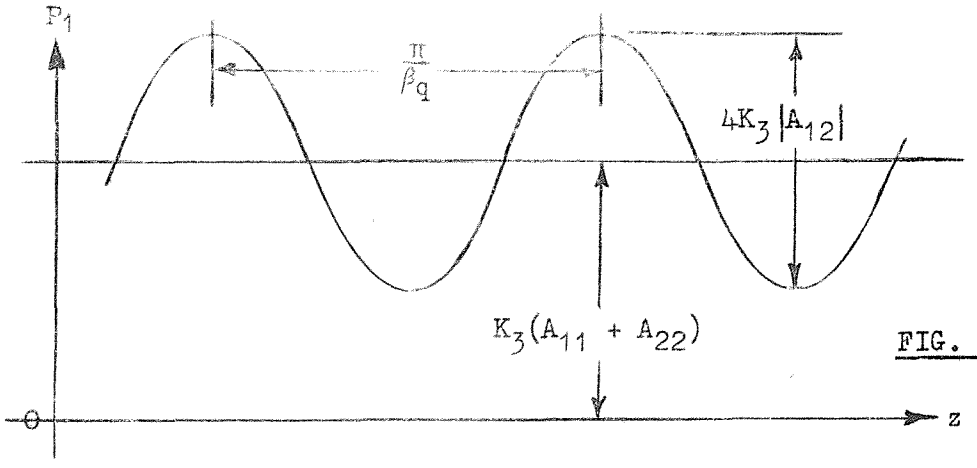


FIG. 7.1

Knowing $K_3|A_{12}|$ and $K_3(A_{11} + A_{22})$, $K_3S$ can be found using equation 2.57:

$$K_3S = K_3\left[(A_{11} + A_{22})^2 - 4|A_{12}|^2\right]^{\frac{1}{2}} \qquad (7.8)$$

Relative values of S can thus be measured for various beam operating conditions. Of particular interest is the effect of virtual cathode formation on S, and it is hoped to study the change of S when the beam-current hysteresis loop is traversed. Little is known of the way a virtual cathode affects beam noise and there have been no reports to date on the effects of hysteresis on the noise parameters S and $\Pi$. If possible the change of S with vortex formation will be studied but, as vortices form only in a beam from a poorly emitting cathode and at reduced magnetic focusing fields, a considerable increase in S is to be expected.

7.2 Principle of Measurement of $\Pi$

A new method of measuring $\Pi$ using cavities has been devised[62]. As explained below it is thought to have advantages over the method of Saito[32] and that proposed by Okoshi[63], and requires the following modifications to the equipment. The S-measuring tube is altered by replacing the single cavity by two cavities a fixed distance apart. The signals from the two cavities are fed into the microwave measuring apparatus via a magic tee with an attenuator at cavity 1 output and a phase shifter at cavity 2 output, as shown in fig.7.2. Cavity 1 is nearer the electron gun.

To obtain relative measurements of $\Pi$, $K_3S$ is first measured as detailed in section 7.1, using only cavity 1. From the variation of the cavity output with distance the plasma

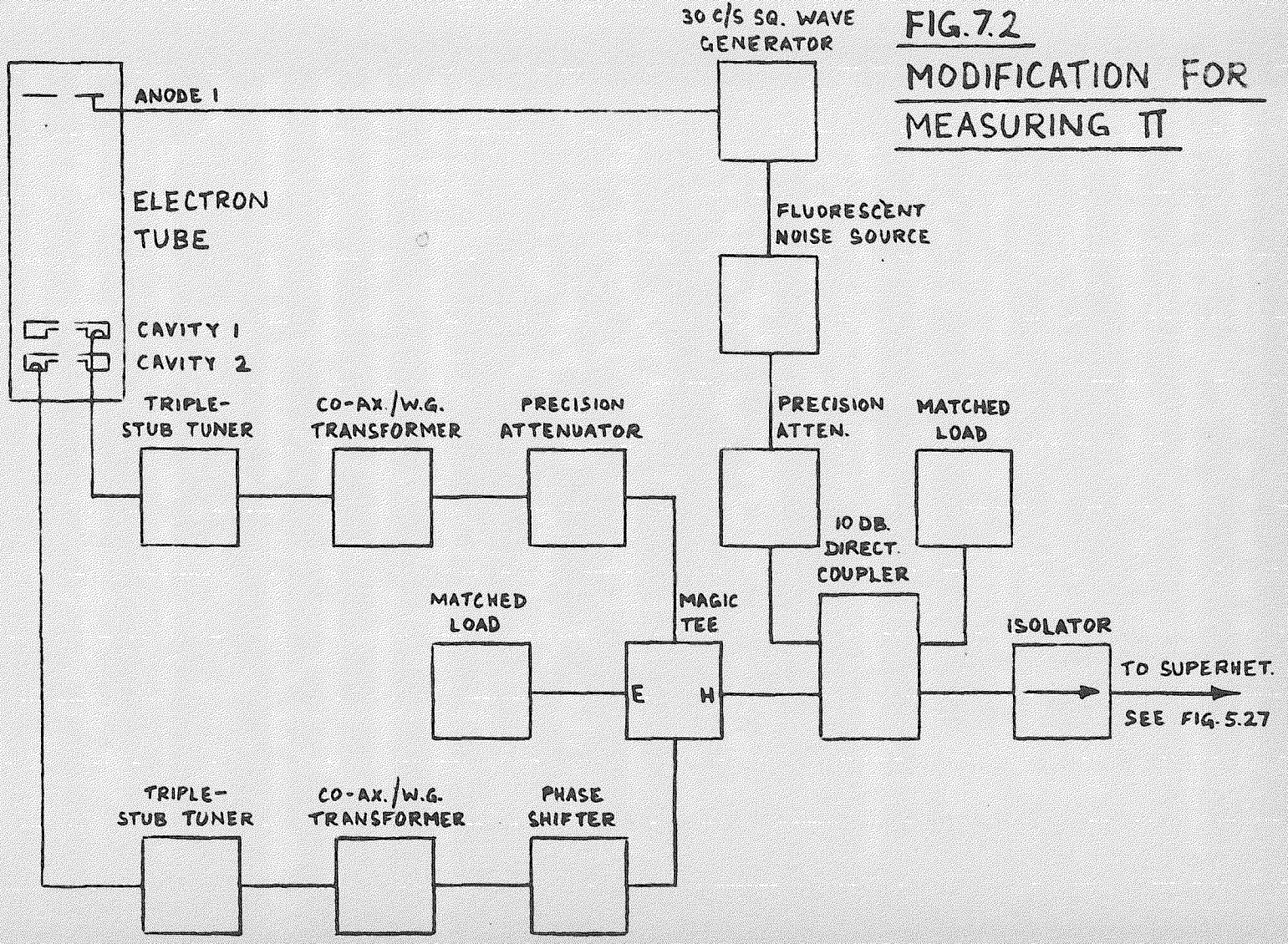


FIG. 7.2
MODIFICATION FOR MEASURING π

propagation constant $\beta_q$ can be found as shown in fig.7.1. If $\Delta z$ is the distance between the cavities, the attenuator in cavity 1 output is set to:

$$L = \cos\beta_q \Delta z \tag{7.9}$$

and the phase shifter in cavity 2 output is set to:

$$\psi = \beta_e \Delta z + \pi \tag{7.10}$$

Referring to Saito's work[32], the output currents from cavity 1 and cavity 2 are:

$$I_1 = K_1 \left[ a_1 e^{j\beta_q z} + a_2 e^{-j\beta_q z} \right] e^{-j\beta_e z} \tag{7.1}$$

$$I_2 = K_1 \left\{ a_1 e^{j\beta_q z} \left[ e^{j\beta_q \Delta z} - jZ\sin\beta_q \Delta z \right] + a_2 e^{-j\beta_q z} \left[ e^{-j\beta_q \Delta z} - jZ\sin\beta_q \Delta z \right] \right\} e^{-j\beta_e (z + \Delta z)} \tag{7.11}$$

where Z is the gap shunt impedance of cavity 1 normalized with respect to the beam impedance. If measurements are taken at the resonant frequency of the cavities over a narrow bandwidth, Z can be considered to be resistive and therefore real.

The output current from the magic tee is:

$$LI_1 + I_2 e^{j\psi} = jK_1 \left\{ \left[ a_1 (Z - 1) + a_2 (Z + 1) \right] \sin\beta_q \Delta z \right\} e^{-j\beta_e z} \tag{7.12}$$

The power measured by the microwave apparatus $P_2$ is proportional to:

$$\overline{\left|LI_1 + I_2 e^{j\psi}\right|^2}$$

$$\text{i.e. } P_2 = K_2\Big\{\overline{|a_1|^2}(Z-1)^2 + \overline{|a_2|^2}(Z+1)^2 + \left[\overline{a_1 a_2^{*}}\, e^{2j\beta_q z} + \overline{a_1^{*} a_2}\, e^{-2j\beta_q z}\right](Z^2-1)\Big\}\sin^2\beta_q\Delta z \tag{7.13}$$

From equations 7.3-7.6, equation 7.13 becomes:

$$P_2 = K_3\Big[A_{11}(Z-1)^2 + A_{22}(Z+1)^2 + A_{12}e^{2j\beta_q z} + A_{21}e^{-2j\beta_q z}\Big](Z^2-1)\sin^2\beta_q\Delta z \tag{7.14}$$

The variation of $P_2$ with z is therefore sinusoidal as shown in fig.7.3.

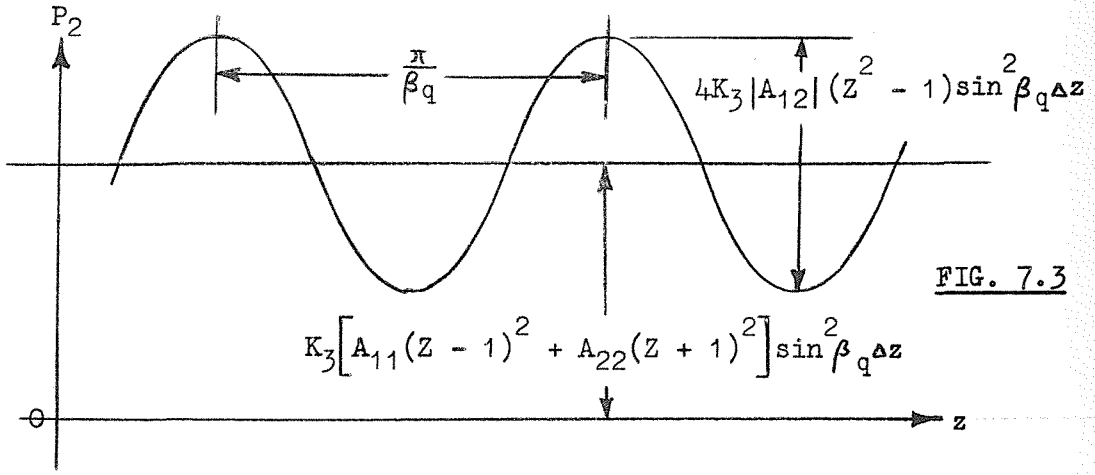


FIG. 7.3

From the S and π measurements (figs. 7.1 and 7.3) we know the following quantities:

$$D = K_3|A_{12}| \tag{7.15}$$

$$E = K_3(A_{11} + A_{22}) \tag{7.16}$$

$$F = K_3|A_{12}|(Z^2 - 1)\sin^2\beta_q\Delta z \tag{7.17}$$

$$G = K_3\left[A_{11}(Z - 1)^2 + A_{22}(Z + 1)^2\right]\sin^2\beta_q\Delta z \tag{7.18}$$

From values D and F, Z can be found:

$$Z = \left[1 + \frac{F}{D}\frac{1}{\sin^2\beta_q\Delta z}\right]^{\frac{1}{2}} \tag{7.19}$$

From values E and G the ratio $\frac{A_{11}}{A_{22}}$ can be found:

$$\frac{A_{11}}{A_{22}} = \frac{(Z + 1)^2\sin^2\beta_q\Delta z - \frac{G}{E}}{\frac{G}{E} - (Z - 1)^2\sin^2\beta_q\Delta z} \tag{7.20}$$

Knowing $K_3(A_{11} + A_{22})$ and $\frac{A_{11}}{A_{22}}$, $K_3\Pi$ can be found from equation 2.58:

$$K_3\Pi = K_3(A_{11} + A_{22})\frac{\frac{A_{11}}{A_{22}} - 1}{\frac{A_{11}}{A_{22}} + 1} \tag{7.21}$$

---

The above derivation does not consider thermal noise produced by the cavities or the finite bandwidth of the measuring system. When these effects are taken into account the method remains essentially the same although some additional terms are required in equations 7.7 and 7.14.

Using these methods, relative values of both S and $\Pi$

can be measured for various beam operating conditions.

A number of precautions must be observed, in particular the choice of cavity spacing. From fig7.3 it can be seen that the amplitude of the $P_2$ against z sine wave and its mean level depend on $\sin^2\beta_q\Delta z$. Ideally, for ease of measurement, these values should be as large as possible i.e. $\Delta z$ should be as near as possible to $\frac{\pi}{2\beta_q}$ ($\frac{1}{4}$ of the plasma wavelength $\lambda_q$) making $\sin^2\beta_q\Delta z \approx 1$. However, if some reduction of the signal input to the measuring system can be tolerated, measurements can be made over a range of plasma wavelengths with a fixed $\Delta z$. If, for example, a drop of 75% in $\sin^2\beta_q\Delta z$ is permissible, $\lambda_q$ can range between $2.4\Delta z$ and $12\Delta z$ giving a variation over a range of 5:1. This range should be quite sufficient for normal investigations involving change of beam operating parameters.

A further reason for taking S measurements with a single-cavity tube before building the double-cavity $\Pi$-measuring apparatus is that S measurements give a good idea of the sort of plasma wavelengths to be expected and enable the two cavities to be spaced for good sensitivity over as wide a range of operating conditions as possible when measuring $\Pi$.

The limitation described above is the only disadvantage this system has over that of Saito[32], where the two cavities were independently movable enabling full sensitivity to be obtained regardless of the value of $\lambda_q$. Moving both cavities

involves considerable additional complications. It almost certainly means using sliding vacuum seals making baking of the tube impossible and a high vacuum difficult to attain. On the other hand, the system described by Okoshi[63], where no moving parts were used, is simple mechanically but very inflexible as far as change of operating conditions is concerned. With such a system measurements can be made at only one value of $\lambda_q$ determined by the cavity spacing. Also adjustment of the transducer section of the electron gun is critical. It is believed that the method of measuring S and $\Pi$ presented here is a good compromise between simplicity of apparatus and versatility of operation

Measurements of both S and $\Pi$ give the full picture of noise on the electron beam. Equation 2.74 shows that the noise figure of a tube using the electron beam under examination depends on the value $(S - \Pi)$. It should therefore be possible to predict the effect on this figure of varying beam operating conditions.

## 8. CONCLUSIONS

It has been pointed out in this thesis that if the necessary care and precautions are taken in the design and construction of low-noise t.w.t's and b.w.a's to minimize other sources of noise, the fundamental limitation on the terminal noise figure is noise on the electron beam due to random emission at the cathode. Making a tube with a very low noise figure is, therefore, mainly a problem of producing an electron gun in which the effect on the beam of random emission is as small as possible.

The theory of noise propagation along electron beams shows that the minimum possible noise figure of a t.w.t. or b.w.a. depends directly on the magnitude of the quantity $(S - \Pi)$. S and $\Pi$ are two noise parameters which remain constant along a beam in which the velocity spread is small compared with the mean velocity, i.e. in a beam which has been accelerated by a potential of more than a few volts. The value of S and $\Pi$ in the single-velocity portion of a beam is determined by the processes in the multi-velocity region immediately in front of the cathode. It is this region which is of prime importance in the study of low-noise electron guns.

Mathematical analysis of a multi-velocity region is not straightforward. In the various proposed theories either severe approximations have been made or numerical calculations have been carried out using computers. It is generally agreed

that a lowering of the quantity $(S - \Pi)$ below the full-shot-noise value takes place in a multi-velocity region.

This reduction of noise is confirmed in practice by the performance of the type of electron gun developed by Currie. This gun incorporates a control electrode near the cathode which extends the low-velocity region and, it is believed, brings about a reduction of $(S - \Pi)$. Another feature of the gun is the formation of a virtual cathode which causes some rather unusual d.c. beam characteristics and which is accompanied by changes in the beam structure. The effect of virtual cathode formation on beam noise is not clear.

In this thesis the results of investigations into the effect of virtual cathode formation on the beam structure and the beam current characteristics of a Currie gun are reported. Two tubes with fluorescent-screen collectors were used. The change of beam current with variation of electrode voltages showed that the virtual cathode formed between anodes 1 and 2. Formation of the virtual cathode was accompanied by a reduction of current in the centre of the annulus only, so that the solid annulus appeared to split into two concentric beams.

When the control electrode voltage was swept at a relatively low frequency ($< 1$kc/s) hysteresis was observed in the beam current under certain conditions, due to an apparent reluctance of the virtual cathode to form. This effect is believed to be caused by the formation and trapping of positive ions

which delayed the formation of the virtual cathode by neutralizing the space charge. The sudden reduction of current when the virtual cathode formed is thought to be caused by rapid ion drainage from the virtual cathode region. These ideas are supported by approximate calculations of ion formation and drainage times.

Other unusual effects observed were noise in the beam current and distortion of the beam structure by vortices. The main cause of both these effects is believed to be poor emission.

The unusual characteristics of the Currie gun are of real interest only if they affect in some way the operation of a microwave tube. It is evident that the noise observed in the beam current could cause modulation of the gain, and vortex disturances, if large enough, could bring about interception of the electron beam. To eliminate these undesirable effects the usual precautions of ensuring good emission, accurate gun alignment and a high vacuum must be observed.

Of particular interest is the effect of a virtual cathode and hysteresis on electron beam noise. A tube built for studying these effects is described, together with the microwave measuring apparatus. However, up to the time of writing no results have been obtained. The tube has a movable electron gun and a single cavity to pick up the noise on the beam enabling the noise parameter S to be measured.

A new method of measuring both S and $\Pi$ is proposed which has certain advantages over other methods. Only a simple modification of the S-measuring tube is necessary consisting of the addition of a second fixed cavity.

## 9. ACKNOWLEDGEMENTS

The author wishes to thank the following for their help in carrying out work described in this thesis:

Professor E.E.Zepler and Professor G.D.Sims for making available the full facilities of the Department of Electronics.

Mr. G.R.Nudd for his assistance during the latter part of the project and Mr. G.Newell in whose workshop much of the constructional work was carried out.

Mr. N.W.W.Smith and Mr A.J.Gander of the Mullard Research Laboratories for providing electron tube parts and construction facilities.

The Ministry of Defence for financing the project, especially Mr. J.F.Gallagher who sponsored the work.

In particular the author would like to acknowledge the invaluable assistance and guidance received from Dr. W.A.Gambling who supervised the project.

## 10. REFERENCES

1. F.N.H.Robinson.

Microwave Shot Noise in Electron Beams and the Minimum Noise Factor of Travelling-Wave Tubes and Klystrons.

Jnl. Brit.I.R.E., 14, 79 (1954).

2. S.Bloom and R.W.Peter.

A Minimum Noise Figure for the Travelling-Wave Tube.

R.C.A. Rev., 15, 252 (1954).

3. J.R.Pierce.

A Theorem Concerning Noise in Electron Streams.

Jnl. Appl. Phys., 25, 931 (1954).

4. J.R.Pierce and W.E.Danielson.

Minimum Noise Figure of Travelling-Wave Tube with Uniform Helices.

Jnl. Appl. Phys., 25, 1163 (1954).

5. T.E.Everhart.

Concerning the Noise Figure of a Backward-Wave Amplifier.

Proc. I.R.E., 43, 444 (1955).

6. H.A.Haus.

Noise in One-Dimensional Electron Beams.

Jnl. Appl. Phys., 26, 560 (1955).

7. H.A.Haus and F.N.H.Robinson.

Minimum Noise Figure of Microwave Amplifiers.

Proc. I.R.E., 43, 981 (1955).

8. H.A.Haus.

Signal and Noise Propagation along Electron Beams.

Noise in Electron Devices, Technology Press and John Wiley and Sons, Ch.3, p.77 (1959).

9. G.M.Branch and T.G.Mihran.

Plasma-Frequncy Reduction Factors in Electron Beams.

Trans. I.R.E., ED-2, 3 (1955).

10. H.Nyquist.

Thermal Agitation of Electric Charge in Conductors.

Phys. Rev., 32, 110 (1928).

11. R.Kompfner.

The Travelling-Wave Tube as an Amplifier at Microwaves.

Proc. I.R.E., 35, 124 (1947).

12. R.W.Peter.

Low-Noise Travelling-Wave Amplifier.

R.C.A. Rev., 13, 344 (1952).

13. W.Shottky.

Spontaneous Current Fluctuations in Various Conductors.

Ann. Physik, 57, 541 (1918).

14. A.J.Rack.

Effect of Space Charge and Transit Time on the Shot Noise in Diodes.

Bell Tech. Jnl., 17, 592 (1947).

15. P.K.Tien.

A Dip in the Minimum Noise Figure of Beam-Type Microwave Amplifiers.

Proc. I.R.E., 44, 938 (1956).

16. P.K.Tien and J.Moshman.

Monte-Carlo Calculation of Noise near the Potential Minimum of a High-Frequency Diode.

Jnl. Appl. Phys., 27, 1067 (1956).

17. A.E.Siegman and D.A.Watkins.

Potential-Minimum Noise in the Microwave Diode.

Trans. I.R.E., ED-4, 82 (1957).

18. A.E.Siegman, D.A.Watkins ans Hsung-Cheng Hsieh.

Density-Function Calculations of Noise Propagation on an Accelerated Multi-Velocity Electron Beam.

Jnl. Appl. Phys., 28, 1138 (1957).

19. A.E.Siegman.

Analysis of Multi-Velocity Electron Beams by the Density-Function Method.

Jnl. Appl. Phys., 18, 1132 (1957).

20. M.R.Currie and D.C.Forster.

Low-Noise Tunable Preamplifiers for Microwave Receivers.

Proc. I.R.E., 46, 570 (1958).

21. M.R.Currie.

A New Type of Low-Noise Electron Gun for Microwave Tubes.

Proc. I.R.E., 46, 911 (1958).

22. M.R.Currie and D.C.Forster.

New Mechanism of Noise Reduction in Electron Beams.

Jnl. Appl. Phys., 30, 94 (1959).

23. M.Caulton and G.E.St.John.

S-Band Travelling-Wave Tube with Noise Figure Below 4dB.

Proc. I.R.E., 49, 911 (1958).

24. B.G.Bosch and K.B.Niclas.

Ultra-Low-Noise Travelling-Wave Tube with Simple Elecron Gun Structure.

Proc. I.R.E., 50, 324 (1962).

25. B.G.Bosch, K.B.Niclas and H.Thienel.

Investigations on Very-Low-Noise Travelling-Wave Tubes.

Proc. 4th Int. Congress on Microwave Tubes, p.458 (1962).

26. J.G.Armstrong.

Study of an Ultra-Low-Noise Travelling-Wave Tube Gun.

I.E.E. conference on the Design and Use of Microwave Valves (1963).

27. J.M.Hammer and M.E.Thomas.

Travelling-Wave Tube Noise Figures of 1.0dB at S-Band.

Proc. I.E.E.E., 52, 207 (1964).

28. J.Berghammer.

Space-Charge Effects in Ultra-Low Noise Electron Guns.

R.C.A. Rev., 21, 369 (1960).

29. B.Salzberg and A.V.Haeff.

Effects of Space Charge in the Grid - Anode Region of Vacuum Tubes.

R.C.A. Rev., 2, 336 (1938).

30. A.L.Eichenbaum and J.M.Hammer.

Limiting Current Effects in Low-Noise Travelling-Wave-Tube Guns.

R.C.A. Rev., 23, 420 (1962).

31. A.Zacharius and L.D.Smullin.

Noise Reduction in Electron Beams.

Trans. I.R.E., ED-7, 172 (1960).

32. S.Saito.

New Method of Measuring the Noise Parameters in an Electron Beam.

Trans. I.R.E., ED-5, 264 (1961).

33. W.M.Mueller.

Reduction of Beam Noisiness by means of a Potential Minimum away from the Cathode.

Proc. I.R.E., 49, 642 (1961).

34. J.M.Hammer.

Measured Values of Noise Spectra, S and $\Pi$, of Ultra-Low-Noise Beams.

Proc. I.E.E.E., 51, 390 (1963).

35. C.K.Birdsall and W.B.Bridges.

Space-Charge Instabilities in Electron Diodes and Plasma Converters.

Jnl. Appl. Phys., 32, 2611 (1961).

36. W.B.Bridges and C.K.Birdsall.

Space-Charge Instabilities in Electron Diodes II.

Jnl. Appl. Phys., 34, 2946 (1963).

37. J.Berghammer.

Noise Smoothing by Reactive Damping in Finite Multi-Velocity Electron Beams.

R.C.A. Rev., 22, 185 (1961).

38. W.M.Mueller and M.R.Currie.

Noise Propagation on Uniformly Accelerated Electron Beams.

Jnl. Appl. Phys., 30, 1876 (1959).

39. J.Berghammer.

Landau Damping of Space-Charge Waves.

Jnl. Appl. Phys., 33, 1499 (1962).

40. M.Caulton, B.Hershenov and F.Paschke.

Experimental Evidence of Landau Damping in Electron Beams.

Jnl. Appl. Phys., 33, 800 (1962).

41. T.G.Mihran.

R.F. Current Behaviour in Electron Beams with D.C. Velocity Spread.

Jnl. Appl. Phys., 33, 1582 (1962).

42. N.W.Robinson.

Bakeable High-Vacuum Seals.

Jnl. Sci. Instrum., 34, 121 (1957).

43. J.Holden, L.Holland and L.Laurenson.

Bakeable Vacuum Seals using Aluminium-Wire Gaskets.

Jnl. Sci. Instrum., 36, 281 (1959).

44. J.E.Ryley and W.A.Gambling.

A Current-Stabilized D.C. Supply Rated at 30A 4kW using Semiconductor Components.

Jnl. Sci. Instrum., 39, 600 (1962).

45. R.L.Garwin.

Efficient Precision Current Regulator for Low-Voltage Magnets.

Rev. Sci. Instrum., 29, 223 (1958).

46. S.D.Johnson and J.R.Singer.

Precision Current Regulator using Transistors.

Rev. Sci. Instrum., 29, 1026 (1958).

47. R.L.Garwin, D.Hutchinson, S.Penman and G.Shapiro.

Efficient Precision Current Regulator for High-Power Magnets.

Rev. Sci. Instrum., 30, 105 (1959).

48. K.C.Brog and F.J.Milford.

High-Precision Large-Current Regulator.

Rev. Sci. Instrum., 31, 321 (1960).

49. J.C.S.Richards.

A Transistorized Current Stabilizer for an Electromagnet.

Electronic Engineering, 32, 22 (1960).

50. A.J.Blundell, A.E.Garside, A.E.Hibberd and I.Williams.

Silicon Power Rectifiers.

Proc. I.E.E., 108A, 273 (1961)

51. H.R.Lowry.

Industrial Applications of Silcon Controlled Rectifiers.

Proc. I.E.E., 106B, 1295 (1959).

52. Controlled Rectification using Trinistor Switches.

Westinghouse Semiconductor Application Report No.2.

53. T.Moreno.

Microwave Transmission Design Data.

Dover Publications Inc. (1958).

54. E.L.Ginzton.

Microwave Measurements.

Mc.Graw Hill Book Co. Inc. (1957).

55. W.R.Beam and R.D.Hughes.

Microwave Noise Source Modulator and Power Supply.

Trans. I.R.E., ED-4, 185 (1957).

56. A. von Engel.

Ionized Gases.

Clarendon Press (1955).

57. H.H.Atkinson.

Limiting Currents and Neutralization in Cylindrical Electron Beams.

Proc. 4th Int. Congress on Microwave Tubes, p.559 (1962).

58. C.C.Cutler.

Spurious Modulation of Electron Beams.

Proc. I.R.E., 44, 61 (1956).

59. A.D.Sutherland.

Relaxation Instabilities in High-Perveance Electron Beams.

Trans. I.R.E., ED-7, 268 (1960).

60. R.L.Kyhl and H.F.Webster.

Breakup of Hollow Cylindrical Electron Beams.

Trans. I.R.E., ED-3, 172 (1956).

61. H.F.Webster.

Structure in Magnetically-Confined Electron Beams.

Jnl. Appl. Phys., 18, 1388 (1957).

62. G.R.Nudd, J.E.Ryley and W.A.Gambling.

A New Method of Measuring the Noise Parameters of an Electron Beam.

In course of publication.

63. T.Okoshi.

A New Method of Measuring the Noise Parameters S and $\Pi$ of an Electron Beam.

Trans. I.E.E.E., ED-11, 37 (1964).